

Hard exclusive production of two pions in $\gamma\gamma$ -collisions within the SCET factorization approach

N. Kivel

Helmholtz Institut Mainz, Johannes Gutenberg-Universität, D-55099 Mainz, Germany
Institut für Kernphysik, Johannes Gutenberg-Universität, D-55099 Mainz, Germany

ABSTRACT: We perform an analysis of power suppressed contributions for large angle pion pairs production in gamma gamma collisions. Using the soft collinear effective theory (SCET) framework we derive a factorization formula which is described as a sum of hard and soft contributions. The soft contribution is an important part for the consistent description of power corrections which can be described by matrix elements of SCET-I operators within the SCET framework. For hard power suppressed amplitude we consider an approximation by twist-3 chiral enhanced contributions. We define a physical subtraction scheme in order to cancel endpoint singularities in collinear convolution integrals. In this case the subleading correction is described by well defined expression with the known angular behavior. The latter is determined by hard scattering subprocess and can be computed at the leading logarithmic approximation.

The obtained results are applied to a phenomenological analysis of existing data. Using the leading and subleading power contributions and fitting two unknown nonperturbative amplitudes as a free parameters we can consistently describe the existing data for $\pi^+\pi^-$ and $\pi^0\pi^0$ production. We suggest to measure one more hadronic cross section which can be accessed in the unpolarized e^+e^- scattering. These data will help to reduce theoretical ambiguities in the phenomenological analysis and to understand the production mechanism of the considered reaction.

¹ On leave of absence from St. Petersburg Nuclear Physics Institute, 188350, Gatchina, Russia

Contents

1	Introduction	1
2	General information about the process $\gamma\gamma \rightarrow \pi\pi$	4
2.1	Kinematics, amplitudes and cross sections	4
2.2	Leading twist approximation	6
3	A toy integral with the soft-overlap contribution	9
3.1	Interpretation of the result in soft collinear effective theory	14
4	Factorization of the subleading amplitudes in SCET	19
4.1	Soft Collinear Effective Theory approach: general remarks	19
4.2	The hard contributions within the SCET framework	21
4.3	The soft-overlap contribution within the SCET framework	25
4.3.1	The soft-overlap contribution with operator $O_n^{(4)} O_{\bar{n}}^{(4)}$	27
4.3.2	The soft-overlap contribution with operators $O_n^{(6)} O_{\bar{n}}^{(i)}$	30
4.3.3	The soft-overlap contributions with photon states	32
4.4	Summary of the SCET analysis	39
5	Calculation of the amplitude in the physical subtraction scheme	39
5.1	The leading-order hard coefficient functions of the soft contribution	40
5.2	Subleading amplitude in the physical subtraction scheme	42
6	Phenomenological analysis of BELLE data	45
6.1	Phenomenological analysis using model-II for pion DA	48
6.2	Phenomenological analysis using CZ-model of pion DA	52
7	Discussion	55
A	Higher twist distribution amplitudes	56
B	The list of SCET interactions	58

1 Introduction

A factorization theorem for large angle production of mesons have been suggested long time ago in Ref.[1]. The amplitude of such process is given by a convolution integral of a hard kernel with light-cone distribution amplitudes (DAs). The hard kernel describes hard subprocess $\gamma\gamma \rightarrow \bar{q}q + \bar{q}q$ and can be computed systematically in the perturbation theory. The DA describes the nonperturbative overlap of the two quarks with outgoing meson state and can not be computed from the first principles.

An interesting case is given by particular process $\gamma\gamma \rightarrow \pi\pi$. The large scattering angles correspond to a region where Mandelstam variables are large $s \sim -t \sim -u \gg \Lambda_{QCD}^2$. The asymptotic behavior of the cross section was obtained in Ref.[1] in the framework of the factorization approach

$$\frac{d\sigma^{\gamma\gamma \rightarrow \pi\pi}}{d\cos\theta} \sim \frac{f_\pi^4}{s^3} \frac{1}{\sin^4\theta}. \quad (1.1)$$

Here θ is the scattering angle in center-of-mass frame, $f_\pi = 131\text{MeV}$ is the pion decay constant. A comprehensive phenomenological analysis of this reaction was later carried out in Ref.[2].

The cross section of pion production was already measured at sufficiently large energy in several experiments [3, 4]. The most precise measurements in the region up to $\sqrt{s} = 4\text{GeV}$ were performed by BELLE collaboration [5, 6], see also review [7]. Comparison of these accurate data with the theoretical calculations shows a significant underestimate of the absolute values of the cross sections [8]. The largest discrepancy between the theory and experiment is observed for the neutral pion production.

There are various attempts to find an explanation of this problem. Within the QCD factorization framework it is suggested to use a broad model for the pion distribution amplitude. In this case the virtualities of the hard particles are assumed to be much smaller than the large external kinematical variables and therefore one can use a relatively large value of the QCD coupling $\alpha_s \simeq 0.4$ [2, 9, 10]. Such approach allows to reach a certain qualitative agreement with the $\pi^+\pi^-$ data but cannot explain the discrepancy in the $\pi^0\pi^0$ channel. In Ref.[10] it is proposed that the large contribution in this channel can arise at higher orders in α_s due to the specific three gluon exchange diagrams.

Other possible scenario which explains the mismatch between the leading-order pQCD predictions and the data implies a different idea about the underlying QCD dynamics. It is assumed that the leading-order contribution becomes dominant only at very large energies which are considerably larger than the energies of existing experiments. Such scenario suggest a different shape of the pion DA which yields small values of the cross sections. The model for pion DA is obtained from the process $\gamma^*\gamma \rightarrow \pi^0$ or using the pion electromagnetic form factor computed in the QCD sum rule technique [11, 13–16]. The discrepancy in this case must be explained by a large numerical effect of power suppressed corrections. A bulk of this effect is associated with the so-called soft-overlap mechanism. Such configuration describes a soft-overlap of hadronic states and appear only as a power correction to the leading asymptotic contribution in Eq.(1.1). Nevertheless it was found that numerically this contribution is large and even dominant at some moderate values of the hard scale Q . The soft-overlap contribution is especially important if the leading-order approximation is of order α_s and therefore can be suppressed numerically.

This idea was implemented for description of large angle meson production in $\gamma\gamma \rightarrow MM$ process within the handbag model in Refs.[17, 18]. In this model the soft-overlap contribution is described by the two-pion matrix element which is associated with the two-pion distribution amplitude. The important feature is that this function depends only from the total energy s . This allows one to compute the angular behavior of the amplitude

because it is completely defined by the hard subprocess. In Ref.[17] it was shown that handbag model gives $1/\sin^4\theta$ behavior for the pion cross sections similar to the leading power term in Eq.(1.1). The unknown normalization of the two-pion distribution amplitude was fitted from the data. This automatically ensures a large value of the $\pi^0\pi^0$ cross section and gives the ratio $R = d\sigma^{\pi^0\pi^0}/d\sigma^{\pi^+\pi^-} = 1/2$.

Despite interesting results the handbag model has many problematic points which have to be better understood. Some critical remarks are considered in Refs. [9, 10]. The most difficult challenge is to develop a consistent formulation of the soft-overlap configuration in order to describe it on a systematic way. This is important in order to avoid a double counting with the power corrections arising from the hard power suppressed configurations. Then such framework allows one to reduce a model dependence of theoretical description to a minimum. Motivated by this task we try to develop such approach in present paper.

Our main task is to develop the QCD factorization approach beyond the leading power approximation. Such development can not be done only by computation of subleading hard contributions. It is well known that such corrections are often ill defined because collinear convolution integrals have the so-called endpoint divergencies. These singularities appear due to the overlap of collinear and soft regions. The complete description in this case can be only carried out including a contribution with soft particles. A description of such configurations can be performed in the framework of effective field theory which takes into account soft and collinear modes. Such effective theory was constructed recently and known as soft collinear effective theory (SCET) [19–24].

In the SCET framework the factorization is carried out in two steps. At first step one factorizes the hard modes (particles with momenta $p_\mu \sim Q$). After integration of hard modes the full QCD is reduced to the effective theory SCET-I. This field theory includes the hard-collinear, collinear and soft degrees of freedom. The hard-collinear modes describe particles with the virtualities $p_{hc}^2 \sim Q\Lambda$, where the Λ is a soft scale of order Λ_{QCD} . A further factorization is possible if the hard scale Q is sufficiently large so that the hard-collinear scale $\mu_{hc}^2 \sim Q\Lambda$ is a good expansion parameter in pQCD. Integrating out hard-collinear particles one obtains the effective theory with soft and collinear particles which is called SCET-II. Such a scheme provide a systematic definition of the soft-overlap configurations and allows one to study the endpoint region in a consistent way.

The region of *moderate* values of Q^2 can be defined as a region where the hard-collinear scale is still relatively small $\mu_{hc}^2 \leq 1 - 1.5\text{GeV}^2$ and further expansion do not provide a good approximation. The kinematical region of existing experiments corresponds to $Q \leq 3 - 4\text{GeV}$. One can easily see that in this region the hard-collinear scale is not large enough $\mu_{hc}^2 \leq 1.2 - 1.6\text{GeV}^2$ where we take $\Lambda \simeq 400\text{MeV}$. Therefore in this case one can perform only the factorization of the hard modes. In this case the soft-overlap contributions can be defined as a matrix elements of SCET-I operators. Such contributions must be included into factorization scheme together with the hard configurations described by pure collinear operators. We expect that this method will help us to obtain a complete and consistent theoretical description of power suppressed corrections.

Our paper is organized as follows. In section 2 we specify notation and kinematics and briefly review the leading twist results. In section 3 we study a scalar integral using

expansion by momentum regions. The toy integral has contributions associated with the collinear and soft regions. We demonstrate that the overlap of the soft and collinear regions introduce the endpoint divergencies. We show that these singularities cancel in the sum of collinear and soft contributions leaving a large logarithm. We also discuss the factorization scheme of this integral in the effective theory framework.

In section 4 we perform an analysis of relevant subleading operators within the SCET framework. First we consider the hard contribution and required collinear operators. We compute the subleading hard contribution given by the chiral enhanced twist-3 pion distribution amplitude. We will show that factorization also include SCET-I operators which describe the relevant soft contributions. Using SCET approach we obtain that there is only one such operator. Using these results we derive a factorization formula which describe the power correction at order $1/Q^2$. In section 5 we compute the hard kernels for the soft contribution. Then we explain how to define a physical subtraction scheme in order to avoid the end-point singularities in the collinear convolution integrals. Section 6 is devoted to a phenomenological analysis. We compare the obtained results with data and discuss different scenarios associated with the different models of the pion DA. A summary and discussion of obtained results is given in section 7. In Appendix we provide a useful information about higher twist distribution amplitudes and SCET Lagrangian.

2 General information about the process $\gamma\gamma \rightarrow \pi\pi$

2.1 Kinematics, amplitudes and cross sections

In order to describe the process $\gamma(q_1)\gamma(q_2) \rightarrow \pi(p)\pi(p')$ we choose center-of-mass system (c.m.s.) $\mathbf{p} + \mathbf{p}' = 0$ with pion momenta directed along z -axis. Mandelstam variables are defined as

$$s = (q_1 + q_2)^2 \equiv W^2, \quad t = (p - q_1)^2, \quad u = (p - q_2)^2, \quad (2.1)$$

In c.m.s. the particle momenta read

$$p = \frac{W}{2}(1, 0, 0, \beta), \quad p' = \frac{W}{2}(1, 0, 0, -\beta), \quad (2.2)$$

$$q_1 = \frac{W}{2}(1, \sin\theta, 0, \cos\theta), \quad q_2 = \frac{W}{2}(1, -\sin\theta, 0, -\cos\theta), \quad (2.3)$$

where θ is the scattering angle and β is the pion velocity

$$\beta = \sqrt{1 - \frac{4m_\pi^2}{s}}. \quad (2.4)$$

We will also use the auxiliary light-cone vectors

$$n = (1, 0, 0, -1), \quad \bar{n} = (1, 0, 0, 1), \quad (n \cdot \bar{n}) = 2. \quad (2.5)$$

In this paper we consider the kinematical region where $s \sim -t \sim -u \gg m_\pi^2$ therefore we neglect pion mass. Then the light-cone decomposition of the momenta read

$$p \simeq W \frac{\bar{n}}{2}, \quad p' \simeq W \frac{n}{2}, \quad (2.6)$$

$$q_1 = \frac{(1 - \cos \theta)}{2} W \frac{n}{2} + \frac{(1 + \cos \theta)}{2} W \frac{\bar{n}}{2} + q_\perp, \quad (2.7)$$

$$q_2 = \frac{(1 + \cos \theta)}{2} W \frac{n}{2} + \frac{(1 - \cos \theta)}{2} W \frac{\bar{n}}{2} - q_\perp, \quad (2.8)$$

with

$$q_\perp^2 = \frac{s}{4}(1 - \cos^2 \theta). \quad (2.9)$$

The process $\gamma\gamma \rightarrow \pi\pi$ is described by the matrix element

$$\langle \pi(p), \pi(p') \text{ out} | \gamma(q_1)\gamma(q_2) \text{ in} \rangle = i(2\pi)^4 \delta(p_1 + p_2 - q_1 - q_2) M_{\gamma\gamma \rightarrow \pi\pi}, \quad (2.10)$$

where the amplitude

$$M_{\gamma\gamma \rightarrow \pi\pi} = e^2 \varepsilon_\mu(q_1) \varepsilon_\nu(q_2) M_{\gamma\gamma \rightarrow \pi\pi}^{\mu\nu}, \quad (2.11)$$

with the following hadronic tensor

$$M_{\gamma\gamma \rightarrow \pi\pi}^{\mu\nu} = i \int d^4x e^{-i(q_1 x)} \langle \pi(p), \pi(p') | T \{ J_{\text{em}}^\mu(x), J_{\text{em}}^\nu(0) \} | 0 \rangle. \quad (2.12)$$

Here J_{em}^μ denotes the electromagnetic current and $e^2 = 4\pi\alpha \simeq 4\pi/137$. It is convenient to pass to the pion isotopic coordinates $(\pi^\pm, \pi^0) \rightarrow (\pi^1, \pi^2, \pi^3)$ and consider the matrix element describing the process $\gamma\gamma \rightarrow \pi^a \pi^b$

$$T_{ab}^{\mu\nu} = i \int d^4x e^{-i(q_1 x)} \langle \pi^a(p), \pi^b(p') | T \{ J_{\text{em}}^\mu(x), J_{\text{em}}^\nu(0) \} | 0 \rangle, \quad (2.13)$$

This amplitude can be parametrized as, see e.g. Ref.[25]

$$\begin{aligned} T_{ab}^{\mu\nu} = & M_{++}^{\mu\nu} \left\{ \delta^{ab} T_{++}^{(0)}(s, t) + \delta^{a3} \delta^{b3} T_{++}^{(3)}(s, t) \right\} \\ & + M_{+-}^{\mu\nu} \left\{ \delta^{ab} T_{+-}^{(0)}(s, t) + \delta^{a3} \delta^{b3} T_{+-}^{(3)}(s, t) \right\} + \dots, \end{aligned} \quad (2.14)$$

where dots denote the additional structures which vanish when contracted with the photon polarization vectors. The two Lorentz tensors in Eq.(2.14) read

$$M_{++}^{\mu\nu} = \frac{1}{2} g^{\mu\nu} - \frac{1}{s} q_1^\nu q_2^\mu, \quad (2.15)$$

$$M_{+-}^{\mu\nu} = \frac{1}{2} g^{\mu\nu} + \frac{s}{4tu} \left\{ \Delta^{\mu\nu} - q_1^\nu q_2^\mu - \frac{\nu}{s} (q_1^\nu \Delta^\mu - q_2^\mu \Delta^\nu) \right\}, \quad (2.16)$$

where we defined $\nu = t - u = -2(q_1 \cdot \Delta)$ and $\Delta = p_1 - p_2$. Two tensor structures $M_{\pm\pm}^{\mu\nu}$ describe the appropriate photon helicity amplitudes $M_{\lambda_1 \lambda_2}$ and satisfy following relations¹

$$q_1^\mu M_{\pm\pm}^{\mu\nu} = q_2^\nu M_{\pm\pm}^{\mu\nu} = 0, \quad M_{++}^{\mu\nu} M_{+-}^{\mu\nu} = 0, \quad M_i^{\mu\nu} M_i^{\mu\nu} = \frac{1}{2}. \quad (2.17)$$

The amplitudes $T_{\pm\pm}^{(0,3)}$ are symmetric under crossing $(t, u) \rightarrow (u, t)$. The pion state in Eq.(2.10) is C -even and can be decomposed onto isospin states with $I = 0, 2$. For physical pion states the amplitude defined in Eq.(2.12) we obtain

$$M_{\gamma\gamma \rightarrow \pi^+ \pi^-}^{\mu\nu} = M_{++}^{\mu\nu} T_{++}^{(0)} + M_{+-}^{\mu\nu} T_{+-}^{(0)}, \quad (2.18)$$

¹Usually one defines four helicity amplitudes M_{++} , M_{--} , M_{+-} and M_{-+} . However for the pion production $M_{++} = M_{--}$ and $M_{+-} = M_{-+}$ and for brevity we do not write M_{--} and M_{-+} .

$$M_{\gamma\gamma\rightarrow\pi^0\pi^0}^{\mu\nu} = M_{++}^{\mu\nu} (T_{++}^{(0)} + T_{++}^{(3)}) + M_{+-}^{\mu\nu} (T_{+-}^{(0)} + T_{+-}^{(3)}). \quad (2.19)$$

The cross sections read

$$\frac{d\sigma^{\pi^+\pi^-}}{d\cos\theta} = \frac{\pi\alpha^2}{16s} (|T_{++}^{(0)}|^2 + |T_{+-}^{(0)}|^2), \quad (2.20)$$

$$\frac{d\sigma^{\pi^0\pi^0}}{d\cos\theta} = \frac{\pi\alpha^2}{32s} (|T_{++}^{(0)} + T_{++}^{(3)}|^2 + |T_{+-}^{(0)} + T_{+-}^{(3)}|^2), \quad (2.21)$$

where pion mass is neglected.

2.2 Leading twist approximation

In the region where $s \sim -t \sim -u \gg \Lambda_{\text{QCD}}$ the amplitude of process $\gamma\gamma \rightarrow \pi\pi$ can be described within the factorization framework. The leading order expressions was derived in Ref.[1], see also Refs.[26, 27]. Let us briefly discuss these results. Let us write the amplitude as a sum

$$T_{+\pm}^{(i)}(s, \theta) = A_{+\pm}^{(i)}(s, \theta) + B_{+\pm}^{(i)}(s, \theta), \quad (2.22)$$

where $A_{+\pm}^{(i)}$ and $B_{+\pm}^{(i)}$ denote the leading and subleading power contributions, respectively. The leading-twist and leading-order in α_s contribution is given by the one gluon exchange diagrams as in Fig.1.

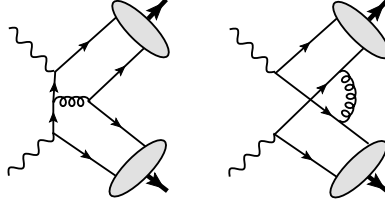


Figure 1. An example of the leading-order diagrams describing large-angle pion production. The shaded blobs denote the pion DAs.

The nonperturbative dynamics is described by the twist-2 pion distribution amplitude (DA) which is defined as a following matrix element

$$f_\pi \varphi_\pi(x) = i \int_{-\infty}^{\infty} \frac{d\lambda}{\pi} e^{-i(2x-1)(p' \cdot \bar{n}) \lambda} \langle \pi^-(p') | \bar{d}(\lambda \bar{n}) \not{n} \gamma_5 u(-\lambda \bar{n}) | 0 \rangle. \quad (2.23)$$

with the pion decay constant $f_\pi = 131\text{MeV}$. Corresponding coefficient functions have been computed in Ref.[1]. The explicit expressions read

$$A_{++}^{(0)}(s, \theta) = -A_{++}^{(3)}(s, \theta) = -\frac{(4\pi f_\pi)^2 \alpha_s C_F}{s \pi N_c} \frac{1}{1 - \cos^2 \theta} \left\langle \frac{1}{x} \right\rangle^2, \quad (2.24)$$

$$A_{+-}^{(0)}(s, \theta) = -\frac{(4\pi f_\pi)^2 \alpha_s C_F}{s \pi N_c} \left\{ \frac{1}{1 - \cos^2 \theta} \left\langle \frac{1}{x} \right\rangle^2 - \frac{1}{9} J(\theta) \right\} \quad (2.25)$$

$$A_{+-}^{(3)}(s, \theta) = \frac{(4\pi f_\pi)^2 \alpha_s C_F}{s \pi N_c} \left\{ \frac{1}{1 - \cos^2 \theta} \left\langle \frac{1}{x} \right\rangle^2 - \frac{1}{4} J(\theta) \right\}. \quad (2.26)$$

In these equations we used that the pion DA is symmetrical function: $\varphi_\pi(1-x) = \varphi_\pi(x)$. We also define $C_F = (N_c^2 - 1)/2N_c$ and α_s denotes the QCD running coupling. The convolution integrals are defined by

$$\left\langle \frac{1}{x} \right\rangle = \int_0^1 dx \frac{\varphi_\pi(x)}{x}, \quad (2.27)$$

and

$$J(\theta) = \int_0^1 dx \varphi_\pi(x) \int_0^1 dy \varphi_\pi(y) \frac{1}{x\bar{x}} \frac{1}{y\bar{y}} \frac{(\bar{x}\bar{y} + xy)(x\bar{x} + y\bar{y})}{(\bar{x}\bar{y} + xy)^2 - (\bar{x}\bar{y} - xy)^2 \cos^2 \theta}, \quad \bar{x} \equiv 1 - x. \quad (2.28)$$

Using Eqs.(2.18) and (2.19) one easily finds the physical amplitudes. In particular, for $\pi^0\pi^0$ production one obtains

$$A_{++}^{(0)}(s, \theta) + A_{++}^{(3)}(s, \theta) = \mathcal{O}(\alpha_s^2), \quad (2.29)$$

$$A_{+-}^{(0)}(s, \theta) + A_{+-}^{(3)}(s, \theta) = -\frac{(4\pi f_\pi)^2 \alpha_s C_F}{s} \frac{5}{\pi N_c} \frac{1}{36} J(\theta). \quad (2.30)$$

Notice that the integral $J(\theta)$ is real and therefore all leading twist amplitudes at leading-order are real. This is explained by the absence of any s -channel cut in the leading-order diagrams.

A detailed phenomenological analysis based on the leading twist formulas (2.24)-(2.26) is considered in Ref.[2]. Here we briefly discuss numerical estimates for the cross sections. In order to apply the leading twist description one has to specify a model for the pion DA. Following to standard approach we present these function as series over Gegenbauer polynomials

$$\varphi_\pi(x, \mu) = 6x\bar{x} \sum_n a_{2n}(\mu) C_{2n}^{3/2}(2x-1). \quad (2.31)$$

The coefficients a_{2n} defined by this equation are multiplicatively renormalizable at the leading logarithmic approximation. We consider few models which can be defined as following.

$$\text{model-I: } \mu = 1\text{GeV}, \quad a_0 = 1, \quad a_2 = 0.25, \quad a_{2n} = 0, \quad n > 2. \quad (2.32)$$

This simple model is based on the estimate suggested in Ref[12]. The following two models

$$\text{model-II: } \mu = 1\text{GeV}, \quad a_0 = 1, \quad a_2 = a_4 = a_6 = 0.1, \quad a_8 = 0.034, \quad a_{2n} = 0, \quad n > 8, \quad (2.33)$$

$$\text{model-III: } \mu = 2.4\text{GeV}, \quad a_0 = 1, \quad a_2 = 0.157, \quad a_4 = -0.192, \quad a_6 = 0.226, \quad a_{2n} = 0, \quad n > 4, \quad (2.34)$$

have been recently suggested in Refs. [13] and [15], respectively. One more alternative model was suggested in [33]

$$\text{set-CZ: } \mu = 1\text{GeV}, \quad a_0 = 1, \quad a_2 = 2/3, \quad a_{2n} = 0, \quad n > 2, \quad (2.35)$$

The running coupling will be computed at the scale $\mu_R = 0.8W\text{GeV}$ for the models I-III. For CZ-model we will use fixed value $\mu_R = 1.3\text{GeV}$ as in Ref.[2]. The inverse moment defined in Eq. (2.27) can be presented as a sum

$$\left\langle \frac{1}{x} \right\rangle = 3(1 + a_2 + a_4 + \dots + a_{2n} + \dots). \quad (2.36)$$

Then for the different models one obtains ($\mu = 1\text{GeV}$)

$$\left\langle \frac{1}{x} \right\rangle_{\text{I}} = 3.75, \quad \left\langle \frac{1}{x} \right\rangle_{\text{II}} = 4.00, \quad \left\langle \frac{1}{x} \right\rangle_{\text{III}} = 4.05, \quad \left\langle \frac{1}{x} \right\rangle_{\text{CZ}} = 5. \quad (2.37)$$

The integral $J(\theta)$ defined in Eq.(2.28) will be computed numerically. In Refs. [1, 2] it is found that this integral provides a small numerical effect. Therefore the main difference between the different models of pion DA is provided by the inverse moment (2.37) and by the value of running coupling α_s . For simplicity, we will also neglect an imaginary part which appear in the timelike kinematics from various large logarithms.

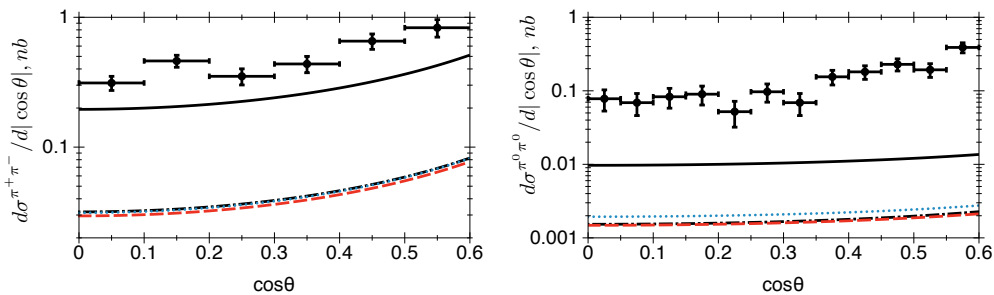


Figure 2. The cross sections as a function of $\cos\theta$ computed at the leading twist approximation at fixed $W = 3.05\text{GeV}$. The black solid line corresponds CZ-model, red dashed curve describes model-I, black dot-dashed and blue dotted curves describe model-II and III, respectively. The data are taken from Refs.[5, 6]

In Fig.2 we show the leading twist estimates for differential cross sections in comparison with BELLE data [5, 6] at $W = 3.05\text{GeV}$. For the pion DA defined by models I-III we fix the hard scale as $\mu = 2.4\text{GeV}$. The relatively low value of the scale for CZ-model yields $\alpha_s(1.7\text{GeV}^2) = 0.395$. In this case such choice is dictated by a large role of the endpoint region where $x \sim 1$ or $x \sim 0$. In this region the virtualities of hard partons are relatively small and this leads to a smaller value of the hard scale in phenomenological calculations.

From Fig.2 we conclude that the leading twist approximation provide a reasonable description of the angular behavior but predicts a very small absolute normalization. The cross section computed with the models I-III is about an order of magnitude below the data.

A more realistic estimate is obtained only with the CZ-model in case of $\pi^+\pi^-$ production. This model yields much larger results because the wide profile of the DA provides a larger value of the inverse momentum $\langle 1/x \rangle$ and also due to larger value of α_s . In this case one cannot exclude a sizable contribution from the higher-order radiative corrections. Some work in this direction is presented in Ref.[34].

On the other hand a description of the cross section for $\pi^0\pi^0$ production remains very problematic for all models of pion DA. Potentially large contributions are compensated in the expressions (2.29) and (2.30). Therefore in this case any leading twist estimate provides very small numerical value for the cross section as shown in Fig.2. In Ref.[10] it is suggested that, probably, some specific higher-order radiative corrections can help to solve this problem.

An alternative description can be developed if one assumes that power suppressed contributions are quite large at some moderate values of hard scale Q^2 . A large numerical contribution in this case can be generated by the soft-overlap mechanism. In Refs.[17, 18] this idea is used in order to develop the handbag model. In present work we continue to study the role of the soft-overlap contribution using the SCET factorization framework.

3 A toy integral with the soft-overlap contribution

In this section we consider a specific Feynman integral in order to demonstrate the relevance of the hard-collinear modes in description of the soft-overlap mechanism. We will show that the factorization of the soft contribution requires to introduce the hard-collinear and the soft modes. We will also see that the overlap of collinear and soft regions introduces the endpoint singularities in the collinear convolution integrals. These divergencies cancel only in the sum of collinear and soft contributions.

Let us consider the following scalar integral

$$J = \int dk \frac{m^2}{[k^2 - m^2] [(k + p')^2] [(k + q')^2] [(k + \bar{y}p')^2 - m^2]}, \quad (3.1)$$

where we assume that $p' \simeq Qn/2$, $q' \simeq \bar{Q}\bar{n}/2$ so that $p'^2 = q'^2 = 0$ and $-q'^2 \equiv Q^2 = 2(p' \cdot q') \gg m^2$. For the integral measure we imply

$$dk = \mu^{2\varepsilon} e^{\varepsilon\gamma_E} \frac{d^D k}{i\pi^{D/2}}, \quad D = 4 - 2\varepsilon. \quad (3.2)$$

We also assume that all propagators in the square brackets in Eq.(3.1) are defined with the standard $+i\varepsilon$ prescription. This integral can be associated with the diagram in Fig.3 where all particles are scalar. The dimensionless variable y describes a fraction of the total

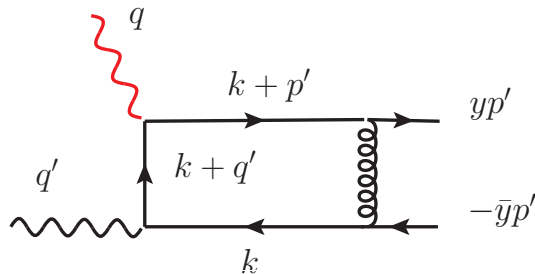


Figure 3. The graphical interpretation of the toy integral in Eq.(3.1).

momentum p' carried by the outgoing “quark”, we also use the short notation $\bar{y} = 1 - y$.

The integral J (3.1) is ultraviolet (UV) and infrared (IR) finite and can be easily computed in $D = 4$. Using the standard technique one obtains

$$J = \frac{1}{\bar{y}Q^2} \left\{ -\text{Li}(y) + \frac{\pi^2}{6} \right\} + \frac{m^2}{\bar{y}Q^4} \left(\ln \frac{m^2}{Q^2} + \dots \right) + \mathcal{O}(1/Q^6), \quad (3.3)$$

where the mass m is considered as a soft scale, $\text{Li}(z)$ denotes the Spence function (or dilogarithm, see definition in Eq.(4.40)) and the dots denote simple non-logarithmic contributions which will be not considered for brevity.

Let us obtain the expansion in Eq. (3.3) by identifying the momentum configurations that give non-vanishing contributions to the integral. For that purpose we recompute the integral (3.1) using the technique known as expansion by momentum regions [35–37].

Below we will use the small parameter $\lambda \sim \sqrt{m/Q}$ which is convenient for the estimate of the various terms in the effective theory. Using this parameter and defining the light-cone coordinates as $(p \cdot n, p \cdot \bar{n}, p_\perp) \equiv (p_+, p_-, p_\perp)$ one finds

$$q \sim p_h \sim Q(1, 1, 1), \quad q' \sim p_c \sim Q(1, \lambda^4, \lambda^2), \quad p' \sim p_c \sim Q(\lambda^4, 1, \lambda^2), \quad (3.4)$$

where p_h and p_c denote a generic hard and collinear momenta, respectively. In addition we will also need the soft p_s and hard-collinear p_{hc} momenta which scale as

$$p_s \sim Q(\lambda^2, \lambda^2, \lambda^2), \quad p_{hc} \sim Q(1, \lambda^2, \lambda) \text{ or } p_{hc} \sim Q(\lambda^2, 1, \lambda). \quad (3.5)$$

The hard region. In the hard region $k \sim p_h$, see Eq.(3.4). In this case the expression for the integral reads

$$J_h = \int dk \frac{m^2}{[k^2][(k+p')^2][(k+q')^2][(k+p'_2)^2]} = \frac{m^2}{\bar{y}Q^4} \left(\frac{2}{\varepsilon} + 2 \ln \mu^2/Q^2 \right). \quad (3.6)$$

This integral can be easily computed in dimensional regularization using the Feynman parameters.

The n -collinear region. In this region $k \sim p_c \sim p'$, see Eq.(3.4). Performing the expansion of the integrand in this region we obtain

$$J_n \simeq \int dk \frac{m^2}{[k^2 - m^2][(k+p')^2][(k+p'_2)^2 - m^2]} \left(\frac{1}{[2(kq')]} - \frac{k^2}{[2(kq')]^2} \right) = J_{0n} + J_{2n}, \quad (3.7)$$

The first integral J_{0n} is of order λ^0 and UV and IR finite. Computation this integral yields

$$J_{0n} = \frac{1}{\bar{y}Q^2} \left(-\text{Li}(y) + \frac{\pi^2}{6} \right). \quad (3.8)$$

Comparing with the exact answer in Eq.(3.3) we find that this term reproduces the leading power term of order $1/Q^2$.

The second integral in Eq.(3.7) is subleading and scales as $J_{2n} \sim \lambda^4$. In order to compute this integral we use a simple trick $k^2 = [k^2 - m^2] + m^2$ in the numerator (3.7) in order to cancel the propagator $[k^2 - m^2]^{-1}$. This gives the sum of the two integrals: one

of them is UV-divergent (without the propagator $[k^2 - m^2]^{-1}$). Computing these integrals with the help of light-cone variables in $D = 4 - 2\varepsilon$ one finds

$$J_{2n} = -\frac{m^2}{\bar{y}Q^4} \left(\frac{\mu^2}{m^2}\right)^\varepsilon \frac{1}{\varepsilon} + \frac{m^2}{\bar{y}Q^4} \int_0^{p'_-} \frac{dk_-}{p'_- - k_-} + \dots \quad (3.9)$$

The first term on the *rhs* has pole $1/\varepsilon$ which originates from the UV-divergent integral. The second UV finite integral gives the second contribution on the *rhs* (3.9) which is IR-divergent and cannot be defined without an additional regularization. This singularity can be interpreted as the endpoint divergency in the collinear convolution integral.

The \bar{n} -collinear region. In this case $k \sim p_c \sim q'$ and already the leading term in the expansion is of order λ^4

$$J_{\bar{n}} \simeq \frac{1}{\bar{y}} \int dk \frac{1}{[2(kp')]^2} \frac{m^2}{[k^2 - m^2] [(k + q')^2]}. \quad (3.10)$$

The straightforward calculation of this integral with the help of the light-cone variables gives

$$J_{\bar{n}} = -\frac{1}{2} \frac{m^2}{\bar{y}Q^4} \frac{1}{\varepsilon} \left(\frac{\mu^2}{m^2}\right)^\varepsilon \int_0^1 \frac{dk_+}{[k_+]^2} (1 - k_+)^{-\varepsilon}. \quad (3.11)$$

In order to obtain this expression we computed the integral over k_- using residues and then integrated over the transverse momentum k_\perp . The pole $1/\varepsilon$ is again due to the UV-divergency of the integral over the transverse momentum k_\perp . However the remaining integral over dk_+ is power divergent in the region $k_+ \sim 0$.

In order to resolve this ambiguity let us rewrite the integrand as a sum of the following terms

$$\frac{1}{[k^2 - m^2] [(k + q')^2]} = \frac{1}{[k^2 - m^2]} \left(\frac{1}{[(k + q')^2]} - \frac{1}{[2(kq')]} \right) + \frac{1}{[k^2 - m^2] [2(kq')]}, \quad (3.12)$$

This yields two contributions

$$J_{\bar{n}} = \frac{1}{\bar{y}} \int dk \frac{m^2}{[2(kp')]^2} \frac{1}{[k^2 - m^2] [2(kq')]} - \frac{1}{\bar{y}} \int dk \frac{m^2}{[2(kp')]^2} \frac{k^2}{[k^2 - m^2] [(k + q')^2] [2(kq')]} = J_{1\bar{n}} + J_{2\bar{n}}. \quad (3.13)$$

Computing the the first integral $J_{1\bar{n}}$ one obtains scaleless and power divergent integral

$$J_{1\bar{n}} \sim \int_0^\infty \frac{dk_+}{k_+^2} \int \frac{dk_\perp}{k_\perp^2 + m^2} = 0. \quad (3.14)$$

Therefore we assume that this integral vanishes and can be neglected. Computation of the second integral yields

$$J_{2\bar{n}} = -\frac{1}{\bar{y}} \int dk \frac{m^2}{[2(kp')]^2} \frac{k^2}{[k^2 - m^2] [(k + q')^2] [2(kq')]} = -\frac{m^2}{\bar{y}Q^4} \left(\frac{\mu^2}{m^2}\right)^\varepsilon + \frac{m^2}{\bar{y}Q^4} \int_0^{q'_+} \frac{dk_+}{k_+^2} \ln[1 - k_+/q'_+] (q'_+ - 2k_+). \quad (3.15)$$

The first term on the *rhs* has UV-pole $1/\varepsilon$ which appears from the integration over k_\perp . The second term has already only the logarithmic singularity when $k_+ \rightarrow 0$. Here we again observe that the UV and IR singularities in Eq.(3.15) enter additively. Again, in order to compute integral $J_{2\bar{n}}$ one needs an additional regularization prescription.

The soft region. In this case $k \sim p_s$, see Eq.(3.5). Expansion of the integrand in this region yields two contributions of order λ^2 and λ^4

$$J_s \simeq \frac{1}{\bar{y}} \int dk \frac{m^2}{[k^2 - m^2] [2(kp')]^2 [2(kq')]} \left\{ 1 - \frac{k^2}{[2(kq')]^2} - \frac{k^2}{2(kp')} - \frac{k^2 - m^2}{2(kp'_2)} \right\}. \quad (3.16)$$

Computation of these integrals in $D = 4 - 2\varepsilon$ yields the scaleless integrals. This is a well known problem when one has to introduce an additional auxiliary regularization. Some of the soft integrals in Eq.(3.16) are even power divergent. As a result such contributions can even generate fictitious subleading terms which are not presented in the exact answer. Consider the first contribution in Eq.(3.16). It is easy to see that it scales as

$$J_{1s} = \frac{1}{\bar{y}} \int dk \frac{m^2}{[k^2 - m^2] [2(kp')]^2 [2(kq')]} \sim \lambda^2, \quad (3.17)$$

and gives the power correction of order $1/Q^3$ which is not presented in the exact answer (3.3). A more detailed investigation shows that the corresponding integral is power divergent and therefore must be considered as scaleless and therefore vanishes.

In order to see this let us introduce an additional auxiliary regularization. We consider the following regularized integral

$$J_{1s}^{\text{reg}} = \frac{m^2}{\bar{y}} \frac{1}{Q^2 p'_-} \frac{1}{2} \int \frac{dk_-}{[k_-]} \int \frac{dk_+}{[k_+ - \tau_+]^2} \frac{dk_\perp}{[k_+ k_- - k_\perp^2 - m^2]}, \quad (3.18)$$

where we use the light-cone variables (k_+, k_-, k_\perp) and introduce regularization parameter τ_+ . We assume that τ_+ transforms in the same way as k_+ under longitudinal boost $k_+ \rightarrow \alpha k_+$. Notice that without the prefactor $\sim 1/p'_-$ the integral is not invariant with respect to longitudinal boosts because the factor $1/[k_+ + \tau_+]^2$ in the denominator (3.18). As a result the computation of this integral leads to a power divergent contribution when $\tau_+ \rightarrow 0$. Taking the integral over k_+ by residues and integrating over k_\perp we obtain

$$J_{1s}^{\text{reg}} = \left(\frac{\mu^2}{m^2} \right)^\varepsilon \frac{m^2}{\bar{y}} \frac{1}{Q^2 p'_- \tau_+}. \quad (3.19)$$

Assuming that $\tau_+ \sim m$ we obtain the contribution of order λ^2 . On the other hand such contribution can not appear in the exact integral J (3.3) because we do not have appropriate external soft momenta. Hence we can conclude that the scaleless integrals which are power divergent can be neglected. The main lesson from this consideration is that one must consider only such soft integrals which are boost invariant and therefore have only the logarithmic endpoint singularities.

Following this argumentation the third and the fourth terms on *rhs* of Eq.(3.16) can also be neglected. Hence only the second term $\sim k^2/[2(kq')]^2$ in Eq.(3.16) provides a

non-vanishing contribution of order λ^4 . Therefore we get

$$J_s = \frac{m^2}{\bar{y}Q^4} \int dk \frac{-k^2}{[k^2 - m^2] [k_+]^2 [k_-]^2}. \quad (3.20)$$

The overlap between the collinear and soft regions can be easily established taking the soft limit in the collinear integrals in Eqs.(3.7) and (3.10). It is easy to see that

$$[J_n]_s = [J_{\bar{n}}]_s = J_s. \quad (3.21)$$

This explains that the IR-divergencies in the collinear integrals are related with the overlap of the soft and collinear regions.

Notice that integral J_{1s} in Eq.(3.17) also appears in the soft limit of the well defined collinear integral J_{0n} in Eq.(3.7) but this does not provide any IR-divergencies. On the other hand the overlap with the same soft integral $J_{1s} = J_{1\bar{n}}$ in the collinear integral $J_{\bar{n}}$, see Eq.(3.13), gives the power divergent integral in Eq.(3.11). Hence we can conclude that subtractions of such spurious soft integrals is important in order to clarify the endpoint behavior of collinear integrals.

We find that the contributions of other possible regions provide scaleless or power suppressed integrals and therefore can be neglected. For instance, the expansion in the hard-collinear regions $k \sim p_{hc}$ defined in Eq.(3.5) yields the scaleless integrals because we do not have external hard-collinear particles. Hence we can conclude that expansion of the integral J up to order λ^4 must be reproduced by the sum of the following integrals

$$J = J_h + J_n + J_{\bar{n}} + J_s. \quad (3.22)$$

Let us now compute each integral in the *rhs* and to check that we reproduce the exact answer in Eq.(3.3).

Formally the soft integral (3.20) is scaleless in dimensional regularization and therefore cannot be defined without an additional regularization. In present case it is convenient to introduce the auxiliary analytic regularization as in Refs.[36, 37]. Following this prescription we introduce two regulators $\lambda_{1,2}$ by substituting in Eq.(3.1)

$$\frac{1}{[(k+p')^2][(k+q')^2]} \rightarrow \frac{\nu^{2(\lambda_1+\lambda_2)}}{[(k+p')^2]^{1+\lambda_1} [(k+q')^2]^{1+\lambda_2}}, \quad (3.23)$$

where ν is the corresponding regularization scale. Calculation of the regularized integrals yields

$$J_{2n}^{\text{reg}} = \int dk \frac{\nu^{2(\lambda_1+\lambda_2)} m^2}{[k^2 - m^2] [(k+p')^2]^{1+\lambda_1} [(k+\bar{y}p')^2 - m^2] [2(kq')]^{(2+\lambda_2)}} \frac{-(1+\lambda_2)k^2}{[2(kq')]^{(2+\lambda_2)}} \quad (3.24)$$

$$= \frac{m^2}{Q^4 \bar{y}} \left(-\frac{1}{\varepsilon} + \ln m^2/\mu^2 - \frac{1}{\lambda_2 - \lambda_1} + \ln Q^2/\nu^2 + \dots \right), \quad (3.25)$$

$$J_{2\bar{n}}^{\text{reg}} = \frac{1}{Q^2 \bar{y}} \int dk \frac{\nu^{2(\lambda_1+\lambda_2)} m^2}{[k^2 - m^2] [2(kp')]^{2+\lambda_1} [(k+q')^2]^{1+\lambda_2}} \\ = \frac{m^2}{Q^4 \bar{y}} \left(-\frac{1}{\varepsilon} + \ln m^2/\mu^2 + \frac{1}{\lambda_2 - \lambda_1} + \ln \nu^2/m^2 + \dots \right), \quad (3.26)$$

$$J_s^{\text{reg}} = \frac{1}{\bar{y}} \int dk \frac{\nu^{2(\lambda_1+\lambda_2)} m^2 (-k^2)}{[k^2 - m^2] [2(kp')]^{2+\lambda_1} [2(kq')]^{2+\lambda_2}} = 0, \quad (3.27)$$

where dots denote simple non-logarithmic terms as before. The soft integral in this regularization prescription remains scaleless and therefore vanishes. However additional poles $\sim 1/(\lambda_2 - \lambda_1)$ appears in the collinear integrals. These poles and scale ν cancel in the sum leaving the large rapidity logarithm $\ln Q^2/m^2$

$$J_{2n}^{\text{reg}} + J_{2\bar{n}}^{\text{reg}} = \frac{m^2}{Q^4 \bar{y}} \left(-\frac{2}{\varepsilon} + 2 \ln m^2/\mu^2 + \ln Q^2/m^2 + \dots \right). \quad (3.28)$$

The total expression for the sum of the collinear and soft integral reads

$$J_{\bar{n}}^{\text{reg}} + J_n^{\text{reg}} + J_s^{\text{reg}} = \frac{1}{Q^2} \left\{ -\text{Li}_2[y] + \frac{\pi^2}{6} \right\} + \frac{m^2}{Q^4 \bar{y}} \left(-\frac{2}{\varepsilon} + 2 \ln m^2/\mu^2 + \ln Q^2/m^2 + \dots \right). \quad (3.29)$$

Using Eq.(3.6) one can easily observe that the pole $1/\varepsilon$ cancel in the sum of the all integrals (3.22) and the expansion in Eq.(3.3) is reproduced. From the structure of different logarithms in Eq.(3.29) we conclude that the simple large logarithm in Eq.(3.3) is reproduced by the sum of collinear and rapidity logarithms.

3.1 Interpretation of the result in soft collinear effective theory

Let us perform interpretation of the different contributions in terms of operators and matrix elements in the effective theory of soft and collinear particles.

The hard contribution describes the configuration where all particles in the loop integral are hard and therefore the loop diagram in this case can be interpreted as a next-to-leading correction to a hard coefficient H . Contracting the hard subdiagram to a "point" we obtain the light-cone leading-order matrix element constructed from two fields. Therefore we can write

$$J_h \simeq \text{FT} \langle 0 | B_c | \gamma \rangle H_{\text{nlo}} * \text{FT} \langle \bar{q}q | \psi_c^\dagger(\eta_1 \bar{n}) \psi_c(\eta_2 \bar{n}) | 0 \rangle = H_{\text{nlo}} * \phi_{qq}, \quad (3.30)$$

The symbol FT denotes the Fourier transformation with respect to light-cone coordinates η_i . The asterisk denote the convolution integrals with respect to the corresponding collinear fractions. The fields ψ_c and B_c denote the collinear "quark" and "photon" fields in the effective theory.

The n -collinear contribution $k \sim p'$ is given by the sum of two integrals $J_{0n} \sim \lambda^0$ and $J_{2n} \sim \lambda^4$, see Eq.(3.7). In both cases the hard subdiagram is generated by the "quark" propagator $k^2 + 2(kq')$. The "nonperturbative" subdiagram is given by remaining collinear "quark" and "gluon" propagators. The leading order contribution J_{0n} can be identified with the convolution of a hard tree kernel with the one-loop contribution to the leading collinear matrix element

$$J_{0n} = \text{FT} \langle 0 | B_c | \gamma \rangle H_{\text{lo}} * \text{FT} \langle \bar{q}q | \psi_c^\dagger \psi_c | 0 \rangle^{\text{nlo}} = H_{\text{lo}} * \phi_{qq}^{\text{nlo}}. \quad (3.31)$$

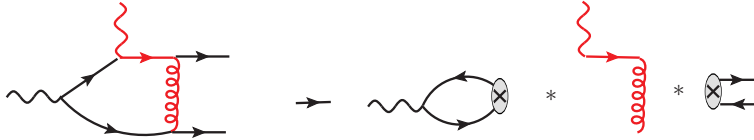


Figure 4. Graphical illustration of the factorization in the \bar{n} -collinear region. The hard lines are shown by red color.

This contribution is finite and do not have any large evolution logarithms because the underlying scalar field theory with is superrenormalizable.

The subleading contribution J_{2n} is given by the next-to-leading term in the expansion of the hard propagator with respect to the small momentum k^2 . Therefore we can also identify it with the convolution of a hard tree kernel with the one-loop correction to a collinear matrix element. But this matrix element must be already associated with the higher twist collinear operator. Corresponding operator is constructed from two “quark” fields and derivatives in order to reproduce the factor $k^2/[2(kq')]^2$ in the expansion (3.7). In position space such subleading operator can be written as

$$\psi_c^\dagger(0) \left\{ \frac{1}{2}(x\bar{n})(n\partial) + \frac{1}{2}x_{\perp i}x_{\perp j}\partial_i\partial_j \right\} \psi_c(x)|_{x=x_+} \equiv \psi_c^\dagger \mathcal{P}(x, \partial)\psi_c. \quad (3.32)$$

Schematically the subleading contribution can be represented as

$$J_{2n} = C_{1o} * \text{FT} \langle \bar{q}q | \psi_c^\dagger \mathcal{P}(x, \partial)\psi_c | 0 \rangle^{\text{nl}} = C_{1o} * \varphi_{qq}^{\text{nl}}. \quad (3.33)$$

The UV-divergence appearing in this contribution (the pole $1/\varepsilon$ in Eq.(3.9)) can be associated with the renormalization of the subleading light-cone operator. The IR-singularity in the integral in Eq.(3.9) can be interpreted as the endpoint divergency in the collinear convolution integral in Eq(3.33) denoted by asterisk.

The \bar{n} -collinear contribution $k \sim q'$ defines the configuration which only appears starting from one-loop. We identify this contribution only with the integral $J_{2\bar{n}}$ in Eq.(3.13). In this configuration the hard part is described by tree subdiagram with one the “gluon” exchange as illustrated in Fig.4. Shrinking the hard subdiagram one obtains the four-fermion collinear operator $\left[\psi_c^\dagger \psi_c \right]_{\bar{n}} \left[\psi_c^\dagger \psi_c \right]_n$. The \bar{n} -collinear quarks describe the loop integral which can be associated with the matrix element of the operator $\left[\psi_c^\dagger \psi_c \right]_{\bar{n}}$ between the real “photon” and vacuum state. This matrix element can be interpreted as the light-cone distribution amplitude of the “photon”. Therefore this collinear contribution can be schematically described as

$$J_{2\bar{n}} = \text{FT} \langle \bar{q}q | \psi_c^\dagger \psi_c | 0 \rangle * T * \text{FT} \langle 0 | \psi_c^\dagger \psi_c | \gamma \rangle = \phi_{qq}^{\text{lo}} * T * \phi_\gamma, \quad (3.34)$$

where T denotes the hard coefficient function. This contribution also has UV-divergency which can be associated with the mixing of the operators $\psi_c^\dagger \psi_c$ and B_c describing the photon matrix element. The IR-singularity in Eq.(3.15) is interpreted as the endpoint divergency in the convolution integral with “photon” distribution amplitude ϕ_γ .

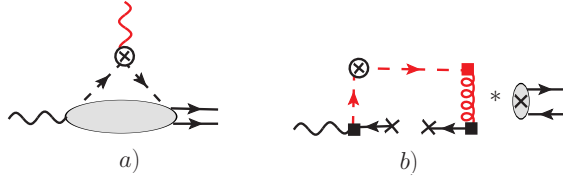


Figure 5. The graphical interpretation of factorization in the soft region. The diagram *a*) illustrates the factorization of the hard mode. The crossed vertex denote the operator $\psi_n^\dagger \psi_{\bar{n}}$, the gray blob corresponds to the matrix element in Eq.(3.35). The diagram *b*) describes the factorization of the hard-collinear particles (red lines). The soft quarks are shown by the solid lines with the crosses. The solid squares denote the effective vertices in the soft-collinear effective theory.

We observe that both collinear contributions have the endpoint divergencies in the collinear convolution integrals. These divergencies indicate an overlap between the collinear and soft domains. Therefore in order to define collinear contributions one has to define a regularization which allows one to the soft regions. This regularization prescription must be used uniformly for collinear and soft contributions in order to avoid a double counting.

The soft contribution described by the integral J_s in Eq.(3.20) does not have any hard propagator $\sim 1/p_h^2$. In this case the hard subgraph can be identified with the tree level vertex describing the scattering of the virtual “photon” with the hard-collinear “quark” : $\gamma^* q_{hc}(q' + k) \rightarrow q_{hc}(p + k)$. Factorizing the hard modes one obtains the matrix element in an effective theory

$$J_s = C_\gamma \langle \bar{q}q | \psi_n^\dagger \psi_{\bar{n}} | \gamma \rangle_{\text{SCET}} \quad (3.35)$$

where fields ψ_n^\dagger and $\psi_{\bar{n}}$ describe the hard-collinear quarks and $C_\gamma = 1$ is the hard kernel.

This matrix element is described by hard-collinear, collinear and soft particles. Only this modes define the soft integral in Eq.(3.20). Therefore this integral can be understood in the framework of the soft collinear effective theory that is indicated by the subscript SCET. The factorization of the hard modes is illustrated by the diagram in Fig.5a. The interactions of hard-collinear fields and soft fields are described by the corresponding SCET Lagrangian which we will not define here. Integrating over the hard-collinear fields we reduce the matrix element (3.35) to the matrix elements of the soft and collinear fields. This is illustrated in Fig.5b and can be described as

$$\begin{aligned} \langle \bar{q}q | \psi_n^\dagger \psi_{\bar{n}} | \gamma \rangle_{\text{SCET}} &\simeq \text{FT} \langle \bar{q}q | \psi_c^\dagger \psi_c | 0 \rangle (y) * J_n(y, Qk_+) * \text{FT} \langle 0 | \psi_s^\dagger \psi_s | 0 \rangle (k_+, k_-) \\ &* J_{\bar{n}}(Qk_-) \text{FT} \langle 0 | B_c | \gamma \rangle = \phi_{qq}^{\text{lo}} * J_n * S * J_{\bar{n}}, \end{aligned} \quad (3.36)$$

where J_n and $J_{\bar{n}}$ correspond to the hard-collinear subdiagrams with the in each collinear sector. The soft matrix element is not local and the asterisks also denote the convolution integral with respect to the soft fractions $k_\pm \sim m$.

Combining together the contributions from all regions one can write the factorization formula for the integral J

$$J = H * \phi_{qq} + [C * \varphi_{qq}]_{\text{reg}} + [\phi_{qq} * T * \phi_\gamma]_{\text{reg}} + C_\gamma [\phi_{qq} * J_n * S * J_{\bar{n}}]_{\text{reg}} + \mathcal{O}(\lambda^6) \quad (3.37)$$

where the brackets $[\dots]_{\text{reg}}$ indicate the additional regularization prescription required for the separation of the collinear and soft modes. This factorization introduces the additional factorization scale dependence which must cancel in sum of the all three contributions. In the calculation carried out above we use the analytical regularization. In this case the soft integral remains scaleless and vanishes. It is important to keep in mind that this does not mean the absence of the soft contribution. In this case the soft contribution is implicitly included into the collinear integrals and therefore into the definitions of the collinear matrix elements. This example illustrates that the definition of the collinear matrix elements is scheme dependent and may differ from one which is usually accepted in the collinear factorization framework (when one does not have any endpoint singularities). If one uses a different regularization scheme then the collinear and soft contributions can be different and therefore the soft contribution must be always added into the factorization formula. A one more approach to define the collinear contributions is to define subtractions which remove the soft configurations from the collinear integrals as suggested in Refs.[38, 39].² In any case a correct description of the endpoint region can not be performed without a consistent definition of the soft contribution.

A specific feature of the discussed integral is the simple logarithmic structure. In a renormalizable field theory, like QCD, one usually obtains a large double logarithm. In such case the auxiliary factorization scale ν can be used for a resummation of large rapidity logarithms, see e.g. Ref.[40] .

One more important observation is related to the interpretation of the spurious power suppressed contributions within the SCET approach. It was demonstrated that in the soft region one of such contribution even predicts power correction of order λ^2 (or correction suppressed as $1/Q$). However corresponding soft integrals are power divergent and must be neglected. In the SCET framework such spurious contributions can be generated by appropriate T -products when matching to SCET-II.

Consider the scalar theory discussed in this section. In this case one can easily find the counting rules for different fields: $\phi_{hc} \sim \lambda$, $\phi_c \sim \lambda^2$, $\phi_s \sim \lambda^2$. Appropriate SCET Lagrangian can be also easily derived and we skip these details here. Then the soft integral J_{1s} is obtained from T -product

$$J_{1s} = \langle \bar{q}q | \mathcal{O} | \gamma \rangle_{\text{SCET}} = \langle \bar{q}q | T \left\{ \mathcal{O}, \mathcal{L}_{\text{int}}^{(2,\bar{n})}, \mathcal{L}_{\text{int}}^{(2,n)}, \mathcal{L}_{\text{int}}^{(1,n)} \right\} | \gamma \rangle \sim \lambda^2, \quad (3.38)$$

with the SCET operator

$$\mathcal{O} = \psi_{hc,n}^\dagger(0) \psi_{hc,\bar{n}}(0) \sim \mathcal{O}(\lambda^2), \quad (3.39)$$

and the interaction vertices

$$\mathcal{L}_{\text{int}}^{(2,\bar{n})} = \int d^4x \psi_{hc,\bar{n}}^\dagger(x) B_{c,\bar{n}}(x) \psi_s(x) \sim \mathcal{O}(\lambda^2), \quad (3.40)$$

$$\mathcal{L}_{\text{int}}^{(2,n)} = m \int d^4x \psi_s^\dagger(x) A_{hc,n}(x) \psi_{c,n}(x) \sim \mathcal{O}(\lambda^2), \quad (3.41)$$

$$\mathcal{L}_{\text{int}}^{(1,n)} = m \int d^4x \psi_{c,n}^\dagger(x) A_{hc,n}(x) \psi_{hc,n}(x) \sim \mathcal{O}(\lambda). \quad (3.42)$$

² In SCET this method is known as zero-bin subtractions.

where we assume $m \sim \lambda^2$ and multipole expansion of the arguments for the soft fields.³ This shows that certain T -products which appear within the SCET framework describe the power divergent integrals which was suggested to set to zero identically. Therefore such constructions in the effective theory are fictitious and one has to study various contractions of the hard-collinear fields more carefully in order to make a conclusion about their relevance.

In absence of external soft momenta (as in our example) one can obtain a good criteria using transformation properties of soft convolution integrals under longitudinal boosts

$$n \rightarrow \alpha n, \quad \bar{n} \rightarrow \alpha^{-1} \bar{n}. \quad (3.43)$$

If the soft integral is not invariant under (3.43) then it is power divergent and corresponding T -product can be neglected. For instance, for the soft convolution integral J_{1s} in Eq.(3.17) one obtains

$$I_s = \int \frac{d(\bar{n} \cdot k)}{(\bar{n} \cdot k)} \int \frac{d(n \cdot k)}{(n \cdot k)^2} \frac{dk_{\perp}}{[(n \cdot k)(\bar{n} \cdot k) - k_{\perp}^2 - m^2]} \rightarrow \alpha^{-1} I_s. \quad (3.44)$$

Then the answer for this integral must transform in the same way that leads to the power divergent expression in Eq. (3.19).

In case of QCD the analogous contributions are described by the similar integrals but with a soft function instead of the soft “quark” propagator (see more details in Sec. 4.3.2)

$$I_s \sim \int \frac{dk_+}{k_+^2} \int \frac{dk_-}{k_-} S(k_+ k_-), \quad (3.45)$$

The soft function $S(k_+ k_-)$ is invariant under longitudinal boosts and therefore depend on the product of the light-cone fractions. The power divergency can be easily seen performing rescaling of the one light-cone variable. For instance, using $k'_- = k_+ k_-$ one finds

$$I_s \sim \int \frac{dk_+}{k_+^2} \int \frac{dk'_-}{k'_-} S(k'_-). \quad (3.46)$$

Therefore this property can not be related with the nonperturbative sector. We assume that such integrals are similar to the “traditional” scaleless integrals like $\int d^D k/k^{2n}$. In what follow we assume that such contributions are fictitious and we will also set them to zero.

The relevant soft contribution (3.20) is described by the higher order T -product obtained by expansion of the argument of the soft field in the interaction vertex in Eq.(3.40):

$$\mathcal{L}_{\text{int}}^{(\bar{n})} = \int d^4 x \psi_{hc, \bar{n}}^\dagger(x) B_{c, \bar{n}}(x) \left\{ \frac{1}{2} (x \bar{n}) (n \partial) + \frac{1}{2} x_{\perp i} x_{\perp j} \partial_i \partial_j \right\} \psi_s(x). \quad (3.47)$$

Therefore we find that certain T -products which describe transition from SCET-I to SCET-II are scaleless and power divergent. The given consideration of the toy integral provides us an evidence that such contribution can be safely excluded from a consideration. This conclusion will be very important for an analysis of soft-overlap configurations which we consider in the next section.

³Remind that any external collinear state scales as $|p_c\rangle \sim \lambda^{-2}$.

4 Factorization of the subleading amplitudes in SCET

4.1 Soft Collinear Effective Theory approach: general remarks

In what follow we assume that it is enough to consider particles which have hard p_h , hard-collinear p_{hc} , collinear p_c and soft p_s momenta. The light-cone components $(pn, p\bar{n}, p_\perp) \equiv (p_+, p_-, p_\perp)$ of the corresponding momenta scale as

$$p_h \sim Q(1, 1, 1), \quad p_h^2 \sim Q^2, \quad (4.1)$$

$$p_{hc} \sim Q(1, \lambda^2, \lambda) \quad \text{or} \quad p'_{hc} \sim Q(\lambda^2, 1, \lambda), \quad p_{hc}^2 \sim Q^2 \lambda^2 \sim Q\Lambda, \quad (4.2)$$

$$p_c \sim Q(1, \lambda^4, \lambda^2) \quad \text{or} \quad p'_c \sim Q(\lambda^4, 1, \lambda^2), \quad p_c^2 \sim Q^2 \lambda^4 \sim \Lambda^2, \quad (4.3)$$

$$p_s \sim Q(\lambda^2, \lambda^2, \lambda^2), \quad p_s^2 \sim Q^2 \lambda^4 \sim \Lambda^2. \quad (4.4)$$

Here Q and Λ denote generic large and soft scales, respectively. Further we will again use the small dimensionless parameter $\lambda \sim \sqrt{\Lambda/Q}$. We assume that we do not need other specific modes in order to describe factorization of the power suppressed amplitudes. Then we expect that factorization approach consist of the following two steps. First, we integrate out the hard modes and reduce full QCD to the effective theory. Corresponding effective Lagrangian is constructed from the hard-collinear and soft particles. This effective theory is denoted as SCET-I. If the hard scale Q^2 is so large that the hard collinear scale $\mu_{hc} \sim \sqrt{Q\Lambda}$ is a good parameter for the perturbative expansion then one can perform the second step and integrate out the hard-collinear modes. This reduces SCET-I to the effective theory describing only collinear and soft particles and known as SCET-II.

The different formulation of the SCET can be found in Refs.[19–24]. In our work we use the technique developed in the position space in Refs.[23, 24]. For the SCET fields we use following notations. The fields ξ_n^C , $A_{\mu C}^n$ and $\xi_{\bar{n}}^C$, $A_{\mu C}^{\bar{n}}$ denote the hard-collinear ($C = hc$) or collinear ($C = c$) quark and gluon fields associated with momentum p' and p , respectively, see Eq.(2.6). As usually, the hard-collinear and collinear quark fields satisfy to

$$\not{n}\xi_n^C = 0, \quad \not{\bar{n}}\xi_{\bar{n}}^C = 0. \quad (4.5)$$

The fields q and A_μ^s describe soft quarks and gluons with the soft momenta (4.4). We will use the standard set of convenient notation for the gauge invariant combinations

$$\chi_n^C(\lambda\bar{n}) \equiv W_n^\dagger(\lambda\bar{n})\xi_n^C(\lambda\bar{n}), \quad \bar{\chi}_n^C(\lambda\bar{n}) \equiv \bar{\xi}_n^C(\lambda\bar{n})W_n(\lambda\bar{n}), \quad (4.6)$$

$$\mathcal{A}_{\mu C}^n(\lambda\bar{n}) \equiv \left[W_n^\dagger(\lambda\bar{n})D_{\mu C}W_n(\lambda\bar{n}) \right], \quad (4.7)$$

where the covariant derivative $D_{\mu C} = i\partial_\mu + gA_{\mu C}^n$ acts inside the brackets and the hard-collinear or collinear gluon Wilson line (WL) read:

$$W_n(z) = \text{P exp} \left\{ ig \int_{-\infty}^0 ds \bar{n} \cdot A_C^n(z + s\bar{n}) \right\}. \quad (4.8)$$

In the wide-angle kinematics we have the energetic particles propagating with large energies in four directions. Therefore it is useful to introduce two more auxiliary light-cone vectors associated with the photon momenta: q_1 and q_2

$$\bar{v}^\mu = \frac{2q_1^\mu}{\sqrt{s}}, \quad v^\mu = \frac{2q_2^\mu}{\sqrt{s}}, \quad (\bar{v} \cdot v) = 2. \quad (4.9)$$

Using the vectors \bar{v}, v we also introduce the hard-collinear quark and gluon fields in the similar way as before just changing $(n, \bar{n}) \rightarrow (v, \bar{v})$.

The explicit expression for the SCET-I Lagrangian in position space can be found in Refs.[23, 24]. This Lagrangian being expanded in the small parameter λ is given by the sum

$$\mathcal{L}_{\text{SCET}}^{(n)} = \mathcal{L}_{\xi\xi}^{(0,n)} + \mathcal{L}_{\xi\xi}^{(1,n)} + \mathcal{L}_{q\xi}^{(1,n)} + \mathcal{O}(\lambda^2), \quad (4.10)$$

where $\mathcal{L}_{\xi\xi}^{(\lambda,n)} \sim \mathcal{O}(\lambda)$ and the explicit expressions read

$$\mathcal{L}_{\xi\xi}^{(0,n)} = \bar{\xi}_n^{hc}(x) (i n \cdot D + g n \cdot A^s(x_-) + i \not{D}_\perp (i \bar{n} \cdot D)^{-1} i \not{D}_\perp) \xi_n^{hc}(x), \quad (4.11)$$

$$\mathcal{L}_{q\xi}^{(1,n)} = \bar{\xi}_n^{hc}(x) i \not{D}_\perp W_n q(x_-) + \bar{q}(x_-) W_n^\dagger i \not{D}_\perp \xi_n^{hc}(x). \quad (4.12)$$

where $D_\mu = i\partial_\mu + g A_\mu^n$, $x_- = \frac{1}{2}(x\bar{n})n$, A_μ^s denotes the soft gluon field. The expression for the subleading term $\mathcal{L}_{\xi\xi}^{(1,n)}$ is a bit lengthy and we will not write it here. The similar expressions are also valid for the other collinear sectors associate with the directions \bar{n}, v, \bar{v} .

The matching from SCET-I to SCET-II is performed by substituting in SCET-I Lagrangian

$$\xi^{hc} \rightarrow \xi^c + \xi^{hc}, \quad A_{hc} \rightarrow A_c + A_{hc} \quad (4.13)$$

and integrating over the hard-collinear fields. A more detailed description of this step can be found in Refs.[41, 42] in the hybrid representation and in Ref.[43] in the position space formulation.

The power counting rules for different SCET operators can be fixed using the power counting of the SCET fields. The counting rules for the SCET fields can be obtained from the corresponding propagators in momentum space and read (see for instance Ref.[23])

$$\xi_n^{hc} \sim \lambda, \quad \bar{n} \cdot A_{hc}^n \sim 1, \quad A_{\perp hc}^n \sim \lambda, \quad n \cdot A_{hc}^n \sim \lambda^2, \quad (4.14)$$

$$\xi_n^c \sim \lambda^2, \quad \bar{n} \cdot A_c^n \sim 1, \quad A_{\perp c}^n \sim \lambda^2, \quad n \cdot A_c^n \sim \lambda^4, \quad (4.15)$$

$$A_\mu^s \sim \lambda^2, \quad q \sim \lambda^3. \quad (4.16)$$

In order to determine the counting rules for physical amplitudes one also needs to define the counting for external hadronic states. In c.m.s frame the outgoing pions are made of energetic collinear partons therefore assuming the conventional normalization of hadronic states one obtains

$$\langle \pi(p_c) | \sim \lambda^{-2}. \quad (4.17)$$

4.2 The hard contributions within the SCET framework

The hard contributions are described by convolution of a hard coefficient function with the matrix elements of collinear operators describing the overlap with the outgoing pion states. Only a collinear operator in SCET can be matched onto hadronic states because the invariant mass of a hadron is restricted to order $Q^2\lambda^4 \sim \Lambda^2$.

Consider first the leading power contribution discussed in Sec.2.2. In the operator form the hard contribution can be presented as

$$T \{J_{\text{em}}^\mu(0), J_{\text{em}}^\nu(x)\}_{\text{hard}} = H^{\mu\nu} * O_n^{(4)} O_{\bar{n}}^{(4)} + \mathcal{O}(\lambda^9), \quad (4.18)$$

where asterisk denotes the convolution integrals in position space. The leading twist-2 operator $O_n^{(4)}$ in SCET notation can be written as

$$O_n^{(4)} = \bar{\chi}_n^c \not{n} \gamma_5 \chi_n^c \sim \mathcal{O}(\lambda^4). \quad (4.19)$$

The arguments of the fields are on the light-cone and not shown for simplicity. All collinear operators $O_{n,\bar{n}}^{(4)}$ are color singlet and have appropriate flavor structure.

In order to compute the amplitude one has to take the matrix element from Eq.(4.18). The soft and collinear modes are decoupled in leading SCET-II Lagrangian [41, 43] and therefore the matrix element of the collinear operators can be factorized

$$\langle p, p' | O_n^{(4)} O_{\bar{n}}^{(4)} | 0 \rangle_{\text{SCETII}} = \langle p | O_n^{(4)} | 0 \rangle_{\text{SCETII}} \langle p' | O_{\bar{n}}^{(4)} | 0 \rangle_{\text{SCETII}}. \quad (4.20)$$

It is easy to see that collinear operator $O_n^{(\lambda)}$ has the minimal possible order $\lambda = 4$, i.e.

$$\langle \pi(p) | O_n^{(\lambda)} | 0 \rangle_{\text{SCETII}} = 0, \quad \lambda < 4. \quad (4.21)$$

Therefore we obtain the first operator with the nonvanishing matrix element only at order λ^8 . Substituting in Eq.(4.20) the parametrization of matrix elements (2.23) and performing the Fourier transformation of the hard kernel H we obtain the factorization formulas discussed in Sec.2.2. The scaling behavior of the amplitudes can be easily obtained using the SCET counting rules that gives

$$A_{+\pm}^{(i)} \sim \underbrace{\langle p' | O_n^{(4)} | 0 \rangle_{\text{SCETII}}}_{\lambda^2} * H^{\mu\nu} * \underbrace{\langle p | O_{\bar{n}}^{(4)} | 0 \rangle_{\text{SCETII}}}_{\lambda^2} \sim \lambda^4 \sim \Lambda^2/Q^2. \quad (4.22)$$

In order to prove the leading power factorization formula within the SCET framework one must demonstrate the absence of an appropriate soft-overlap configuration of the same order $\sim \lambda^8$. We will do this later performing an analysis of the soft contributions.

The hard power corrections to the leading-order result (4.18) are defined by subleading collinear operators. The set of the required operators $O_n^{(i)} \sim \mathcal{O}(\lambda^i)$ can be described by the two operator subsets order λ^6 (twist-3) and λ^8 (twist-4). Using the SCET notations these operators can be introduced as following.

The twist-3 operators

$$O_n^{(6)} = \left\{ \bar{\eta}_n^\alpha \not{n}_\perp \gamma^\beta \gamma_5 \chi_n^c, \bar{\chi}_n^c \not{n}_\perp \gamma^\beta \gamma_5 \eta_n^\alpha, \bar{\chi}_n^c \not{n}_\perp \mathbf{A}_\perp^n \gamma_5 \chi_n^c \right\}, \quad (4.23)$$

where we use the following notation

$$\eta_n^\alpha(x) = (i\bar{n} \cdot \partial)^{-1} W_n^\dagger(x) iD_{\perp c}^\alpha \xi_n^c(x) \sim \mathcal{O}(\lambda^4), \quad (4.24)$$

$$\bar{\eta}_n^\alpha(x) = \bar{\xi}_n^c(x) i\overleftarrow{D}_{\perp c}^\alpha W_n(x) (i\bar{n} \cdot \overleftarrow{\partial})^{-1} \sim \mathcal{O}(\lambda^4). \quad (4.25)$$

The set of the appropriate twist-4 operators can be schematically introduced as

$$\begin{aligned} O_n^{(8)} = & \left\{ \bar{\eta}_n^\alpha \not{n} \gamma_{\perp\beta} \gamma_5 \mathcal{A}_\perp^n \chi_n^c, \bar{\chi}_n^c \not{n} \gamma_{\perp\beta} \gamma_5 \mathcal{A}_\perp^n \eta_n^\alpha, \bar{\eta}_n^\alpha \not{n} \gamma_{\perp\beta} \tilde{\mathcal{A}}_\perp^n \chi_n^c, \right. \\ & \bar{\chi}_n^c \not{n} \gamma_{\perp\beta} \tilde{\mathcal{A}}_\perp^n \eta_n^\alpha, \bar{\chi}_n^c \not{n} \gamma_5 (\bar{n} \cdot \mathcal{A}^n) \chi_n^c, \bar{\chi}_n^c \not{n} (\bar{n} \cdot \tilde{\mathcal{A}}^n) \chi_n^c, \\ & \left. \bar{\chi}_n^c \not{n} \gamma_5 \mathcal{A}_{\mu\perp}^n \mathcal{A}_{\nu\perp}^n \chi_n^c, \bar{\chi}_n^c \not{n} \tilde{\mathcal{A}}_{\mu\perp}^n \mathcal{A}_{\nu\perp}^n \chi_n^c, \bar{\chi}_n^c \Gamma_1 \chi_n^c, \bar{\chi}_n^c \Gamma_2 \chi_n^c \right\}, \end{aligned} \quad (4.26)$$

where $\tilde{\mathcal{A}}_{\mu\perp}^{(8)} = \frac{1}{2} i \varepsilon_{\mu\alpha n \bar{n}} \mathcal{A}_\perp^\alpha$, the symbols Γ_i in the four-quark operator denote the appropriate Dirac matrices.

In Appendix A we also provide the QCD definitions well-known in the literature. The QCD operators can be represented within the SCET framework as the operators listed in Eqs.(4.23),(4.26). More details about this correspondence can be also found in Ref.[44]. Obviously, the analogous set of the operators can also be defined in the \bar{n} -collinear sector. Matrix elements of the operators in Eqs.(4.23), (4.26) define the higher twist distribution amplitudes of pion.

Notice that all twist-3 operators are chiral odd. The first two operators in set $O_n^{(6)}$ in Eq.(4.23) are the two-particle operators. They play an important role in phenomenology because their matrix elements include the so-called chirally enhanced DAs [50]. The DAs of these operators can be represented as a sum of the three-particle DA defined by the three-particle operator $\bar{\chi}_n^c(z_1) \not{n} \mathcal{A}_\perp^n(z_2) \gamma_5 \chi_n^c(z_3)$ and two-particle contribution which is proportional to the large numerical factor $m_\pi^2/(m_u + m_d)$, see the details in Appendix A.

The set of the twist-4 operators $O_n^{(8)}$ consists of three-particle (first and second lines) and four-particle operators. The QCD definitions of the three-particle DAs can also be found in Appendix A. ⁴

Including all possible subleading contributions we obtain

$$\begin{aligned} T \{ J_{\text{em}}^\mu(0), J_{\text{em}}^\nu(x) \}_{\text{hard}} = & H^{\mu\nu} * O_n^{(4)} O_{\bar{n}}^{(4)} + \sum T_6^{\mu\nu} * O_n^{(6)} O_{\bar{n}}^{(6)} \\ & + \sum T_8^{\mu\nu} * \{ O_n^{(4)} O_{\bar{n}}^{(8)} + O_n^{(8)} O_{\bar{n}}^{(4)} \} + \mathcal{O}(\lambda^{13}), \end{aligned} \quad (4.27)$$

where the sum over all operators which enter in the sets $O_n^{(6,8)}$ is implied, the kernels $T_i^{\mu\nu}$ denote the hard coefficient function. In Eq.(4.27) we excluded the contributions of order λ^{10} provided by the operators like $O_n^{(4)} O_{\bar{n}}^{(6)}$. Such combinations can be neglected because corresponding coefficient functions vanish in the massless QCD ($O_n^{(4)}$ and $O_{\bar{n}}^{(6)}$ have different Dirac structure). It is easy to see that subleading contributions in Eq.(4.27) are given by the operators of order λ^{12} .

The full description of the subleading contribution in Eq.(4.27) is very complicated because of large number of the various subleading operators. Let us at first step, in order to

⁴There are also two-particle twist-4 DAs which can be expressed through the twist-2 and twist-4 DAs. For simplicity we do not introduce them here.

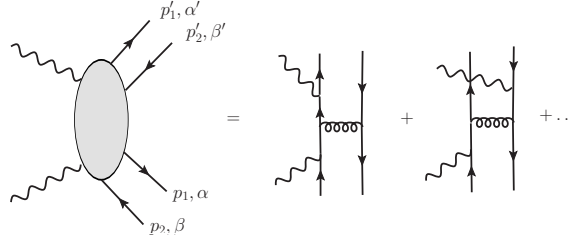


Figure 6. Graphical representation of the function $D_{ab}^{\mu\nu}(p_i, p'_i)$ defined in Eq.(4.29).

simplify the calculations, to restrict the following consideration only by the specific chiral enhanced contribution. Such approximation might also be justified phenomenologically due to relatively large normalization coefficients of the corresponding DAs. The consideration of other contributions we postpone for future work. Therefore in what follow we assume that

$$T \{J_{\text{em}}^\mu(0), J_{\text{em}}^\nu(x)\}_{\text{hard}} \simeq H^{\mu\nu} * O_n^{(4)} O_{\bar{n}}^{(4)} + T^{\mu\nu} * O_{\chi n}^{(6)} O_{\chi \bar{n}}^{(6)}. \quad (4.28)$$

where the operator $O_{\chi n}^{(6)}$ denotes the chiral enhanced contributions.

In order to compute the hard kernel $T^{\mu\nu}$ one has to consider the diagrams which are similar to those in Fig.1 but with the appropriate twist-3 projections for pion DAs. We will use a technique suggested in Refs.[49, 53]. In this case a compact expression for the subleading amplitudes $B_{+\pm}^{(i,h)}$ (2.22) can be written as

$$\delta^{ab} B_{+\pm}^{(0,h)}(s, \theta) + \delta^{a3} \delta^{b3} B_{+\pm}^{(3,h)}(s, \theta) = \frac{(f_\pi \mu_\pi)^2}{16} \int_0^1 dx \hat{M}_{\beta'\alpha'}(x, p') \int_0^1 dy \hat{M}_{\beta\alpha}(y, p) \times \left[2M_{1,2}^{\mu\nu} D_{ab}^{\mu\nu}(p_i, p'_i) \right]_{\alpha'\beta;\alpha\beta'}, \quad (4.29)$$

where $D_{ab}^{\mu\nu}(p_i, p'_i)$ denotes the sum of all diagrams describing the hard subprocess $\gamma\gamma \rightarrow (q\bar{q})_n + (q\bar{q})_{\bar{n}}$. The external momenta of the outgoing quarks are shown in Fig.6. The light-cone expansions of quark momenta read

$$p_1 \simeq yp + r_\perp, \quad p_2 \simeq \bar{y}p - r_\perp, \quad (4.30)$$

$$p'_1 \simeq xp' + k_\perp, \quad p'_2 \simeq \bar{x}p' - k_\perp. \quad (4.31)$$

Twist-3 quark projectors \hat{M} in Eq.(4.29) are given by

$$\hat{M}_{\alpha\beta}(y, p) = \phi_p(y) [\gamma_5]_{\beta\alpha} - p_\lambda [\sigma^{\lambda\rho} \gamma_5]_{\beta\alpha} \frac{i}{6} \left[\frac{n^\rho}{(p \cdot n)} \phi'_\sigma(y) - \phi_\sigma(y) \frac{\partial}{\partial r_\perp^\rho} \right], \quad (4.32)$$

$$\hat{M}_{\beta'\alpha'}(x, p') = \phi_{p'}(x) [\gamma_5]_{\beta'\alpha'} - p'_\lambda [\sigma^{\lambda\rho} \gamma_5]_{\beta'\alpha'} \frac{i}{6} \left[\frac{\bar{n}^\rho}{(p' \cdot \bar{n})} \phi'_\sigma(x) - \phi_\sigma(x) \frac{\partial}{\partial k_\perp^\rho} \right]. \quad (4.33)$$

Here for the DAs $\phi_{p,\sigma}$ we use only the chiral enhanced pieces

$$\phi_p(x) = 1, \quad \phi_\sigma(x) = 6x\bar{x}, \quad \phi'_\sigma(x) = 6(1 - 2x). \quad (4.34)$$

The expressions in Eqs.(4.32) and (4.33) include the differentiations with respect to the relative transverse momenta r_\perp and k_\perp . After the differentiation one can put $r_\perp = k_\perp = 0$. In order to compute the traces in expression Eq.(4.29) we used package *FeynCalc* [54]. We obtained the following results

$$B_{++}^{(0,h)}(s, \theta) \simeq B_{++}^{(3,h)}(s, \theta) \simeq 0 + \mathcal{O}(\alpha_s^2), \quad (4.35)$$

$$B_{+-}^{(0,h)}(s, \theta) = \frac{\alpha_s C_F (4\pi f_\pi)^2 \mu_\pi^2}{4\pi N_c s} \left\{ (e_u^2 + e_d^2) \frac{(3 - \eta^2)}{(1 - \eta^2)} I_s + \frac{2e_u e_d}{(1 - \eta^2)} I(\eta) \right\}, \quad (4.36)$$

$$B_{+-}^{(3,h)}(s, \theta) = \frac{\alpha_s C_F (4\pi f_\pi)^2 \mu_\pi^2}{4\pi N_c s} \frac{(e_u - e_d)^2}{(1 - \eta^2)} I(\eta), \quad (4.37)$$

where $\eta = \cos \theta$. We also introduced special notations for the two types of the collinear convolution integrals. The singular integrals are given by

$$I_s = \int_0^1 dy \int_0^1 dx \left(\frac{1}{y\bar{x}} + \frac{1}{x\bar{y}} \right). \quad (4.38)$$

The finite collinear integrals can be computed that yields

$$I(\eta) = 8 - 4\eta \ln \left[\frac{1 + \eta}{1 - \eta} \right] + 2(3 - \eta^2) \left\{ \text{Li} \left[\frac{1 + \eta}{2} \right] + \text{Li} \left[\frac{1 - \eta}{2} \right] - \frac{2\pi^2}{3} - \ln^2 \frac{1 + \eta}{1 - \eta} + \frac{1}{2} \left(\ln^2 \frac{1 + \eta}{2} + \ln^2 \frac{1 - \eta}{2} \right) \right\}, \quad (4.39)$$

where $\text{Li}[z]$ denotes the Spence function defined by

$$\text{Li}(z) = - \int_0^z dt \frac{\ln(1 - t)}{t}. \quad (4.40)$$

The simple description of the singular and regular integrals is possible due to the different isotopic factor in front of the appropriate diagrams. The regular integral $I(\eta)$ is only provided by the diagrams where photons couple to the different quark lines (like the second diagram in Fig.1). Therefore these diagrams are not singular and corresponding convolution integrals can be computed explicitly. At large values of scattering angle $\eta \sim 0$ (remind that $\eta = \cos \theta$ hence $\theta \sim 90^\circ$) we obtain

$$I(\eta \rightarrow 0) = 8 - 3\pi^2 + \eta^2(\pi^2 - 20) + \mathcal{O}(\eta^4). \quad (4.41)$$

From obtained results we also conclude that there are no chiral enhanced corrections to the amplitudes $B_{++}^{(i,h)}$ at leading order in α_s . These amplitudes obtain corrections from the twist-3 three-particle DA which are not considered in this paper.

The end-point singularities accumulated in the integral I_s originate in the diagrams where both photons couple to the same quark line. The integral I_s in Eq.(4.37) is real and has the logarithmic endpoint divergencies. For simplicity we do not introduce any explicit regularization for I_s . The nice feature is that at leading-order in α_s the divergent integrals does not depend on the scattering angle θ . As we have seen in Sec. 3 the endpoint singularities indicate that there is an overlap between the soft and collinear regions and in order to develop a consistent description of the power corrections it is necessary to include the appropriate soft-overlap contributions which will be considered in the next section.

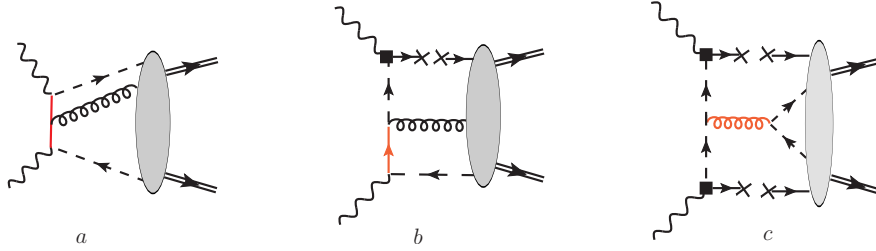


Figure 7. The diagrams illustrating the different groups of the SCET operators in Eq.(4.43). The solid red lines show the hard subdiagrams, the dashed fermion and solid gluon lines denote the hard-collinear particles. The solid lines with the crosses show the soft particles. The black squares denote vertices in the effective theory.

4.3 The soft-overlap contribution within the SCET framework

We suppose that the complete factorization is described by the sum of the hard (4.27) and soft contributions

$$T \{J_{\text{em}}^\mu(0), J_{\text{em}}^\nu(x)\} = T \{J_{\text{em}}^\mu(0), J_{\text{em}}^\nu(x)\}_{\text{hard}} + T \{J_{\text{em}}^\mu(0), J_{\text{em}}^\nu(x)\}_{\text{soft}}, \quad (4.42)$$

The soft-overlap contributions depends on the three scales: hard $\mu_h \sim Q^2$, hard-collinear $\mu_{hc} \sim \sqrt{\Lambda Q}$, and soft $\mu_s \sim \Lambda$. The factorization in this case is performed by integration over hard and hard-collinear modes. Performing the factorization of the hard modes we reduce T -product of the electromagnetic currents to a set of SCET-I operators $O^{(k)} \sim \lambda^k$ constructed from the hard-collinear fields

$$T \{J_{\text{em}}^\mu(0), J_{\text{em}}^\nu(x)\}_{\text{soft}} = \sum_i C_i^{\mu\nu} * O_i^{(k)}. \quad (4.43)$$

We divide these operators on the three groups according to their possible structure. The simplest group is described by the operators consist of hard-collinear fields from the n - and \bar{n} -collinear sectors. Such configuration can be illustrated by diagram in Fig.7 (a). Shrinking the hard lines (hard subgraph) to a “point” we obtain the two-jet operator $\sim \bar{\chi}_n^{hc} \mathcal{A}_{\perp hc}^n \chi_{\bar{n}}^{hc}$. Here we show the hard-collinear gluon just for illustration, a more detailed analysis is given below. Corresponding contributions can be interpreted as a soft overlap between the outgoing pions.

The second group can be associated with the operators which appear if one of the electromagnetic currents on lhs of Eq.(4.43) is matched onto subleading SCET operator with soft quark field(s)

$$J_{\text{em}} \simeq \bar{q} \gamma_\perp \chi_v^{hc} + \mathcal{O}(\lambda^5). \quad (4.44)$$

This possibility is illustrated in Fig.7 (b). Shrinking the hard subgraph we obtain the three-jet hard-collinear operator $\sim \bar{\chi}_v^{hc} \gamma \mathcal{A}_{\perp hc}^n \chi_{\bar{n}}^{hc}$. These contributions can be interpreted as a soft overlap contributions between photon and outgoing pions. In the toy integral considered in Sec.3 such contribution can be associated with the soft J_s , see interpretation in Fig.5.

The third group SCET operators correspond to the configuration when the both electromagnetic currents on *lhs* of Eq.(4.43) are matched onto SCET subleading operators as in Eq.(4.44). Such possibility is illustrated in Fig.7 (c). Shrinking the hard subgraph we obtain the four-jet hard-collinear operator $\sim \bar{\chi}_v^{hc} \Gamma \chi_{\bar{v}}^{hc} \bar{\chi}_n^{hc} \Gamma \chi_{\bar{n}}^{hc}$. In this case one faces with the soft overlap configuration between the all external states.

The main purpose of the following consideration is to establish the SCET-I operators which can overlap with the hard configurations described in Eq.(4.28). Then we include corresponding soft-overlap contributions into the factorization formula in order to have a consistent description of the subleading corrections. In order to establish the order and structure of the soft-overlap contribution we consider the matching of the SCET-I operator $O^{(k)}$ in Eq.(4.43) onto SCET-II operators with the appropriate structure. Technically this can be done performing the substitution (4.13) constructing appropriate T -products in the intermediate theory with hard-collinear, collinear and soft fields [41–43].

We start our analysis from the two-jet operators of the first group which are built from the hard-collinear fields of n - and \bar{n} sectors. Computation of the relevant T -product gives the following expression

$$T \left\{ O^{(k)}, \mathcal{L}_{\text{int}}^{(l_1, n)}, \mathcal{L}_{\text{int}}^{(m_1, \bar{n})}, \dots \right\} \simeq O_n^{(i)} * J_n * O_S * J_{\bar{n}} * O_{\bar{n}}^{(j)}, \quad (4.45)$$

where the jet-functions J_n and $J_{\bar{n}}$ describe the contractions of the hard-collinear fields. They can be computed from the appropriate SCET diagrams. The operators $O_{n, \bar{n}}^{(j)}$ and O_S are built only the collinear and soft fields, respectively. In what follow we will call the expression on *rhs* of (4.45) by soft-collinear operator. If the soft-collinear operator in Eq.(4.45) has the same order as the collinear operator $O_n^{(i)} O_{\bar{n}}^{(j)} \sim \lambda^{i+j}$ describing the hard contribution then we can conclude that SCET-I operator $O^{(k)}$ is relevant for the description of the soft-collinear overlap and must be included in Eq.(4.43).

Technically it is convenient to compute the hard-collinear contractions in each collinear sector independently considering soft and collinear fields as external fields. Taking into account that the SCET operator $O^{(k)}$ from the first group can be presented as a simple product of two hard-collinear operators

$$O^{(k)} = O^{(k_1, n)} O^{(k_2, \bar{n})}, \quad (4.46)$$

Therefore we can write

$$T \left\{ O^{(k)}, \mathcal{L}_{\text{int}}^{(l_1, n)}, \mathcal{L}_{\text{int}}^{(m_1, \bar{n})}, \dots \right\} \simeq T \left\{ O^{(k_1, n)}, \mathcal{L}_{\text{int}}^{(l_1, n)}, \dots \right\} T \left\{ O^{(k_2, \bar{n})}, \mathcal{L}_{\text{int}}^{(m_1, \bar{n})}, \dots \right\}. \quad (4.47)$$

Computation of the T -products in each hard-collinear sector yields

$$T \left\{ O^{(k_1, n)}, \mathcal{L}_{\text{int}}^{(l_1, n)}, \dots \right\} \simeq O_n^{(i)} * J_n * S, \quad (4.48)$$

$$T \left\{ O^{(k_2, \bar{n})}, \mathcal{L}_{\text{int}}^{(m_1, \bar{n})}, \dots \right\} \simeq \bar{S} * J_{\bar{n}} * O_{\bar{n}}^{(j)}. \quad (4.49)$$

where symbols S and \bar{S} denote the soft operators. Combining (4.48) and (4.49) we obtain the expression in Eq.(4.45) with the soft operator

$$O_S = S \bar{S}. \quad (4.50)$$

Combining T -products (4.48) and (4.49) we have impose certain constraints on the operators $O^{(k)}$. We will exclude the operators with the odd number of the transverse indices like

$$O_{\perp}^{(k)}[\text{odd}] = \{ \bar{\chi}_n^{hc} \gamma_{\perp}^{\mu} \chi_n^{hc}, \bar{\chi}_n^{hc} \mathcal{A}_{\perp hc}^n \mathcal{A}_{\perp \mu hc}^n \chi_n^{hc}, \dots \} \quad (4.51)$$

The matrix elements of such operators vanish due to the Lorentz invariance

$$\langle p, p' | O_{\perp}^{(k)}[\text{odd}] | 0 \rangle_{\text{SCET}} = 0. \quad (4.52)$$

The chiral-odd operators $O^{(k)}$ like $\bar{\chi}_n^{hc} \chi_n^{hc}$, $\bar{\chi}_n^{hc} \gamma_5 \chi_n^{hc}$ and so on can also be neglected because the corresponding coefficient functions vanish in massless quark limit.

Using that collinear and soft fields are factorized in SCET-II Lagrangian one finds

$$\langle p, p' | O_n^{(i)} * J_n * O_S * J_{\bar{n}} * O_{\bar{n}}^{(j)} | 0 \rangle \simeq \langle p' | O_n^{(i)} | 0 \rangle * J_n * \langle 0 | O_S | 0 \rangle * J_{\bar{n}} * \langle p | O_{\bar{n}}^{(j)} | 0 \rangle. \quad (4.53)$$

This implies that the soft operator O_S must have nonvanishing matrix element in Eq.(4.53).

In what follows our task is to find all operators Eq.(4.45) which provide the overlap with the configurations describing the hard contribution in Eq.(4.28).

4.3.1 The soft-overlap contribution with operator $O_n^{(4)} O_{\bar{n}}^{(4)}$

We start our analysis from the soft-overlap configuration which is described by the collinear operator $O_n^{(4)} O_{\bar{n}}^{(4)}$. In order to obtain the full soft-collinear operator we consider first the T -products in the one collinear sector

$$T \left\{ O^{(k_1, n)}, \mathcal{L}_{\text{int}}^{(l_1, n)}, \dots \right\} \simeq O_n^{(4)} * J_n * S. \quad (4.54)$$

The simplest possible set of the operators of order λ can be described as

$$O^{(1, n)} = \{ \bar{\chi}_n, \chi_n, \mathcal{A}_{\perp}^n \}, \quad (4.55)$$

Here and further we do not write explicitly the label hc for the hard-collinear fields assuming $\xi^{hc} \equiv \xi$. The first and second operators describes the hard-collinear quark and antiquark, respectively. The analysis of the quark and antiquark configurations are very similar and we consider only the quark operator. The gluon operator can appear only in the next-to-leading in α_s hard coefficient function and therefore is subleading.

It is not possible to built any T -product (4.54) which yields the required soft-collinear operator of order λ^4 or smaller. Consider first the case of the quark operator $\bar{\chi}_n$. In order to obtain the two collinear quark fields for $O_n^{(4)}$ one needs at least two insertions of the vertices $\mathcal{L}_{\text{int}}^{(1, n)}$ which include collinear fields $\bar{\xi}_n^c$ and ξ_n^c . Such vertices can be obtained from the leading-order Lagrangian $\mathcal{L}^{(0, n)}$ with the help of the substitution (4.13). In this configuration only soft quark can appear as a soft field. Hence in order to have soft quark field in rhs (4.54) one needs at least one more insertion $\mathcal{L}_{\text{int}}^{(1, n)}$ with the soft quark. Therefore one obtains T -products of order λ^4 . Using the SCET Lagrangian we found the following three possibilities

$$T \left\{ \bar{\chi}_n, \mathcal{L}_{\text{int}}^{(1, n)}[\bar{\xi}^c A_{\perp} A_{\perp} \xi], \mathcal{L}_{\text{int}}^{(1, n)}[\bar{\xi} A_{\perp} A_{\perp} \xi^c], \mathcal{L}_{\text{int}}^{(1, n)}[\bar{q} A_{\perp} \xi] \right\} \simeq O_n^{(4)} * J_n * \bar{q}, \quad (4.56)$$

$$T \left\{ \bar{\chi}_n, \mathcal{L}_{\text{int}}^{(1, n)}[\bar{\xi}^c A_{\perp} A_{\perp} \xi], \mathcal{L}_{\text{int}}^{(2, n)}[\bar{q} A_{\perp} \xi^c] \right\} \simeq O_n^{(4)} * J_n * \bar{q}, \quad (4.57)$$

$$T \left\{ \bar{\chi}_n, \mathcal{L}_{\text{int}}^{(1, n)}[\bar{\xi}^c A_{\perp} A_{\perp} \xi], \mathcal{L}_{\text{int}}^{(2, n)}[\bar{\xi} A_{\perp} A_{\perp}^s \xi^c] \right\} \simeq O_n^{(4)} * J_n * A_{\perp}^s, \quad (4.58)$$

where in the square brackets $\mathcal{L}_{\text{int}}^{(1,n)}[\dots]$ we show the field structure of the interaction terms. The explicit expressions for these SCET interactions can be found in Appendix B. Remind that field q denotes the soft quark.

However all these T -products include the odd number of the transverse hard-collinear gluon fields A_{\perp} . In order to contract them one can insert one more three gluon vertex $\mathcal{L}_{\text{int}}^{(0,n)}[\partial_{\perp} A_{\perp} A_{\perp} A_{\perp}]$. However due to the transverse derivative the obtained loop integrals vanish because we do not have external hard-collinear transverse momenta. Hence using the quark (antiquark) operator $\bar{\chi}_n$ one can not obtain the soft-collinear operator (4.54) of order λ^4 .

Consider now the gluon operator in Eq.(4.55). In this case the required T -product can be described as

$$T \left\{ \mathcal{A}_{\perp}^n, \mathcal{L}_{\text{int}}^{(3,n)} [\bar{\xi}_n^c A_{\perp}^n A_{\perp}^s \xi_n^c] \right\} \simeq O_n^{(4)} * J_n * A_{\perp}^s \sim \lambda^4. \quad (4.59)$$

However in such contribution the collinear operator has isospin zero while we need the operator with isospin one. Therefore T -product in Eq.(4.59) can be neglected. In this case we did not find any other possibility to obtain the soft-collinear operator of order λ^4 with the required structure.

Therefore we demonstrated the absence of the soft-collinear operator which can overlap with the leading-order collinear operator $O_{\bar{n}}^{(4)} O_n^{(4)}$. Therefore the leading order formula (4.18) is valid to all orders in α_s .

The hard corrections described in Eq.(4.18) are suppressed by relative factor λ^4 . Is this estimate also valid for the the soft corrections in Eq.(4.43)? As we agreed before we shall neglect the soft-collinear configurations with $O_{\bar{n}}^{(4)} O_n^{(4)}$ if they are also suppressed by relative factor λ^4 .

In order to estimate corresponding power corrections we need to study the higher order contributions generated by the soft-collinear operators in Eq.(4.54). In particular we are interested in T -products in (4.54) which can provide the soft-collinear operator of order λ^5 . It turns out that such contributions can be easily constructed. The simplest possibility can be described as

$$T \left\{ \bar{\chi}_n, \mathcal{L}_{\text{int}}^{(1,n)} [\bar{\xi}^c A_{\perp} A_{\perp} \xi], \mathcal{L}_{\text{int}}^{(3,n)} [\bar{q} A_{\perp} A_{\perp} \xi^c] \right\} \sim \mathcal{O}(\lambda^5), \quad (4.60)$$

Contractions of the gluon fields in (4.60) yield the diagram with the hard-collinear loop. One more possibility is given by the following T -product

$$T \left\{ \bar{\chi}_n, \mathcal{L}_{\text{int}}^{(2,n)} [\bar{\xi}^c A_{\perp} A_{\perp}^s \xi], \mathcal{L}_{\text{int}}^{(2,n)} [\bar{q} A_{\perp} \xi^c] \right\} \sim \mathcal{O}(\lambda^5), \quad (4.61)$$

where the explicit expressions for the Lagrangians $\mathcal{L}_{\text{int}}^{(2,n)}$ are given in Appendix B. In this case the soft configuration is more complicate and includes also the soft gluon field A_{\perp}^s .

The other configurations of order λ^5 are related with the higher order operators $O^{(2,n)} \sim \lambda^2$

$$O^{(2,n)} = \bar{\chi}_n A_{\perp}^n. \quad (4.62)$$

We postpone the discussion of the Dirac and color structure of the operators $O^{(k,n)}$ until construction of the total soft-overlap contribution (4.53). The appropriate T -product (4.54) which scales as λ^5 are given by

$$T \left\{ \bar{\chi}_n A_\perp^n, \mathcal{L}_{\text{int}}^{(1,n)} [\bar{\xi}^c (n \cdot A) \xi], \mathcal{L}_{\text{int}}^{(2,n)} [\bar{q} A_\perp (\bar{n} \cdot A) \xi^c] \right\} \sim \mathcal{O}(\lambda^5), \quad (4.63)$$

This configuration again describes the digram with hard-collinear loop. The tree level hard-collinear contribution can be obtained using the higher order operator

$$O^{(3,n)} = \bar{\chi}_n^c A_\perp^n. \quad (4.64)$$

This operator already includes one collinear field (it is easy to see that $O^{(3,n)}$ is obtained from $O^{(2,n)}$ using the substitution (4.13)). In this case the required T -product read

$$T \{ \bar{\chi}_n^c A_\perp^n, \mathcal{L}_{\text{int}}^{(2,n)} [\bar{q} A_\perp \xi^c] \} \sim \mathcal{O}(\lambda^5), \quad (4.65)$$

with $\mathcal{L}^{(2,n)}$ shown in Eq.(B.3). The other higher order operators $O^{(k,n)}$ with $k \geq 3$ provide the T -products which have order λ^6 or higher and therefore we will not consider them now. For simplicity we also will not consider the T -products with the gluon operator \mathcal{A}_\perp^n because it suppressed by hard α_s and therefore can be neglected in our calculation.

The relevant T -products for the \bar{n} -collinear sector can be described in the similar way. Therefore we can construct the total soft-collinear operator following to Eq.(4.47). The operators $O^{(k_1,n)}$ and $O^{(k_2,\bar{n})}$ with $k_i \leq 3$ can be combined in the operators $O^{(k)}$ with $k = k_1 + k_2 < 6$. Building the total operator $O^{(k)}$ in Eq.(4.46) we must take into account the restrictions from the Lorentz symmetry already discussed in the previous section. These operators are built from two hard-collinear quark fields and any number of hard-collinear gluon fields. These are chiral-even operators which can only have even transverse Lorentz indices. This allows one to conclude that

$$O^{(k)} = \bar{\chi}_n (n \cdot \mathcal{A}^n)^l \gamma_{\perp \mu_1} \mathcal{A}_{\perp \mu_2}^n \dots \mathcal{A}_{\perp \mu_{2p}}^{\bar{n}} (\bar{n} \cdot \mathcal{A}^{\bar{n}})^m \chi_{\bar{n}}, \quad (4.66)$$

where we assume that all fields in are hard-collinear. Using C -parity we obtain the leading order operator

$$O^{(3)} = \bar{\chi}_n (\mathcal{A}_\perp^n + \mathcal{A}_\perp^{\bar{n}}) \chi_{\bar{n}} + (n \leftrightarrow \bar{n}), \quad (4.67)$$

Combining the T -products of order λ^5 described in Eqs.(4.60),(4.61) and (4.65) we obtain the soft-collinear operators of order λ^{10} which therefore have relative suppression of order λ^2 . All these contributions are described by the operator $O^{(3)}$ or higher order operators obtained from $O^{(3)}$ with the help of substitution (4.13). There are only two T -products which provide the soft-collinear operator of order λ^{10} . Corresponding contributions can be illustrated by diagrams shown in Fig.8. The diagram (a) is described by the combination of T -product as in (4.61) and (4.65)

$$T \left\{ \bar{\chi}_n \mathcal{A}_\perp^{\bar{n}} \chi_{\bar{n}}^c, \mathcal{L}_{\text{int}}^{(2,n)} [\bar{\xi}^c A_\perp A_\perp^s \xi], \mathcal{L}_{\text{int}}^{(2,n)} [\bar{q} A_\perp \xi^c], \mathcal{L}_{\text{int}}^{(2,\bar{n})} [\bar{\xi}^c A_\perp q] \right\}. \quad (4.68)$$

The diagram (b) is provided by the combination of T -products as in (4.60) and (4.65)

$$T \left\{ \bar{\chi}_n \mathcal{A}_\perp^{\bar{n}} \chi_{\bar{n}}^c, \mathcal{L}_{\text{int}}^{(1,n)} [\bar{\xi}^c A_\perp A_\perp \xi], \mathcal{L}_{\text{int}}^{(3,n)} [\bar{q} A_\perp \xi^c], \mathcal{L}_{\text{int}}^{(2,\bar{n})} [\bar{\xi}^c A_\perp q] \right\} \quad (4.69)$$

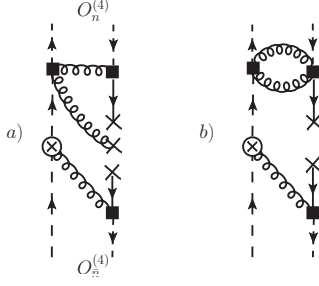


Figure 8. The diagrams of order λ^{10} which are provided by the T -products in Eqs.(4.68) and (4.69), respectively.

This is interesting observation which suggest that there are $1/Q$ corrections associated with the soft contributions. However as we have already seen in Sec.3 such contributions can only provide formal expressions for spurious integrals. Therefore in order to make correct conclusion one has to study the SCET diagrams and show that corresponding soft integrals are not power divergent. For that purpose we need to know their transformation properties under longitudinal boost transformations (3.43).

Consider the diagram in Fig.8 (a). The soft convolution integral reads

$$J_n * S * J_{\bar{n}} \sim \int \frac{dk_2^-}{k_2^-} \int \frac{dk_1^+}{k_1^+} \frac{dk_2^+}{k_2^+} S(k_1^+, k_2^+, k_2^-), \quad (4.70)$$

where the soft correlation function (CF) is defined as⁵

$$S(k_1^+, k_2^+, k_2^-) = \text{FT} \langle 0 | \bar{q}(\lambda_1 n) \mathcal{A}_\perp^s(\lambda_2 n) q(\eta_1 \bar{n}) | 0 \rangle. \quad (4.71)$$

with the Fourier transformation

$$\text{FT} \equiv \int d(x \cdot \bar{n}) e^{ik_1^+(x \cdot \bar{n})} \int d(y \cdot \bar{n}) e^{i(k_1^+ - k_2^+)(y \cdot \bar{n})} \int d(x \cdot n) e^{-ik_2^-(x \cdot n)}. \quad (4.72)$$

From this definition we see that under boost transformations

$$S(k_1^+, k_2^+, k_2^-) \rightarrow \alpha^{-1} S(k_1^+, k_2^+, k_2^-). \quad (4.73)$$

and therefore the soft integral in Eq.(4.70) is not invariant under boosts. Hence this integral is power divergent and therefore vanishes as the spurious contribution. We also checked this conclusion considering the soft limit of the appropriate two-loop QCD diagram. A similar analysis for the diagram in Fig.8 (b) also yields that this diagram is associated with the power divergent soft integral and therefore can be neglected.

4.3.2 The soft-overlap contribution with operators $O_n^{(6)} O_{\bar{n}}^{(i)}$

On order to build the soft-overlap contributions with the twist-3 operators $O_n^{(6)}$ we need to consider T -products with the following structure

$$T \left\{ O^{(k_1, n)}, \mathcal{L}_{\text{int}}^{(l_1, n)}, \dots \right\} \simeq O_n^{(6)} * J_n * S. \quad (4.74)$$

⁵ Here and further in the text we do not show the soft Wilson lines for simplicity.

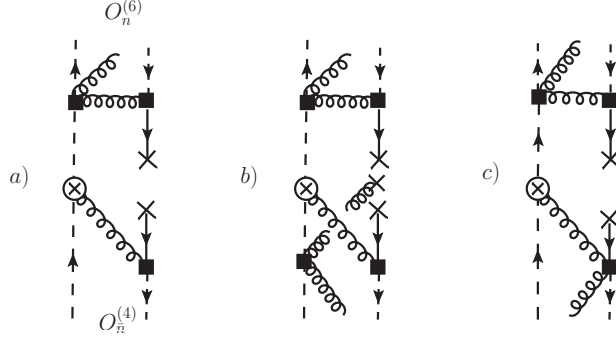


Figure 9. The diagrams describing the T -products with the collinear operators of $O_n^{(6)}O_{\bar{n}}^{(i)}$.

We found that there is only one such T -product of order λ^5 . It can be obtained with the operator $O^{(1,n)} = \bar{\chi}_n$ and reads

$$T \left\{ \bar{\chi}_n, \mathcal{L}_{\text{int}}^{(2,n)} [\bar{\xi}^c A_{\perp}^c A_{\perp} \xi], \mathcal{L}_{\text{int}}^{(2,n)} [\bar{q} A_{\perp} \xi^c] \right\} \sim \mathcal{O}(\lambda^5), \quad (4.75)$$

where the vertices $\mathcal{L}^{(2,n)}$ are described in Eqs.(B.4) and (B.3).

The other T -products (4.74) scale as λ^7 . However combining the contributions of order λ^7 and λ^5 we obtain the soft-collinear operators of order λ^{12} which are suppressed exactly as the hard subleading contribution with $O_n^{(6)}O_{\bar{n}}^{(6)}$. Hence the T -products of order λ^7 must be also considered.

Using various operator $O^{(k,n)}$ we find the following expressions of order λ^7

$$T \left\{ \bar{\chi}_n, \mathcal{L}_{\text{int}}^{(2,n)} [\bar{\xi}^c A_{\perp}^c A_{\perp} \xi], \mathcal{L}_{\text{int}}^{(4,n)} [\bar{q} A_{\perp}^s A_{\perp} \xi^c] \right\}, \quad (4.76)$$

$$T \left\{ \bar{\chi}_n \mathcal{A}_{\perp}, \mathcal{L}_{\text{int}}^{(2,n)} [\bar{q} A_{\perp} \xi^c], \mathcal{L}_{\text{int}}^{(3,n)} [\bar{\xi}^c A_{\perp}^c A_{\perp}^s \xi] \right\}, \quad (4.77)$$

$$T \left\{ \bar{\chi}_n^c \mathcal{A}_{\perp}, \mathcal{L}_{\text{int}}^{(4,n)} [\bar{\xi}^c A_{\perp}^c A_{\perp} q] \right\}, \quad (4.78)$$

$$T \left\{ \bar{\chi}_n^c \mathcal{A}_{\perp}^c, \mathcal{L}_{\text{int}}^{(2,n)} [\bar{q} A_{\perp} \xi_n^c] \right\}. \quad (4.79)$$

One can obtain the soft-collinear operators of order λ^{10} combining the T -products (4.54) and (4.74). Corresponding soft-collinear operators can not overlap with the hard configurations because the collinear operators $O_n^{(4)}$ and $O_{\bar{n}}^{(6)}$ have different chiral structure. Hence these contributions can appear only due to the soft-overlap mechanism. There is only one possibility to obtain the such contribution at order λ^{10} using the combination of T -products in Eq.(4.65) and Eq.(4.75)

$$T \left\{ \bar{\chi}_n \mathcal{A}_{\perp}^{\bar{n}} \chi_{\bar{n}}^c, \mathcal{L}_{\text{int}}^{(2,\bar{n})} [\bar{\xi}^c A_{\perp} q], \mathcal{L}_{\text{int}}^{(2,n)} [\bar{\xi}^c A_{\perp}^c A_{\perp} \xi], \mathcal{L}_{\text{int}}^{(2,n)} [\bar{q} A_{\perp} \xi^c] \right\} \sim \mathcal{O}(\lambda^{10}). \quad (4.80)$$

This configuration can be described by the diagram in Fig.9(a). The operator $O^{(k)} = \bar{\chi}_n \mathcal{A}_{\perp}^{\bar{n}} \chi_{\bar{n}}^c$ is associated with the SCET-I operator $O^{(3)}$ in Eq.(4.67). We again obtain a

correction which is suppressed by factor λ^2 comparing to the leading-order contribution. The soft convolution integral reads

$$J_n * S * J_{\bar{n}} \sim \int \frac{dk_+}{k_+^2} \int \frac{dk_-}{k_-} S(k_+, k_-), \quad (4.81)$$

where the soft CF $S(k_+, k_-)$ is defined as

$$S(k_+, k_-) = \int d(\bar{n} \cdot x) e^{ik_+(\bar{n} \cdot x)} \int d(n \cdot y) e^{-ik_-(n \cdot y)} \langle 0 | \bar{q}(\lambda n) q(\eta \bar{n}) | 0 \rangle. \quad (4.82)$$

The soft operator in Eq.(4.82) is chiral-odd and color singlet. One can easily see that corresponding soft CF is boost invariant and therefore can be written as $S(k_+, k_-) = S(k_+ k_-)$. Hence the corresponding soft integral in Eq.(4.81) is not invariant under boosts. One can easily see that this integral is quite similar to the soft integral J_{1s} in Eq.(3.17). Hence the T -product in Eq.(4.80) describes the spurious integral and can be neglected. One can expect that the soft contributions with the collinear operator $O_n^{(6)} O_{\bar{n}}^{(4)}$ can be obtained from at higher orders $\sim \lambda^{12}$. However we neglect such contributions and therefore we do not consider such operators.

The most important soft-overlap contributions of order λ^{12} are described by the soft-collinear operators with $O_n^{(6)} O_{\bar{n}}^{(6)}$ collinear operator. Corresponding contributions can be constructed from the T -products of λ^5 in (4.75) and λ^7 described in Eqs.(4.77) and (4.78)

$$T \left\{ \bar{\chi}_n \mathcal{A}_\perp^{\bar{n}} \chi_{\bar{n}}, \mathcal{L}_{\text{int}}^{(2, \bar{n})} [\bar{\xi}^c A_\perp q], \mathcal{L}_{\text{int}}^{(3, \bar{n})} [\bar{\xi} A_\perp^c A_\perp^s \xi^c], \right. \\ \left. \mathcal{L}_{\text{int}}^{(2, n)} [\bar{\xi}^c A_\perp^c A_\perp \xi], \mathcal{L}_{\text{int}}^{(2, n)} [\bar{q} A_\perp \xi^c] \right\} \sim \mathcal{O}(\lambda^{12}), \quad (4.83)$$

$$T \left\{ \bar{\chi}_n \mathcal{A}_\perp^{\bar{n}} \chi_{\bar{n}}^c, \mathcal{L}_{\text{int}}^{(4, \bar{n})} [\bar{\xi}^c A_\perp^c A_\perp q], \mathcal{L}_{\text{int}}^{(2, n)} [\bar{\xi}^c A_\perp^c A_\perp \xi], \mathcal{L}_{\text{int}}^{(2, n)} [\bar{q} A_\perp \xi^c] \right\} \sim \mathcal{O}(\lambda^{12}). \quad (4.84)$$

Appropriate diagrams are shown in Fig.9 (b) and (c), respectively. Both diagrams describe the suitable soft convolution integrals which have only the logarithmic singularities.

We can not find other contributions with the more complicate operators $O^{(k)}$ which can provide the soft-overlap operator as in Eq.(4.66) at order λ^{12} . Let us also observe that all operators $O^{(k)}$ in Eqs.(4.83) and (4.84) are related to the leading SCET-I operator $O^{(3)}$ in Eq.(4.67). Therefore corresponding soft-overlap contribution is described by the matrix element of the SCET operator $O^{(3)}$ in Eq.(4.67). This matrix element also describes the soft-collinear operators associated with other possible collinear configurations like $O_n^{(4)} O_{\bar{n}}^{(4)}$, $O_n^{(4)} O_{\bar{n}}^{(6)}$, $O_n^{(8)} O_{\bar{n}}^{(4)}$ which we do not consider in this paper for simplicity.

4.3.3 The soft-overlap contributions with photon states

Some examples of the soft-overlap contributions with photons have been provided earlier, see Fig.7. The specific feature of these configurations is that they are described by the SCET-I operators associated with more than two light-like directions (three and four-jet operators). As a result the analysis of such contributions is more complicate than the corresponding analysis of the two-jet operators carried in the previous sections.

In general, real photon has the nonperturbative component of the wave function and therefore one can define the matrix element which defines the photon DA. The leading twist DA is defined by the chiral-odd operator Ref.[45]

$$O_v^{(4)} = \bar{\chi}_v^c \not{v} \gamma_T \chi_v^c \quad (4.85)$$

where, remind, the auxiliary light-like vectors are v and \bar{v} are defined in Eq.(4.9). The γ_T denotes the suitable transverse projection.⁶ The hard subleading contribution with the nonperturbative photon can be associated with the following collinear operator

$$O_v^{(4)} O_{\bar{n}}^{(6)} O_n^{(4)} \sim \lambda^{14}, \quad (4.86)$$

and the similar operators obtained by appropriate permutation of the collinear indices v, \bar{v} and n, \bar{n} . In order to obtain the nontrivial matrix element we need at least two operators with the chiral-even Dirac structure and therefore we need the subleading operator $O_{\bar{n}}^{(6)}$ in Eq.(4.86). As a result this contribution suppressed as $\mathcal{O}(\lambda^{14})$ and therefore can be neglected. If we use the twist-3 chiral-odd operator for description of the photon DA

$$O_v^{(6)} = \bar{\chi}_v^c \not{v} \mathcal{A}_{\perp\alpha}^v \chi_v^c \sim \lambda^6. \quad (4.87)$$

we also obtain the contribution of order λ^{14} . Therefore the contribution of order λ^{12} can only be obtained from the soft-overlap contributions as suggested in Fig.7 (b, c).

Appropriate SCET operators include the hard-collinear fields associated with the photon and pion momenta. The lowest order operators read

$$O_\gamma^{(3)} = \{ \bar{\chi}_n \gamma_\alpha \mathcal{A}_{\beta\perp}^{\bar{n}} \chi_v, \bar{\chi}_n \gamma_\alpha \mathcal{A}_{\beta\perp}^{\bar{n}} \chi_{\bar{v}}, \{n \leftrightarrow \bar{n}\}, \dots \}, \quad (4.88)$$

$$O_{\gamma\gamma}^{(4)} = \{ \bar{\chi}_v \Gamma \chi_{\bar{v}}, \bar{\chi}_n \Gamma \chi_{\bar{n}}, \dots \}. \quad (4.89)$$

where dots denote the other suitable combinations with similar field structure, the matrix Γ denotes appropriate Dirac and color structures. From Fig.7 (b, c) one can observe that only the operators $O_\gamma^{(3)}$ have hard coefficient functions at leading order in α_s .

Suppose that we consider a configuration where one of the photons interacts with the soft quark, like in Fig.7 (b). Assume that the coupling of the collinear photon to the hard-collinear and soft quarks can be described by the leading order SCET Lagrangian

$$\mathcal{L}_{\text{int}}^{(2,v)}[\bar{\xi} B_c q] = ee_q \int d^4x \bar{\chi}_v \not{B}_c^{(v)} q, \quad (4.90)$$

where $B_{\mu c}^{(v)}$ describes the collinear photon field. Inserting such contribution to the SCET matrix element we obtain

$$\begin{aligned} & \langle p, p' | T \{ O_\gamma^{(3)}, \dots, \mathcal{L}_{\text{int}}^{(l_i, n)}, \mathcal{L}_{\text{int}}^{(2,v)}[\bar{\xi} B_c q] \} | q_2 \rangle \\ & \simeq ee_q \varepsilon_\nu(q_2) \int d^4x e^{-i(q_2 x)} \langle p', p | T \{ O_\gamma^{(3)}, \dots, \mathcal{L}_{\text{int}}^{(l_i, n)}, \bar{\chi}_v \gamma_T^\nu q \} | 0 \rangle, \end{aligned} \quad (4.91)$$

⁶This definition implies a choice v and \bar{v} as the basic light-like vectors.

where dots denote the other SCET interactions. The external collinear photon state yields the factor λ^{-2} . Then inserting interaction (4.90) which is of order λ^2 we compensate this factor. Hence in order to estimate the relative order of the such contribution one needs to estimate of the remaining set of the T -product in Eq.(4.91)

$$\dim \left\{ O_\gamma^{(k)}, \dots, \mathcal{L}_{\text{int}}^{(l_i, n)} \right\} \sim \lambda^{3+\dots+l_i}. \quad (4.92)$$

This allows one to compare this configuration with the two-jet contributions discussed in the previous sections.

Each operator $O_\gamma^{(3)}$ from the set in Eq.(4.88) consists of the three different hard-collinear fields. As a result the SCET matrix element $\langle p, p' | O_\gamma^{(3)} | \gamma \rangle$ defines an amplitude depending on the energy s and scattering angle θ . As a result in this case the hard factorization does not allow one to get any restrictions on the structure of the amplitude.

The further analysis is the same as before: we need to find suitable T -products (4.45) giving the required soft-collinear operators of order λ^{12} or smaller. In order to be specific we consider $O_\gamma^{(3)} = \bar{\chi}_n \gamma_\alpha \mathcal{A}_{\beta\perp}^{\bar{n}} \chi_v$. The construction of the soft-collinear operator can be done in the same way as before combining the contributions from each hard-collinear sector. In order to describe the electromagnetic interaction we use the subleading SCET vertex (4.90). This yields

$$T \{ \chi_v, \bar{\chi}_v \gamma^\nu q \} \simeq J_v^\nu * q. \quad (4.93)$$

The appropriate T -products with the hard-collinear operator $O^{1, n} = \bar{\chi}_n$ were already discussed before, see Eqs.(4.60),(4.61) and (4.75). These terms provide the contributions of order λ^5

$$T \{ \bar{\chi}_n, \dots \} \simeq O_n^{(4,6)} * J_n * \bar{q} \sim \lambda^5. \quad (4.94)$$

The only new element now is the T -product with the gluon field which must have the following structure

$$T \{ \mathcal{A}_{\beta\perp}^{\bar{n}} \} \simeq \bar{S} * J_{\bar{n}} * O_{\bar{n}}^{(i)}. \quad (4.95)$$

We find the following lowest order possibilities

$$T \left\{ \mathcal{A}_{\beta\perp}^{\bar{n}}, \mathcal{L}_{\text{int}}^{(2, \bar{n})} [\bar{q} A_\perp \xi^c], \mathcal{L}_{\text{int}}^{(3, \bar{n})} [\bar{\xi}^c A_\perp A_\perp q] \right\} \simeq [\bar{q} q] * J_{\bar{n}} * O_{\bar{n}}^{(4)} \sim \lambda^6, \quad (4.96)$$

$$T \left\{ \mathcal{A}_{\beta\perp}^{\bar{n}}, \mathcal{L}_{\text{int}}^{(1, \bar{n})} [\bar{\xi} A_\perp q], \mathcal{L}_{\text{int}}^{(2, \bar{n})} [\bar{\xi}^c A_\perp^c A_\perp \xi], \mathcal{L}_{\text{int}}^{(2, \bar{n})} [\bar{q} A_\perp \xi^c] \right\} \simeq [\bar{q} q] * J_{\bar{n}} * O_{\bar{n}}^{(6)} \sim \lambda^6. \quad (4.97)$$

Combining together the contributions in Eqs.(4.93)-(4.95) we obtain only two possible soft-collinear operators of order λ^{12} as described in Eq.(4.92). These operators contain $O_n^{(4)} O_{\bar{n}}^{(4)}$ and $O_n^{(6)} O_{\bar{n}}^{(6)}$. We now focus on the term with the twist-3 collinear operators $O_{n, \bar{n}}^{(6)}$. Corresponding T -product is combined from Eqs. (4.75) and (4.97) that gives

$$\dim \left\{ O_\gamma^{(3)}, \mathcal{L}_{\text{int}}^{(1, \bar{n})}, \mathcal{L}_{\text{int}}^{(2, \bar{n})}, \mathcal{L}_{\text{int}}^{(2, \bar{n})}, \mathcal{L}_{\text{int}}^{(2, n)}, \mathcal{L}_{\text{int}}^{(2, n)} \right\} \sim \lambda^{12}. \quad (4.98)$$

The full T -product can be illustrated by the diagram in Fig.10 (a). Therefore from this result we conclude that this contribution may also be relevant for description of the endpoint singularities in hard term (4.28).

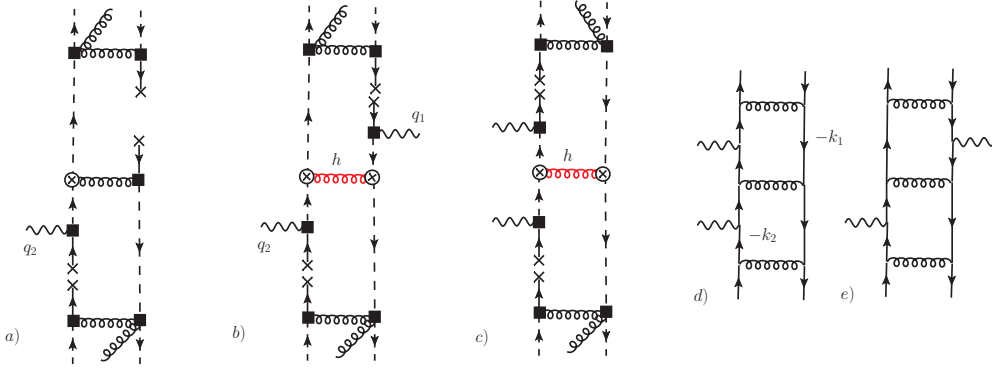


Figure 10. The diagrams illustrating the T -products of the operators $O_\gamma^{(3)}$ and $O_{\gamma\gamma}^{(4)}$. The four-fermion vertices of the operator $O_{\gamma\gamma}^{(4)}$ in diagrams (b) and (c) are shown by two crossed circles connected by red gluon line with index “h”.

The analysis of the operator $O_{\gamma\gamma}^{(4)}$ in Eq.(4.89) is quite similar. Using the same arguments as before one can write

$$\begin{aligned} & \langle p, p' | T \left\{ O_{\gamma\gamma}^{(k)}, \dots, \mathcal{L}_{\text{int}}^{(l_i, n)}, \mathcal{L}_{\text{int}}^{(2, v)}[\bar{\xi} B_c q], \mathcal{L}_{\text{int}}^{(2, \bar{v})}[\bar{\xi} B_c q] \right\} | q_1, q_2 \rangle \\ & \simeq \varepsilon_\mu(q_1) \varepsilon_\nu(q_2) \langle p, p' | O_n^{(i)} * J_n * J_v^\nu * O_S * J_{\bar{v}}^\mu * J_{\bar{n}} * O_{\bar{n}}^{(j)} | 0 \rangle, \end{aligned} \quad (4.99)$$

where jet functions J_i describe the hard-collinear interactions associated with the different light-cone vectors. Then the relative order of the corresponding contribution is defined by the order of the

$$\dim \left\{ O_{\gamma\gamma}^{(4)}, \dots, \mathcal{L}_{\text{int}}^{(l_i, n)} \right\} \sim \lambda^{4+\dots+l_i}. \quad (4.100)$$

The construction of the required T -products follows the same line as before. We use expression (4.75) in order to convert the hard-collinear quark field to the required soft-collinear combination. Combining the known T -products we obtain the contributions of order λ^{12}

$$\dim \left\{ O_{\gamma\gamma}^{(4)}, \mathcal{L}_{\text{int}}^{(2, \bar{n})}, \mathcal{L}_{\text{int}}^{(2, \bar{n})}, \mathcal{L}_{\text{int}}^{(2, n)}, \mathcal{L}_{\text{int}}^{(2, n)} \right\} \sim \lambda^{12}. \quad (4.101)$$

Then the total expression in Eq.(4.99) can be described by diagrams shown in Fig.10 (b, c). These diagrams describe the configurations when colliding photons interact with the same or different quarks. Hence, at least formally, we again obtain the contributions which can overlap with the hard configuration in Eq.(4.28) and therefore can be relevant for description of the endpoint region.

However there are some observations which indicate that these T -product can describe the spurious integrals similar to J_{1s} in the toy model. Indeed, the configurations as in Fig.10 (b) implies that the hard diagram with photons attached to the different spinor lines can also produce the singular endpoint contributions. However from the calculation in Sec.4.2 we obtain the different result: such diagrams provide the regular contributions described by factors $I(\eta)$, see Eq.(4.39). Next, the structure of the hard-collinear diagrams in Fig.10 (a, b, c) is quite similar to diagram in Fig.9 (a) which vanishes. In addition, the angular dependence of the photon soft-overlap contributions is not fixed by the hard

subdiagram. The soft convolution integral also depends on θ and this can potentially provide a more complicate function of θ than one in front of the singular integral I_s in Eq.(4.36). Therefore let us study these diagrams in detail.

The common feature of the photon soft-overlap contributions is related with the four-quark soft CFs. For instance for the diagram in Fig.10 (a) the soft CF is given by the matrix element (remind that we do not show explicitly the soft Wilson lines)

$$\langle 0 | \bar{q}(\lambda_1 n) \Gamma_1 q(\eta_1 \bar{n}) \bar{q}(\eta_2 \bar{n}) \Gamma_2 q(\sigma v) | 0 \rangle, \quad (4.102)$$

where matrices $\Gamma_1 \otimes \Gamma_2$ describe Dirac and color structure. It is clear that this matrix element describes a complicate soft CF. Our consideration can be simplified if we consider the large- N_c limit [46, 47] for the diagrams in Fig.10. In this limit the soft gluon exchanges between the soft quark field in the different loops (or between the different soft quark “propagators”) give always non-planar diagrams which are suppressed by $1/N_c$ comparing to planar diagrams according to large- N_c counting rules [46, 47]. Therefore in the large- N_c picture the soft matrix element in Eq.(4.102) simplifies and can be described as product of the two-quark soft CFs. In case of diagram in Fig.10 (a) this gives

$$\langle 0 | \bar{q}(\lambda_1 n) \Gamma_1 q(\eta_1 \bar{n}) \bar{q}(\eta_2 \bar{n}) \Gamma_2 q(\sigma v) | 0 \rangle \approx \langle 0 | \bar{q}(\lambda_1 n) q(\eta_1 \bar{n}) | 0 \rangle \langle 0 | \bar{q}(\eta_2 \bar{n}) q(\sigma v) | 0 \rangle, \quad (4.103)$$

where each two-quark CF is defined as in Eq.(4.82). In this case the corresponding soft convolution integral reads

$$\begin{aligned} J_n * S * J_{\bar{n}} * J_v &\sim \int_0^\infty \frac{dk_2^-}{[-k_2^-]^2} \int_0^\infty \frac{d(k_2 \cdot v)}{[-(k_2 \cdot v)]} S(k_2^-(k_2 v)) \\ &\times \int_0^\infty \frac{dk_1^+}{[-k_1^+]^2} \int_0^\infty \frac{dk_1^-}{[k_1^- - k_2^-]} S(k_1^+ k_1^-), \end{aligned} \quad (4.104)$$

where momenta k_1 and k_2 can be associated with the momenta of the soft quarks in the loops of diagram in Fig.10 (a). Each soft CF in Eq.(4.104) is invariant under longitudinal boosts and therefore depends only on the products of the appropriate light-cone fractions. Notice that the factorization of the soft CF (4.103) allows one to consider the longitudinal integrals as independent and to compute them using different basis of the light-cone vectors in each loop. In such situation one can consider different types of the longitudinal boosts in each sector. In order to analyze these integrals let us introduce the two auxiliary regulators τ_+ and τ_- which transforms as plus and minus components under longitudinal boosts. Consider now the integrals over k_1^\pm in Eq.(4.104).

$$\int_0^\infty \frac{dk_1^+}{[-k_1^+ - \tau_+]^2} \int_0^\infty \frac{dk_1^-}{k_1^- - k_2^-} S(k_1^+ k_1^-) \quad (4.105)$$

$$= \int_0^\infty dk_1^- S(k_1^-) \int_0^\infty \frac{dk_1^+}{[-k_1^+ - \tau_+]^2} \frac{1}{[k_1^- - k_2^- k_1^+]} \sim a \tau_+^{-1} + b k_2^-, \quad (4.106)$$

where a and b are some constants and $k_i^+ = (n \cdot k_i)$, $k_i^- = (\bar{n} \cdot k_i)$. We observe that the integral is power divergent providing $\sim \tau_+^{-1}$. Computing two remaining integrals in

Eq.(4.104) we obtain

$$\int_0^\infty \frac{dk_2^-}{[k_2^- + \tau_-]^2} \int_0^\infty \frac{d(k_2 \cdot v)}{(k_2 \cdot v)} S(k_2^-(k_2 \cdot v)) [a\tau_+^{-1} + b k_2^-] \quad (4.107)$$

$$= \int_0^\infty \frac{d(k_2 \cdot v)}{(k_2 \cdot v)} S((k_2 \cdot v)) \int_0^\infty dk_2^- \frac{a\tau_+^{-1} + b k_2^-}{[k_2^- + \tau_-]^2} \sim \frac{a}{\tau_+ \tau_-} + \dots \quad (4.108)$$

Hence we obtain that the soft convolution integral obtained from the diagram in Fig.10 (a) is power divergent and therefore vanishes. The similar consideration allows one to obtain the same results for the two diagrams in Fig.10 (b, c). This allows us to conclude that the T -products associated with diagrams in Fig.10 (a, b, c) describe the spurious contributions at leading-order of $1/N_c$ expansion.

Consider now the hard contribution $B_{+-}^{0,h}$ which has integral with the endpoint singularities. At large- N_c limit it can be easily estimated using the Eq.(4.36)

$$B_{+-}^{0,h} \sim f_\pi^2 \mu_\pi^2 \alpha_s C_F / N_c \sim f_\pi^2 \mu_\pi^2 / N_c.$$

The fictitious contributions of diagrams in Fig.10 (a, b, c) at large- N_c limit are of the same order. Hence suppressed by $1/N_c$ configurations which were neglected in Eq.(4.104) are irrelevant for the matching of the endpoint singularities of the amplitude $B_{+-}^{0,h}$ in Eq.(4.36). The subleading in $1/N_c$ configurations might be important for descriptions of the endpoint singularities which only appear at the next-to-leading order in α_s in the hard amplitudes $B_{+\pm}^{i,h}$, i.e. suppressed by $1/N_c$ contributions can be associated with the subleading logarithms. In our analysis we will not consider such contributions. Let us also remind that our conclusion is only valid for the chiral enhanced contributions.

The obtained conclusions can be verified by investigating the appropriate two-loop QCD diagrams shown in Fig.10 (d, e) and using the expansion by momentum regions. Within this technique one can see that the soft regions of these diagrams yield the SCET diagrams in Fig.10 (a, b, c). The two-quark soft CFs in this case are described by integrals from the propagators of the soft quarks with mass m which plays the role of the soft scale.

In order to be concrete let us consider the diagram D_d in Fig.10 (d) in such configuration when the soft limit corresponds to the SCET diagram in Fig.10 (a). Expansion of the corresponding QCD expression in the soft limit $k_{1,2} \sim m$ yields

$$D_d^{s,s} \sim \int dk_2 \frac{m}{[k_2^2 - m^2] [-(v \cdot k_2)] [-k_2^-]^2} \int dk_1 \frac{m}{[k_1^2 - m^2] [-k_1^+]^2 [k_1^- - k_2^-]} \quad (4.109)$$

Notice that contribution of each soft quark propagator is given by chiral-odd term that provides the mass factor m in the numerator. This expression reproduces the structure of the integral in Eq.(4.104). Computing the soft integral (4.109) with the regulators τ_\pm as in Eqs.(4.105) and (4.107) we confirm the qualitative result obtained in Eq.(4.108).

In order to see the overlap of the collinear and soft regions one can also consider the contributions from the collinear regions. The collinear contributions with $k_1 \sim p'$, $k_2 \sim p$ can be interpreted as the convolution of the tree level hard kernel with the one-loop collinear matrix elements for which we assume the appropriate twist-3 projections. Taking the soft

limit for collinear contributions and comparing with the soft contribution in Eq.(4.109) we can see a possible overlap with the soft region. Following this line we find that the soft limit of the collinear contributions does not match exactly the soft expression for these two loop diagrams. The soft limit of the collinear contribution yields

$$D_d^{n/s, \bar{n}/s} \sim \int dk_1 \frac{m}{[k_1^2 - m^2] [-k_1^+]^2 [k_1^-]} \int dk_2 \frac{m}{[k_2^2 - m^2] [-k_2^-]^2 [-(v \cdot k_2)]}, \quad (4.110)$$

We see that the soft integrals in Eq.(4.110) are completely factorized. One immediately see that each soft integral is similar to the spurious integral J_{1s} in Eq.(3.17). Therefore $D_d^{n/s, \bar{n}/s} = 0$ and we do not have an overlap between the collinear and soft regions. In cases when only one of the momenta k_1 or k_2 is taken to be soft one obtains $D_d^{n, \bar{n}/s} = D_d^{n/s, \bar{n}} = 0$ up to power suppressed contributions.

The analogous results are also valid for the second diagram Fig.10 (e) and for the configurations associated with the diagrams in Fig.10 (a, b, c). Therefore we confirm that in the perturbation theory the formal SCET T -products associated with the diagrams in Fig.10 (a, b, c) also describe the inessential power divergent integrals.

One more possibility to obtain the photon soft-overlap contribution is provided by the operators of order λ^8

$$O_\gamma^{(8)} = \bar{\chi}_v \Gamma \chi_n O_{\bar{n}}^{(6)}, \dots, \quad (4.111)$$

where Γ denotes a chiral-odd Dirac matrix $\Gamma = \gamma_5, \sigma\gamma_5$ and dots denote similar operators with the different collinear labels. The appropriate contribution can be obtained combining

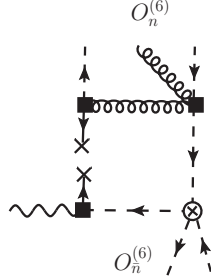


Figure 11. The SCET diagram describing the photon soft-overlap contribution in Eq(4.112). The crossed circle denotes the hard-collinear SCET operator $O_\gamma^{(8)}$.

the T -product of order λ^5 for the hard-collinear field χ_n , see Eq.(4.75), with the photon interaction vertex $\mathcal{L}_{\text{int}}^{(2,v)}$

$$\begin{aligned} \langle p, p' | O_\gamma^{(6)} | q_2 \rangle &= \langle p, p' | O_{\bar{n}}^{(4)} T \left\{ \bar{\chi}_v \gamma_\sigma \chi_n, \mathcal{L}_{\text{int}}^{(2,v)} [\bar{q} B_\perp \xi_v], \dots \right\} | q_2 \rangle \\ &= \langle p' | O_{\bar{n}}^{(6)} | 0 \rangle * J_n * O_S * J_v * \langle p | O_n^{(6)} | 0 \rangle \sim \lambda^8, \end{aligned} \quad (4.112)$$

In Fig.11 we show the SCET diagram generated by the T -product in Eq.(4.112). The SCET vertices $\mathcal{L}_{\text{int}}^{(2,v)}$ and $\mathcal{L}_{\text{int}}^{(2,n)}$ describing the interaction with the soft quark fields restrict the structure of the soft operator in the matrix element. This can be only chiral-odd operator $\sim \langle 0 | \bar{q} q | 0 \rangle$. Then the hard-collinear diagram in Fig.11 has three chiral-odd vertices:

hard-collinear vertex $\bar{\chi}_v \Gamma \chi_n$, collinear operator $O_n^{(6)}$ and the soft operator. As a result this diagram generates a trace with odd number of the γ -matrices and this contribution vanishes.

4.4 Summary of the SCET analysis

Let us briefly summarize the obtained results. We confirm the structure of leading power contribution. It is only described by the hard contribution associated with the leading-twist collinear operator $O_n^{(4)} O_{\bar{n}}^{(4)} \sim \mathcal{O}(\lambda^8)$ defined in Eq.(4.19).

The hard power suppressed contributions are described by suitable collinear operators of order λ^{12} . There are many appropriate collinear operators at this order. In order to simplify our consideration we take into account only the specific chiral enhanced contributions $O_{\chi n}^{(6)} O_{\chi \bar{n}}^{(6)}$ associated with the twist-3 DA of pion, see Eq.(4.23) and discussion in Sec. 4.2. The specific feature of this contribution is that corresponding DA is known exactly in QCD and it is numerically enhanced comparing to other higher-twist corrections. However the corresponding hard coefficient function has the endpoint singularities, see Eq.(4.36), that can be explained by the overlap of collinear and soft regions. We expect that the endpoint singularities must cancel in the sum of hard and a suitable soft-overlap contribution. In SCET-II such soft-overlap contribution is described by a soft-collinear operator of order λ^{12} which is constructed from the same collinear operators $O_{\chi n}^{(6)} O_{\chi \bar{n}}^{(6)}$ and soft fields.

After hard factorization the soft-overlap contribution is described by a set of SCET-I operators. We demonstrated that there is only one SCET-I operator which provides the soft-collinear operator with required properties in SCET-II. Corresponding SCET-I operator $O^{(3)}$ is given in Eq.(4.67) and can be associated with the soft-overlap contribution between the outgoing pions. We also obtain that more complicate soft-overlap configurations with pion and photon states are power suppressed at least to a leading logarithmic accuracy. This is enough in order to obtain a consistent description in our case.

These results allows us to write the following relatively simple formula

$$T \{J^\mu(x), J^\nu(0)\} \simeq H^{\mu\nu} * O_n^{(4)} O_{\bar{n}}^{(4)} + [T^{\mu\nu} * O_{\chi n}^{(6)} O_{\chi \bar{n}}^{(6)}]_{\text{reg}} + C_3^{\mu\nu} * [O^{(3)}]_{\text{reg}}, \quad (4.113)$$

where brackets $[\dots]_{\text{reg}}$ symbolically denote a specific regularization and subtractions scheme which allow one to separate the collinear and soft modes. More detailed discussion of this point will be presented below. Let us note that the hard convolution integral in the third term on *rhs* of Eq.(4.113) is well defined and the corresponding convolution integral does not depend on the specific regularization and therefore the coefficient function $C_3^{\mu\nu}$ is shown outside brackets $[\dots]_{\text{reg}}$.

5 Calculation of the amplitude in the physical subtraction scheme

In this section we compute the hard coefficient function $C_3^{\mu\nu}$ which appears in the soft-overlap contribution in Eq.(4.113). Using this result we define the physical subtraction scheme which allows one to separate unambiguously the regularized contributions

in Eq.(4.113) and to define the hard subleading in λ contribution without the endpoint singularities. Within this framework we obtain the well defined expressions for the physical amplitudes which can be used for a phenomenological analysis.

5.1 The leading-order hard coefficient functions of the soft contribution

Let us clarify the arguments of fields in the required SCET operator $O^{(3)}$ (4.67). We assume that the fields are multipole expanded in the position space. We define this operator as

$$O^{(3)}(\lambda) = \bar{\chi}_n(0) \left(\mathcal{A}_\perp^{(n)}(\lambda\bar{n}) + \mathcal{A}_\perp^{(\bar{n})}(\lambda n) \right) \chi_{\bar{n}}(0), \quad (5.1)$$

where hard-collinear fields $\bar{\chi}_n$ and \mathcal{A}_\perp are defined in Eqs.(4.6) and (4.7). This operator depends on the relative light-cone distance λ between the hard-collinear quark and gluon. Performing the Fourier transformation with respect to λ one introduces the conjugate variable τ which can be interpreted as a fraction of the total hard-collinear momentum carried by gluon. It is convenient to introduce the following momentum space representation

$$\mathcal{A}_\mu^{(n)}(\tau) = \int \frac{d\lambda}{2\pi} P'_+ e^{-i\lambda P'_+ \tau} \mathcal{A}_\mu^{(n)}(\lambda\bar{n}), \quad (5.2)$$

where P' denote the momentum operator in the n -collinear sector. The similar expression holds also for the $\mathcal{A}_\mu^{(\bar{n})}$. Using this compact notation one can define the matrix element directly in the momentum space. Hence we define the SCET-I operator as

$$O^{(3)}(\tau) = \bar{\chi}_n(0) \left(\mathcal{A}_\perp^{(n)}(\tau) + \mathcal{A}_\perp^{(\bar{n})}(\tau) \right) \chi_{\bar{n}}(0). \quad (5.3)$$

The parametrization of the corresponding SCET-I matrix element can be defined as

$$\left\langle \pi^a(p), \pi^b(p') \left| O^{(3)}(\tau) \right| 0 \right\rangle_{\text{SCET-I}} = \delta^{ab} (4\pi f_\pi)^2 f_{\pi\pi}(\tau, s), \quad (5.4)$$

where, just for convenience, we used the dimensional factor $(4\pi f_\pi)^2$, in this section we also do not write explicitly the regularization symbol $[\dots]_{\text{reg}}$ as in Eq.(4.113). The dimensionless SCET amplitude $f_{\pi\pi}(\tau, s)$ depends from the collinear fraction τ and the total energy s and from the factorization scale which is not shown for simplicity.⁷ The evolution of the operators like $O^3(\tau)$ has been studied in Refs.[51, 52].

In Eq.(5.4) we assume that the operator $O^3(\tau)$ is the singlet in the flavor space

$$O_B(\tau) \sim \bar{u}u + \bar{d}d. \quad (5.5)$$

The operator with isospin $I = 1$ cannot contribute in this case because of C -parity. This allows one to conclude that such soft contribution is relevant only for the isoscalar amplitudes $B_{+\pm}^{(0)}$. Therefore the factorization of the soft contributions can be written as

$$B_{+\pm}^{(0,s)}(s, \theta) = (4\pi f_\pi)^2 \int_0^1 d\tau C_{+\pm}^{(0)}(s, \theta, \tau) f_{\pi\pi}(\tau, s), \quad (5.6)$$

⁷Let us emphasize in order to avoid misunderstanding that here we assume the factorization scale associated with the factorization of hard modes while the additional regularization denoted as $[\dots]_{\text{reg}}$ is introduced for a separation of the collinear and soft modes.

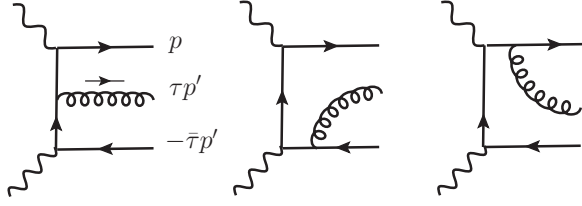


Figure 12. The set of diagrams required for the matching of T-product of the electromagnetic currents onto SCET-I operator $O^{(3)}(\tau)$. We only show the diagrams for the case $\bar{\chi}_n \mathcal{A}_\perp^{(\bar{n})} \chi_{\bar{n}}$. The crossed diagrams are not shown for simplicity. The diagrams describing the other configurations are similar, we also used $\bar{\tau} \equiv 1 - \tau$.

$$B_{+\pm}^{(3,s)}(s, \theta) = \mathcal{O}(\alpha_s). \quad (5.7)$$

We see that the angular dependence of the soft amplitudes is defined by the hard subprocess and therefore can be computed in perturbation theory.

In order to obtain tree level expressions for the coefficient functions $C_{+\pm}^{(0)}$ one has to compute the diagrams shown in Fig.12. The computation is quite standard therefore let us provide the resulting expressions for the soft amplitudes

$$B_{++}^{(0,s)}(s, \theta) = -(e_u^2 + e_d^2) \frac{(4\pi f_\pi)^2}{s} \frac{4}{1 - \eta^2} \int_0^1 d\tau \frac{\tau}{1 - \tau} f_{\pi\pi}(\tau, s), \quad (5.8)$$

$$B_{+-}^{(0,s)}(s, \theta) = -2(e_u^2 + e_d^2) \frac{(4\pi f_\pi)^2}{s} \frac{3 - \eta^2}{1 - \eta^2} \int_0^1 d\tau f_{\pi\pi}(\tau, s), \quad (5.9)$$

where we again used notation $\eta = \cos \theta$. The both helicity amplitudes $B_{+\pm}^{(0,s)}$ are defined by the same SCET amplitude $f_{\pi\pi}$ but through the different convolution integrals with respect to τ . We also observe that the angular behavior (associated with the variable η) in Eqs.(5.8) and (5.9) is different. For definiteness let us assume that the renormalization scale in the amplitude $f_{\pi\pi}$ is fixed to be large $\mu_F \simeq s$.

The obtained expressions in Eqs.(5.8) and (5.9) demonstrate the one important property: the angular behavior of the soft amplitudes is defined by the simple factors $1/(1 - \eta^2)$ and $(3 - \eta^2)/(1 - \eta^2)$ which are factorized from the convolution integrals over τ . This allows one to define the following two SCET amplitudes as

$$\Phi_{++}(s) = \int_0^1 d\tau \frac{\tau}{1 - \tau} f_{\pi\pi}(\tau, s), \quad \Phi_{+-}(s) = \int_0^1 d\tau f_{\pi\pi}(\tau, s). \quad (5.10)$$

The factorization of the angular dependence from the convolution integrals in Eqs.(5.8) and (5.9) provides a very important check of the suggested formalism. In this case the endpoint singularities in the soft term (remind that they are regularized by the special regularization denoted by $[\dots]_{\text{reg}}$) and provided by the amplitudes $\Phi_{+\pm}(s)$ which does not depend on the scattering angle θ . On the other hand the compensation of the endpoint divergencies between the hard and soft contributions in Eq.(4.113) requires a strong correlation of the angular dependence in these contributions. This correlation can be used in order to define a specific subtraction procedure of the endpoint singularities from the hard subleading term

$[T^{\mu\nu} * O_{\chi^n}^{(6)} O_{\chi\bar{n}}^{(6)}]_{\text{reg}}$ in Eq.(4.113) and therefore to obtain well defined expressions for the physical amplitudes.

5.2 Subleading amplitude in the physical subtraction scheme

Combining the results for the hard subleading amplitudes (4.35)-(4.37) and for the soft contributions (5.8)-(5.10) we obtain the following expressions

$$B_{+-}^{(0)}(s, \theta) \simeq -2(e_u^2 + e_d^2) \frac{(4\pi f_\pi)^2}{s} \frac{3 - \eta^2}{1 - \eta^2} [\Phi_{+-}(s)]_{\text{reg}} + \frac{\alpha_s C_F}{4\pi N_c} \frac{(4\pi f_\pi)^2}{s} \frac{\mu_\pi^2}{s} \left[\left\{ (e_u^2 + e_d^2) \frac{(3 - \eta^2)}{(1 - \eta^2)} I_s + \frac{2e_u e_d}{(1 - \eta^2)} I(\eta) \right\} \right]_{\text{reg}} \quad (5.11)$$

$$B_{++}^{(0)}(s, \theta) \simeq -(e_u^2 + e_d^2) \frac{(4\pi f_\pi)^2}{s} \frac{4}{1 - \eta^2} [\Phi_{++}(s)]_{\text{reg}} + [\langle p, p' | O_n O_{\bar{n}} * T_{++} | 0 \rangle]_{\text{reg}}(\theta, s), \quad (5.12)$$

$$B_{++}^{(3)}(s, \theta) \simeq 0, \quad (5.13)$$

$$B_{+-}^{(3)}(s, \theta) \simeq B_{+-}^{(3,h)}(s, \eta) = \frac{\alpha_s C_F}{4\pi N_c} \frac{(4\pi f_\pi)^2}{s} \frac{\mu_\pi^2}{s} \frac{(e_u - e_d)^2}{(1 - \eta^2)} I(\eta). \quad (5.14)$$

The expression for the amplitude $B_{+-}^{(0)}$ in Eq.(5.11) includes the divergent integral I_s in the hard contribution and therefore we use the specific regularization indicated by square brackets. The same situation must take place in the expression in Eq.(5.12). However in this case the endpoint singularities are related to a hard configuration which is not described by the chiral enhanced contributions and therefore have not been computed in our consideration. In order to emphasize this point we denoted in Eq.(5.12) the hard contributions as the matrix element $[\langle p, p' | O_n O_{\bar{n}} * T_{++} | 0 \rangle]_{\text{reg}}$. The amplitudes $B_{\pm\pm}^{(3)}$ do not obtain any soft-overlap contributions and therefore we do not need any special regularization in this case.

In order to proceed further we must define explicitly the regularization and subtraction scheme indicated as $[\dots]_{\text{reg}}$. In order to solve this problem we are going to use the observation made in the previous section: the factorization of the angular dependent factors in the expressions for the soft contributions. The definition of the subtraction scheme given below is very close to the idea which was suggested in description of B -decays in Refs.[48, 49] therefore we will also refer to this receipt as physical subtraction scheme. Consider for instance the amplitude $B_{+-}^{(0)}$. Using that the amplitude Φ_{+-} defined in Eq.(5.10) does not depend on the scattering angle θ we can define it at some fixed angle as following expression θ_0 as

$$[\Phi_{+-}(s)]_{\text{reg}} = \left(-\frac{10}{9} \frac{(4\pi f_\pi)^2}{s} \frac{3 - \eta_0^2}{1 - \eta_0^2} \right)^{-1} \times \left(B_{+-}^{(0)}(s, \theta_0) - \frac{\alpha_s}{4\pi} \frac{(4\pi f_\pi)^2}{s} \frac{\mu_\pi^2}{s} \frac{4}{3} \left[\left\{ \frac{5}{9} \frac{3 - \eta_0^2}{1 - \eta_0^2} I_s - \frac{4}{9} \frac{1}{1 - \eta_0^2} I(\eta_0) \right\} \right]_{\text{reg}} \right) \quad (5.15)$$

where $\eta_0 = \cos \theta_0$ and we also substituted $N_c = 3$, $e_u = 2/3$, $e_d = -1/3$ in order to simplify the analytical expression. This equation defines the soft factor $[\Phi_{+-}(s)]_{\text{reg}}$ through the physical amplitude $B_{+-}^{(0)}(s, \theta_0)$ and the regularized hard contribution. The *rhs* in Eq.(5.15) does not depend on the subtraction angle θ_0 therefore the value θ_0 can be fixed using phenomenological arguments. It is clear that the best choice θ_0 corresponds to a region where our description is expected to be most accurate. In what follow we choose the value $\theta_0 = 90^\circ$ which is equidistant from the forward and backward regions. Then substituting Eq.(5.15) into expression with arbitrary θ (5.11) and using $\theta_0 = 90^\circ$ ($\eta_0 = 0$) we obtain

$$B_{+-}^{(0)}(s, \theta) = \frac{1 - \eta^2/3}{1 - \eta^2} B_{+-}^{(0)}(s, 90^\circ) + \Delta_{+-}^{(0)}(s, \eta), \quad (5.16)$$

with

$$\Delta_{+-}^{(0)}(s, \eta) = \frac{\alpha_s (4\pi f_\pi)^2 \mu_\pi^2}{4\pi} \frac{16}{s} \frac{1}{27(1 - \eta^2)} \left\{ \left(1 - \frac{\eta^2}{3}\right) I(0) - I(\eta) \right\}. \quad (5.17)$$

From this result we observe that the divergent integral I_s cancel. Formally this is the direct consequence of the simple fact: the angular factor $(3 - \eta^2)/(1 - \eta^2)$ in front of divergent integral I_s in Eq.(5.11) is exactly the same as in front of the soft amplitude $\Phi_{+-}(s)$. Let us stress that this coincidence is obtained from the two different matching calculations. More generally, the singular terms on *rhs* of Eq.(5.16) enter only in the combination $\Delta_{+-}^{(0)}$ and must cancel if our factorization formula (5.11) is complete, i.e. it describes the all required configurations (or regions). Then the regularization [...] _{reg} on *rhs* of Eq.(5.16) can be omitted. Therefore the cancellation of the singular term I_s in the expression (5.17) can be considered as a direct confirmation of the SCET analysis carried out in Sec. 4.3. Let us also remind, that the hard contribution $\Delta_{+-}^{(0)}$ in Eq.(5.17) is not complete and can also include other contributions which are related to the different higher twist DAs.

Application of the same scheme for the amplitude $B_{++}^{(0)}$ yields

$$B_{++}^{(0)}(s, \theta) \simeq \frac{B_{++}^{(0)}(s, 90^\circ)}{1 - \eta^2} + \Delta_{++}^{(0)}(s, \eta) \approx \frac{B_{++}^{(0)}(s, 90^\circ)}{1 - \eta^2}. \quad (5.18)$$

where the hard correction $\Delta_{++}^{(0)}$ is given by the appropriate combination of the contributions $[\langle p, p' | O_n O_{\bar{n}} * T_{++} | 0 \rangle](s, \theta) \sim \alpha_s$ described by the higher twist pion DAs associated with the operators O_n and $O_{\bar{n}}$. We neglected these terms assuming that their numerical values are smaller comparing to the chiral enhanced corrections. In Eq.(5.18) we just indicate this possible contribution for clarity.

Let us remind that in expressions given by Eqs.(5.16) and (5.18) we consider only the power suppressed amplitudes $B_{+\pm}^{(i)}$ as defined in Eq.(2.22). The physical subtractions reorganize the formal expansions (5.11) and (5.12) in such way that the soft-overlap contributions are accumulated in the power suppressed amplitudes $B_{+\pm}^{(0)}(s, \theta = 90^\circ)$ which we consider as nonperturbative quantities. The angular behavior of the power suppressed amplitudes $B_{+\pm}^{(i)}$ in the Eqs.(5.16) and (5.18) is obtained from the hard coefficient functions and therefore can be considered as a model independent result. The effect of the power

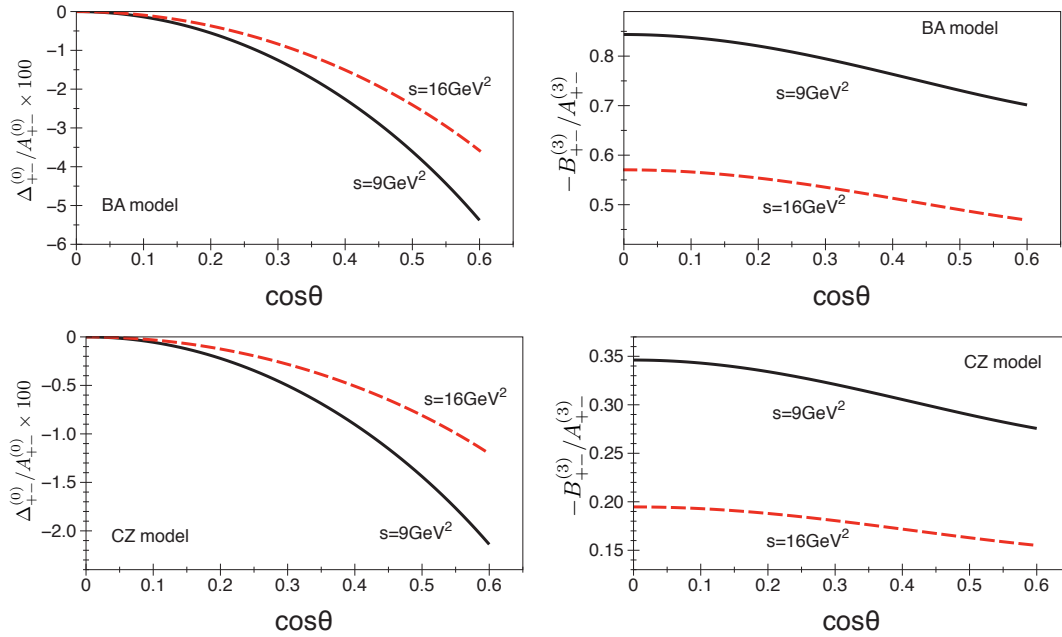


Figure 13. The ratios of the hard subleading power amplitude to the leading power contribution. The first (second) line shows the plots for the BA(CZ)-model of pion DA.

suppressed hard contribution can be associated in our approximation with the corrections described by $\Delta_{+-}^{(0)}$ and $B_{+-}^{(3,h)}$ in Eqs.(5.18) and (5.14), respectively.

It is interesting to compare the hard leading-order contributions with the hard power suppressed corrections. In Fig.13 we show the ratios of the $\Delta_{+-}^{(0)}/A_{+-}^{(0)}$ (left) and $B_{+-}^{(3)}/A_{+-}^{(3)}$ (right) as functions of $\cos\theta$ for two different values of s . In order to compute these ratios we used the leading twist pion DA defined by BA-set, see Eq.(2.33). The renormalization scale μ_R for the running coupling and for the quark masses is fixed to be $\mu_R = 0.8W$ GeV.

The ratio $\Delta_{+-}^{(0)}/A_{+-}^{(0)}$ is relatively small (about few percent) and tends to zero when $\cos\theta \rightarrow 0$. This behavior is the consequence of our subtraction scheme with subtractions at $\theta_0 = 90^\circ$ that ensures $\Delta_{+-}^{(0)}(s, \eta \rightarrow 0) \rightarrow 0$. Therefore we see that numerical effect from the hard chiral enhanced power correction in the amplitude $T_{+-}^{(0)}$ is very small. The result for ratio $B_{+-}^{(3)}/A_{+-}^{(3)}$ is different. In this case the absolute value of the subleading amplitude is comparable to the leading one providing a larger numerical impact. Even at $s = 16\text{GeV}^2$ the effect from the chiral enhanced power correction is of order 40–50%. The amplitudes $B_{+-}^{(3)}$ and $A_{+-}^{(3)}$ enter with opposite signs therefore the value of the combination $B_{+-}^{(3)} + A_{+-}^{(3)}$ is strongly reduced. Hence the effect of the chiral power correction for this amplitude is numerically significant and must be taken into account.

For the CZ-model of the pion DA ($\mu_R = 1.3\text{GeV}$) the relative value of the hard subleading corrections is considerably smaller because the absolute value of the leading contribution is considerably larger in this case. The results for the corresponding ratios are shown in the bottom plots in Fig.13.

Summarizing, in (5.16) and (5.18) we provide the expressions for the power suppressed amplitudes which depend on the two unknown functions $B_{+-}^{(0)}(s, 90^\circ)$ and $B_{++}^{(0)}(s, 90^\circ)$ describing the soft-overlap contribution in the physical subtraction scheme. Now we can combine these results with the leading-twist contributions $A_{+\pm}^{(i)}$ in order to perform a phenomenological analysis of the existing data.

6 Phenomenological analysis of BELLE data

The expressions for the cross sections can be written in the relatively simple form if we present the total amplitudes in the following form

$$T_{++}^{(0)}(s, \theta) = A_{++}^{(0)}(s, \theta) + \frac{1}{1 - \eta^2} B_{++}^{(0)}(s), \quad (6.1)$$

$$T_{+-}^{(0)}(s, \theta) = A_{+-}^{(0)}(s, \theta) + \frac{1 - \eta^2/3}{1 - \eta^2} B_{+-}^{(0)}(s) + \Delta_{+-}^{(0)}(s, \eta), \quad (6.2)$$

$$T_{++}^{(3)}(s, \theta) = A_{++}^{(3)}(s, \theta), \quad (6.3)$$

$$T_{+-}^{(3)}(s, \theta) = A_{+-}^{(3)}(s, \theta) + B_{+-}^{(3,h)}(s, \theta) \quad (6.4)$$

where $\eta = \cos\theta$ and we used that the amplitude $B_{++}^{(3)}$ is small, see (5.13). The expressions describing the leading power contributions $A_{+\pm}^{(i)}$ are given in Eqs.(2.24)-(2.26). The hard subleading amplitudes $B_{+-}^{(3,h)}$ and $\Delta_{+-}^{(0)}$ can be found in Eqs.(5.14) and (5.17), respectively. In Eqs.(6.1) and (6.2) we used for the subleading amplitudes as given in Eqs.(5.16) and (5.18). For the unknown soft-overlap contributions we introduced short notations

$$B_{++}^{(0)}(s, \theta = 90^\circ) \equiv B_{++}^{(0)}(s), \quad B_{+-}^{(0)}(s, \theta = 90^\circ) \equiv B_{+-}^{(0)}(s). \quad (6.5)$$

Using equations (6.1)-(6.4) we can write expressions for the cross sections (2.20) and (2.21) as following

$$\begin{aligned} \frac{d\sigma^{\pi^+\pi^-}}{d\cos\theta} = \frac{\pi\alpha^2}{16s} & \left(\frac{|B_{++}^{(0)}|^2}{(1-\eta^2)^2} + \left(\frac{1-\eta^2/3}{1-\eta^2} \right)^2 |B_{+-}^{(0)}|^2 + |A_{++}^{(0)}|^2 + |A_{+-}^{(0)} + \Delta_{+-}^{(0)}|^2 \right. \\ & \left. + 2A_{++}^{(0)} \frac{\text{Re}[B_{++}^{(0)}]}{1-\eta^2} + 2\frac{1-\eta^2/3}{1-\eta^2} (A_{+-}^{(0)} + \Delta_{+-}^{(0)}) \text{Re}[B_{+-}^{(0)}] \right), \end{aligned} \quad (6.6)$$

$$\begin{aligned} \frac{d\sigma^{\pi^0\pi^0}}{d\cos\theta} = \frac{\pi\alpha^2}{32s} & \left(\frac{|B_{++}^{(0)}|^2}{(1-\eta^2)^2} + \left(\frac{1-\eta^2/3}{1-\eta^2} \right)^2 |B_{+-}^{(0)}|^2 + |A_{+-}^{(0)} + \Delta_{+-}^{(0)} + A_{+-}^{(3)} + B_{+-}^{(3,h)}|^2 \right. \\ & \left. + 2\frac{1-\eta^2/3}{1-\eta^2} (A_{+-}^{(0)} + \Delta_{+-}^{(0)} + A_{+-}^{(3)} + B_{+-}^{(3,h)}) \text{Re}[B_{+-}^{(0)}] \right). \end{aligned} \quad (6.7)$$

In these expressions we used that all hard contributions $A_{+\pm}^{(i)}$, $B_{+-}^{(3,h)}$ and $\Delta_{+-}^{(0)}$ are real and therefore only the real parts $\text{Re}[B_{+\pm}^{(0)}]$ appear in the interference.

Using the known angular behavior of the cross sections in Eqs.(6.6) and (6.7) one can try to describe BELLE data [5, 6] in the region $W = 3 - 4\text{GeV}$ accepting the amplitudes $B_{+\pm}^{(0)}$ as free parameters. In the subsequent analysis we assume that the amplitudes $B_{+\pm}^{(0)}$ are dominated by real parts and

$$\text{Im } B_{+\pm}^{(0)}(s) \approx 0. \quad (6.8)$$

Then at fixed energy s we only have two unknown real parameters $B_{+\pm}^{(0)}(s)$ in order to describe the two differential cross sections.

The part of the nonperturbative input is given by the pion DA. In our numerical estimates we will use two different models described in Eqs. (2.33) and (2.35) (BA- and CZ-model, respectively). The numerical results obtained with the other models defined in Eqs.(2.32) and (2.34) are very close to one obtained with the BA-model.

At the beginning let us consider some qualitative properties of the cross sections described by Eqs.(6.6),(6.7). These expressions allows one to confront the theoretical predictions for the angular behavior at fixed energy s against the data. The angular behavior is described by the known coefficients in front of the soft amplitudes $B_{+\pm}^{(0)}(s)$ and by the different hard amplitudes.

Let us consider a soft approximation obtained neglecting the *all* hard contributions in Eqs.(6.6) and (6.7). Then the cross sections are described only by the quadratical terms $|B_{++}^{(0)}|^2$ and $|B_{+-}^{(0)}|^2$. Their coefficients differ by relatively small factor $(\eta^2/3)/(1-\eta^2)^2$ and therefore we can conclude that such “soft” cross sections behave as approximately as $(1-\eta^2)^{-2}$. From Eqs.(6.6) and (6.7) it is easily to see that the ratio of the cross sections in this case is fixed

$$\left[\frac{d\sigma^{\pi^0\pi^0}}{d\cos\theta} / \frac{d\sigma^{\pi^+\pi^-}}{d\cos\theta} \right]_{\text{soft}} = \frac{1}{2}. \quad (6.9)$$

The deviation from this value in the present formalism can be explained only by the presence of the interference of the computed hard contributions $A_{+\pm}^{(i)}$, $B_{+\pm}^{(3,h)}$ with the unknown soft amplitudes $B_{+\pm}^{(0)}(s, 0)$.

Therefore relatively small deviation from $1/(1-\eta^2)$ behavior can only be visible if the value of the amplitude $B_{+-}^{(0)}$ is quite large.

The linear in $B_{+\pm}$ terms in Eqs.(6.6),(6.7) can also provide a significant numerical effect. Let us consider their behavior in $\cos\theta$. From Eq.(2.24) one finds that $A_{++}^{(0)} \sim 1/(1-\eta^2)$. The combination $(1-\eta^2/3)(A_{+-}^{(0)} + \Delta_{+-}^{(0)})$ which inter in Eq.(6.6) also behaves as $1/(1-\eta^2)$. In Fig.14 we plot the corresponding linear term

$$\rho_{+-}(s, \eta) = (1-\eta^2/3) \left(A_{+-}^{(0)}(s, \eta) + \Delta_{+-}^{(0)}(s, \eta) \right), \quad (6.10)$$

and the approximation which is given by

$$\tilde{\rho}_{+-}(s, \eta) \simeq \frac{\rho_{+-}(s, 0)}{1-\eta^2}. \quad (6.11)$$

at fixed $W = 3\text{GeV}$. From this figure one can see that the difference between the two expressions is quite small for all models of pion DA. This picture is not changed in the

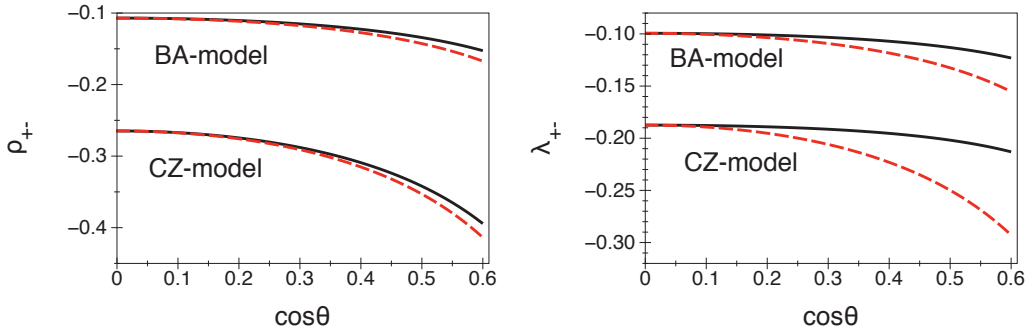


Figure 14. The linear coefficients ρ_{+-} defined in Eq.(6.10) (left figure) and λ_{+-} defined in Eq.(6.13) (right figure) as a functions of $\eta = \cos\theta$ at fixed energy $W = 3\text{GeV}$. The exact values of these coefficients are shown by solid black lines. The approximations $\tilde{\rho}_{+-}$ (6.11) and $\tilde{\lambda}_{+-}$ (6.14) are given by dashed red lines. For the numerical calculations of the amplitudes we used the same input parameters as in Figs.13

region where $W = 3 - 4\text{GeV}$. Therefore to a very good accuracy one can expect that

$$\frac{d\sigma^{\pi^+\pi^-}}{d\cos\theta} \sim \frac{1}{(1-\eta^2)^2}. \quad (6.12)$$

This simple observation allows us to conclude that one can not perform a good extraction of the two amplitudes $B_{+\pm}^{(0)}$ by fitting the differential cross section $d\sigma^{\pi^+\pi^-}/d\cos\theta$.

The qualitative observation (6.12) is in agreement with experimental data [5]. The behavior of the cross section as in Eq.(6.12) was also obtained in handbag model approach Ref.[17]. However within this framework $B_{++}^{(i)} = 0$ that is not agree with the our result in Eq.(6.6).

The linear (with respect to $B_{+\pm}^{(0)}$) contribution in the cross sections for neutral pions in Eq.(6.7) depends only from the amplitude $B_{+-}^{(0)}$. The corresponding hard coefficients reads

$$\lambda_{+-}(s, \eta) = A_{+-}^{(0)}(s, \eta) + \Delta_{+-}^{(0)}(s, \eta) + A_{+-}^{(3)}(s, \eta) + B_{+-}^{(3,h)}(s, \eta). \quad (6.13)$$

The angular behavior of this expression deviates from a simple behavior like $(1-\eta^2)^{-1}$. In Fig.14 we show the exact value $\lambda_{+-}(s, \eta)$ in comparison with the approximation

$$\tilde{\lambda}_{+-}(s, \eta) = \frac{\lambda_{+-}(s, 0)}{(1-\eta^2)}. \quad (6.14)$$

We observe that in this case the deviation from the profile $1/(1-\eta^2)$ reaches 30% for the CZ-model. Therefore if the absolute value of the amplitude $B_{+-}^{(0)}$ is relatively large then the corresponding linear term in the cross section can already provide a sizable numerical effect. In this case the separation of the two amplitudes using the angular behavior can be performed in a better way.

The boundary value $\eta_{\max} = 0.6$ in the energy interval $W = 3 - 4 \text{ GeV}$ corresponds to the values of $|t| = |u| = 1.8 - 3.2 \text{ GeV}^2$. Such values of t and u are still far from the asymptotic domain and we can not exclude a substantial numerical corrections associated with the different subleading contributions. Therefore we admit that our description can be less accurate in the region $\eta \sim 0.6$ for $W = 3 - 4 \text{ GeV}$.

6.1 Phenomenological analysis using model-II for pion DA

We start our phenomenological analysis using the pion DA defined by set-II, see Eq.(2.33). The value of the hard scale is fixed to be $\mu_R = 0.8W$. This scale is used in order to compute the running coupling $\alpha_s(\mu_R)$, the moments $a_{2n}(\mu_R)$ and quark masses in expression for μ_π in Eq.(A.4).

In order to see an effect from the subleading corrections let us consider numerical values of different contributions in the cross sections. Taking $W = 3.05\text{GeV}$, $\cos\theta = 0.05$ we obtain

$$\left(\frac{d\sigma^{\pi^+\pi^-}}{d\cos\theta}\right)_{\text{LT}} = 0.0283, \quad \left(\frac{d\sigma^{\pi^+\pi^-}}{d\cos\theta}\right)_{\text{exp}} = 0.312 \pm 0.039, \quad (6.15)$$

$$\left(\frac{d\sigma^{\pi^0\pi^0}}{d\cos\theta}\right)_{\text{LT}} = 0.0014, \quad \left(\frac{d\sigma^{\pi^0\pi^0}}{d\cos\theta}\right)_{\text{exp}} = 0.078 \pm 0.025, \quad (6.16)$$

$$\frac{d\sigma^{\pi^+\pi^-}}{d\cos\theta} = 0.879|B_{++}^{(0)}|^2 + 0.878|B_{+-}^{(0)}|^2 - 0.259B_{++}^{(0)} - 0.180B_{+-}^{(0)} + 0.0283, \quad (6.17)$$

$$\frac{d\sigma^{\pi^0\pi^0}}{d\cos\theta} = 0.440|B_{++}^{(0)}|^2 + 0.439|B_{+-}^{(0)}|^2 - 0.083B_{+-}^{(0)} + 0.004. \quad (6.18)$$

Here the subscript ‘‘LT’’ denotes the leading-twist approximation. For comparison we also show in Eqs.(6.15) and (6.16) the experimental values from Refs.[5, 6].

Comparing Eqs.(6.16) and (6.18) in the limit $B_{+pm}^{(0)} = 0$ one can see that the hard subleading contribution $B_{+-}^{(3,h)}$ provides a large numerical contribution ($\pi^0\pi^0$ channel). However the absolute value of this correction is still very small in order to obtain the experimental value in Eq.(6.16). This observation is also valid for other values of the scattering angle θ . Hence we conclude that the data can be described only if the soft amplitudes $B_{+\pm}^{(0)}$ are quite large.

If our description of the angular behavior is consistent with the data then we can determine the values of the amplitudes $B_{+\pm}^{(0)}$. In Figs. 15 and 16 we present our results for the fit of the BELLE data [5, 6] for charged and neutral pions, respectively. The results of the two-parameter fit of both data sets are shown in Figs.15 and 16 by dashed lines. In Table 1 we present the numerical values of the amplitudes $B_{+\pm}^{(0)}$ in for each energy W . The data for $\pi^0\pi^0$ production in the region $W = 3.3 - 3.6\text{GeV}$ have a gap because of charmonium production. In this region we can not perform the two-parameter fit of the amplitudes $B_{+\pm}^{(0)}$ and therefore corresponding values can not be obtained using this method. We obtain that in the region $W = 3.05 - 3.65\text{GeV}$ the absolute value of $B_{+-}^{(0)}$ is quite small. The angular separation of the amplitudes cannot be done accurately in this case and this leads to large errors for $B_{+-}^{(0)}$. It demonstrates that application of the expressions in Eqs.(6.6) and (6.7) for the fit of the data does not allow one to determine the unknown amplitudes with a reasonable accuracy without some additional information.

The result of the two-parameter fit allow us to conclude that $|B_{++}^{(0)}| \gg |B_{+-}^{(0)}|$. For larger values of energy $W \geq 3.75\text{GeV}$ the values of $B_{+-}^{(0)}$ in Table 1 are already quite large

Table 1. The values of the amplitudes $B_{\pm\pm}^{(0)}(s)$ obtained from the two-parameter fit of the cross sections provided by BELLE collaboration [5, 6]. The reduced values of χ^2 are computed with dof= 16.

W , GeV	$B_{++}^{(0)}(s, 0)$	$B_{+-}^{(0)}(s, 0)$	χ^2/dof
3.05	-0.47 ± 0.16	0.068 ± 2.96	2.32
3.15	-0.44 ± 0.17	0.057 ± 2.68	1.89
3.65	-0.260 ± 0.34	-0.003 ± 1.7	0.98
3.75	-0.22 ± 0.21	-0.1 ± 0.38	1.28
3.85	-0.17 ± 0.12	0.25 ± 0.14	0.67
3.95	-0.18 ± 0.11	0.15 ± 0.26	0.58

Table 2. Results for the amplitude $B_{++}^{(0)}(s)$ obtained from the one-parameter fit of BELLE data [5] for charged pions.

W , GeV	3.05	3.15	3.25	3.35	3.45
$B_{++}^{(0)}(s, 0)$	-0.48 ± 0.02	-0.44 ± 0.02	-0.39 ± 0.02	-0.35 ± 0.03	-0.30 ± 0.03
χ^2/dof	1.5	2.3	2.5	2.0	1.8

W , GeV	3.55	3.65	3.75	3.85	3.95	4.05
$B_{++}^{(0)}(s, 0)$	-0.27 ± 0.03	-0.29 ± 0.04	-0.27 ± 0.03	-0.23 ± 0.03	-0.20 ± 0.03	-0.15 ± 0.04
χ^2/dof	1.9	0.8	0.8	0.8	0.4	3.6

but the error bars are also large. Guided by these observations we consider a simple model assuming

$$B_{+-}^{(0)} \simeq 0. \quad (6.19)$$

In this case one can perform a more simple one-parameter fit of the data for charged pion in order to define the values of $B_{++}^{(0)}$. Then these values can be used for computation of the cross section for neutral pions. Comparison of the cross section with the data allows one to check the consistency of the model. The obtained results are also shown in Figs. 15 and 16 by solid line. We observe that the difference between one- and two-parameter fits in this case is small.

In Table 2 we present the results for the values $B_{++}^{(0)}$ defined by the one-parameter fit. One can see that the quality of the fit is much better. Such fit has better χ^2 and obtained values have relatively small error bars. However this estimates are no longer unbiased and the small error bars can also arise due to the effect of underfitting⁸. Nevertheless we consider this this model is interesting providing a simple scenario which is consistent with the data.

⁸The author thanks to M.Distler for the discussion of this moment.

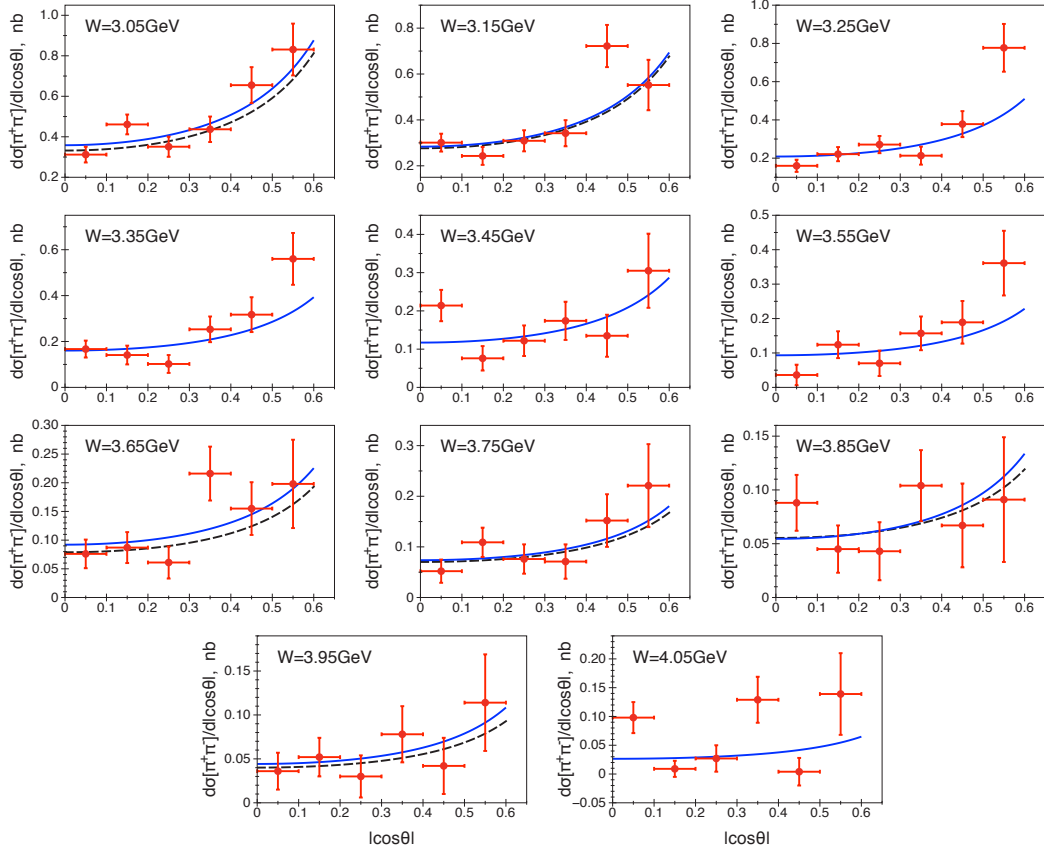


Figure 15. Results of the fit for the charged pion cross section, see discussion in the text. The data are results from BELLE [5].

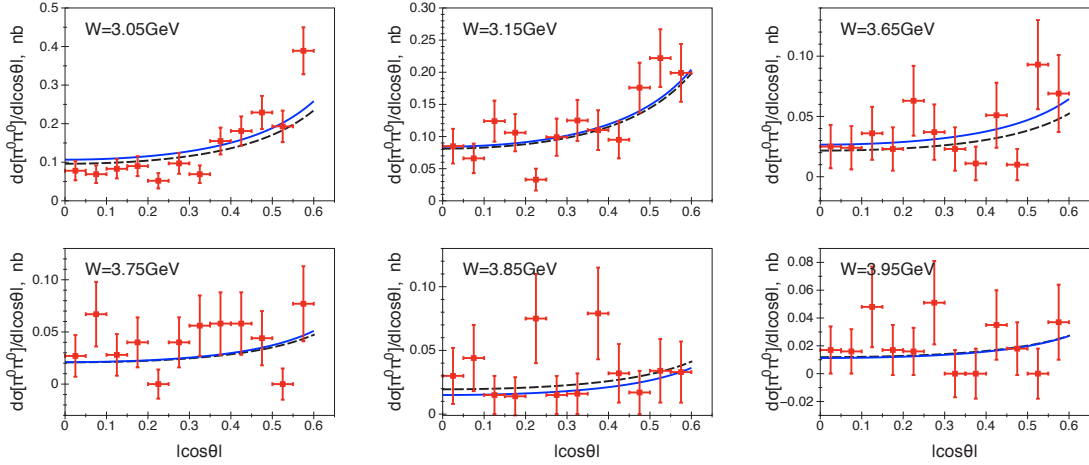


Figure 16. Results of the fit for the neutral pion cross section, see discussion in the text. The data are taken from Ref.[6].

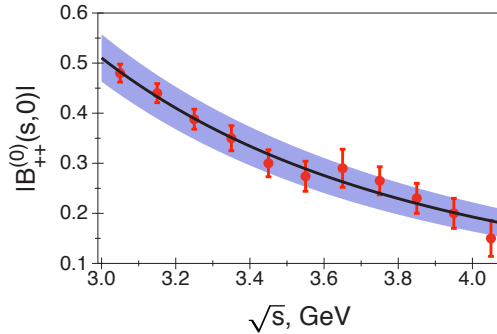


Figure 17. The amplitude $B_{++}^{(0)}(s, 0)$ as a function of energy s .

Substituting the values $B_{++}^{(0)} = -0.48$, $B_{+-}^{(0)} = 0$ in Eq. (6.17) we obtain

$$\frac{d\sigma^{\pi^+\pi^-}}{d\cos\theta}(3.05\text{GeV}, \cos\theta = 0.05) = 0.879|B_{++}^{(0)}|^2 - 0.259B_{++}^{(0)} + 0.0283 \quad (6.20)$$

$$= 0.19_{B_{++}^2} + 0.12_{B_{++}} + 0.0283 \simeq 0.34, \quad (6.21)$$

where the subscripts indicate the corresponding contribution in the upper line. We observe that the interference contribution (linear in $B_{++}^{(0)}$) provides quite sizable numerical effect of order 30%. The similar calculation for the neutral channel yields

$$\frac{d\sigma^{\pi^0\pi^0}}{d\cos\theta} = 0.440|B_{++}^{(0)}|^2 + 0.004 = 0.096 + 0.004 = 0.1. \quad (6.22)$$

In this case the interference depends only from the small amplitude $B_{+-}^{(0)}$ and therefore corresponding numerical effect is negligible. Hence we conclude that the sizable deviation from the simple value 1/2 for the cross section ratio (6.9) can be only obtained due to the linear contribution with the amplitude $B_{++}^{(0)}$ in Eq.(6.6).

Performing an empirical power fit of results in Table 2 we obtain

$$B_{++}^{(0)}(s, 0) = \left(\frac{s_0}{s}\right)^a, \quad \text{with } s_0 = 6.0 \pm 0.3, \quad a = 1.7 \pm 0.15. \quad (6.23)$$

This result is shown in Fig.17. Using SCET framework we obtained in Sec.4 that this amplitude is suppressed in the limit $s \rightarrow \infty$ as $B_{++}^{(0)}(s) \sim \Lambda^4/s^2$. The obtained empirical value of the power exponent a is smaller but not far from this expectation. The large value of the effective scale s_0 in Eq.(6.23) is necessary in order to have a large normalization of the cross section. We expect the nonperturbative dynamical scale defining the behavior of the amplitude $B_{++}^{(0)}(s)$ is the hard-collinear scale $\mu_{hc} \sim \Lambda Q$ where Λ can be interpreted as a typical value of soft particles momenta. We can rewrite the empirical formula in Eq.(6.23) as $B_{++}^{(0)}(s, 0) = \left(\frac{s'_0}{\Lambda W}\right)^{2a}$ where $W \equiv \sqrt{s}$. Taking $\Lambda \simeq 300 - 400\text{MeV}$ we obtain that the value of the intrinsic scale is $s'_0 = \Lambda\sqrt{s_0} \simeq 0.73 - 0.98 \text{ GeV}^2$.

Eq. (6.23) for $B_{++}^{(0)}(s)$ allows one to compute the total cross sections and their ratio. Corresponding results are shown in Figs. 18 and 19. From Fig. 18 it is seen that

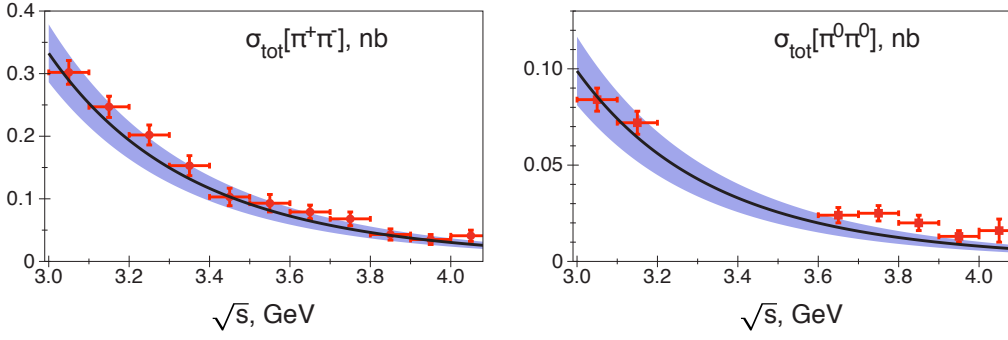


Figure 18. The total cross sections as a functions of energy.

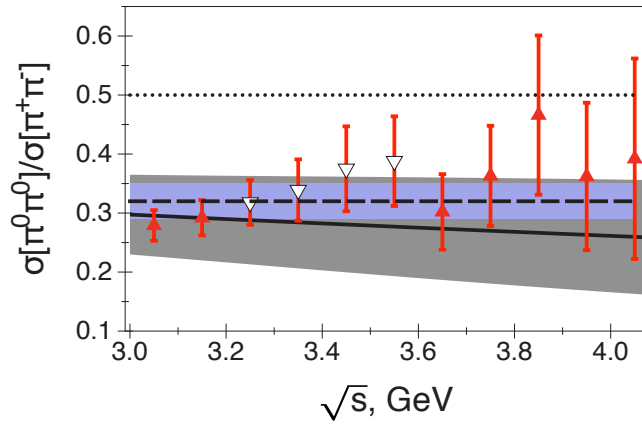


Figure 19. The ratio of the cross sections $\sigma_{tot}^{\pi^0\pi^0}/\sigma_{tot}^{\pi^+\pi^-}$ as a function of the energy. The data are taken from Ref.[6] . The dashed line shows the experimental fit with 1σ error bands. The solid line shows the computed ratio with the 1σ error bands.

obtained $\sigma_{tot}^{\pi^0\pi^0}$ is somewhat smaller than the experimental values. As a result the ratio (solid line in Fig.19) slightly decreases for larger energy W . The gray area around the solid line shows 1σ bands obtained from the errors of the parameters s_0 and a in Eq.(6.23). The fit of the experimental data yields $R = 0.32 \pm 0.03$ [6].⁹ In Fig.19 this result is shown by dashed line with 1σ error bands.

6.2 Phenomenological analysis using CZ-model of pion DA

Using CZ-model defined in Eq.(2.35) and fixing a small value of the renormalization scale $\mu_R = 1.3\text{GeV}$ one obtains a larger contribution from the leading-twist part. In that case the numerical values of the differential cross sections at $W = 3.05$ GeV and $\cos\theta = 0.05$

⁹The results in the region $W = 3.3 - 3.6$ GeV (plotted with open triangles) are not used for the fit in Ref[6].

read (c.f. with the corresponding Eqs.(6.15)-(6.18))

$$\left(\frac{d\sigma^{\pi^+\pi^-}}{d\cos\theta}\right)_{\text{LT}} = 0.18, \quad \left(\frac{d\sigma^{\pi^+\pi^-}}{d\cos\theta}\right)_{\text{exp}} = 0.312 \pm 0.039, \quad (6.24)$$

$$\left(\frac{d\sigma^{\pi^0\pi^0}}{d\cos\theta}\right)_{\text{LT}} = 0.009, \quad \left(\frac{d\sigma^{\pi^0\pi^0}}{d\cos\theta}\right)_{\text{exp}} = 0.078 \pm 0.025, \quad (6.25)$$

$$\frac{d\sigma^{\pi^+\pi^-}}{d\cos\theta} = 0.88|B_{++}^{(0)}|^2 + 0.88|B_{+-}^{(0)}|^2 - 0.65B_{++}^{(0)} - 0.45B_{+-}^{(0)} + 0.18. \quad (6.26)$$

$$\frac{d\sigma^{\pi^0\pi^0}}{d\cos\theta} = 0.44|B_{++}^{(0)}|^2 + 0.44|B_{+-}^{(0)}|^2 - 0.16B_{+-}^{(0)} + 0.014. \quad (6.27)$$

In this case the quality of the two-parameter fit is better: the obtained error bars are smaller. The results for the differential cross sections are shown in Fig.20 and the numerical values of the amplitudes for the different energies W are summarized in Table 3. One can see that in this case the solution is given by large $B_{+-}^{(0)}$ and relatively small $B_{++}^{(0)}$. The coefficient of the linear contribution λ_{+-} defined in (6.13) is quite large and therefore the angular separation works better that explains the better results of the two-parameter fit. The results are presented in Fig.20. The power fit of the obtained points yields

$$B_{++}^{(0)}(s) = \left(\frac{s_0}{s}\right)^a, \quad \text{with } s_0 = 5.8 \pm 1\text{GeV}^2, \quad a = 3.4 \pm 1.2, \quad (6.28)$$

$$B_{+-}^{(0)}(s) = -\left(\frac{s_1}{s}\right)^b, \quad \text{with } s_1 = 6.1 \pm 0.5\text{GeV}^2, \quad b = 1.2 \pm 0.15. \quad (6.29)$$

Corresponding figures with 1σ error bands are shown in Fig.21. The absolute value of

Table 3. The amplitudes $B_{\pm\pm}^{(0)}(s)$ obtained from the two-parameter fit of BELLE data [5, 6] with CZ-model of pion DA (dof=16).

$W, \text{ GeV}$	3.05	3.15	3.65	3.75	3.85	3.95
$B_{++}^{(0)}(s, 0)$	-0.20 ± 0.03	-0.15 ± 0.03	-0.09 ± 0.05	-0.06 ± 0.04	-0.02 ± 0.04	-0.017 ± 0.046
$B_{+-}^{(0)}(s, 0)$	0.59 ± 0.03	0.59 ± 0.03	0.36 ± 0.04	0.37 ± 0.04	0.37 ± 0.03	0.31 ± 0.04
χ^2/dof	2.7	2.2	0.94	1.3	0.7	0.60

$B_{++}^{(0)}$ is smaller comparing to $B_{+-}^{(0)}$ and much stronger suppressed with the energy s . The power behavior of the dominant amplitude $B_{+-}^{(0)}$ is much smaller than the asymptotic prediction $\sim 1/s^2$. An attempt to apply the one-parameter model with $B_{++}^{(0)} \simeq 0$ gives a bad description indicating that $B_{++}^{(0)}$ can not be neglected for the whole energy interval. The total cross sections and their ratio are shown in Figs. 22 and 23. All notations and the error bands are the same as in Figs.18 and 19, respectively.

In case of CZ-model one also needs to take into account the numerical effect provided by the the linear contributions with the amplitudes $B_{\pm\pm}^{(0)}$ in Eqs.(6.6) and (6.7). Substituting

the numerical values for the amplitude in Eqs.(6.26) and (6.27) we obtain ($W = 3.05\text{GeV}$ and $\cos\theta = 0.05$)

$$\frac{d\sigma^{\pi^+\pi^-}}{d\cos\theta} = 0.035_{B_{++}^2} + 0.3_{B_{+-}^2} + 0.13_{B_{++}} - 0.26_{B_{+-}} + 0.18 = 0.38, \quad (6.30)$$

$$\frac{d\sigma^{\pi^0\pi^0}}{d\cos\theta} = 0.018_{B_{++}^2} + 0.15_{B_{+-}^2} - 0.09_{B_{+-}} + 0.014 = 0.09. \quad (6.31)$$

Here the subscripts again show the numerical contribution of the appropriate quadratical or linear terms in Eq's.(6.26) and (6.27). Numerical values in (6.30) and (6.31) demonstrate that all terms are significant for description of the cross sections.

We observe that it is possible to fit the data using very different models of pion DA. Hence our consideration shows that our approach cannot help to constrain pion DA and as a result we can obtain different solutions for the amplitudes $B_{+\pm}^{(0)}$. In this case one needs more information in order to constrain the input parameters. Potentially a precise measurement of the cross section $e^+e^- \rightarrow e^+e^-\pi\pi$ with unpolarized electron beams allows one to obtain more information about the amplitudes of the hadronic subprocess.

The corresponding cross section is described by the two contributions, see the details in Ref.[56]. Schematically the expression for the cross section reads

$$d\sigma^{e^+e^- \rightarrow e^+e^-\pi\pi} = \left\{ A \frac{1}{2} \left(\sigma_{\parallel}^{\gamma\gamma \rightarrow \pi\pi} + \sigma_{\perp}^{\gamma\gamma \rightarrow \pi\pi} \right) + B \left(\sigma_{\parallel}^{\gamma\gamma \rightarrow \pi\pi} - \sigma_{\perp}^{\gamma\gamma \rightarrow \pi\pi} \right) \cos 2\varphi \right\} \frac{d^3p'_1}{E_1} \frac{d^3p'_2}{E_1}, \quad (6.32)$$

where the $\sigma_{\parallel,\perp}^{\gamma\gamma \rightarrow \pi\pi}$ denotes cross sections for the scattering of photons with the parallel (σ_{\parallel}) and orthogonal (σ_{\perp}) linear polarizations. Here the coefficients A and B denote the functions of the kinematical variables and their explicit expressions can be found in Ref.[56]. The azimuth angle φ is defined as the angle between the electron scattering planes in the colliding electron c.m.s., E_i and p'_i denote the scattered electron energies and momenta. In the present work we only investigated the first combination of the cross sections which is proportional to the sum of the helicity amplitudes:

$$\sigma_{\parallel}^{\gamma\gamma \rightarrow \pi\pi} + \sigma_{\perp}^{\gamma\gamma \rightarrow \pi\pi} \sim |T_{++}^{\gamma\gamma \rightarrow \pi\pi}|^2 + |T_{+-}^{\gamma\gamma \rightarrow \pi\pi}|^2. \quad (6.33)$$

Using the angular dependence given by the factor $\cos 2\varphi$ one can also access the second contribution which is sensitive to the difference of the cross sections in Eq.(6.32). This combination is proportional only to the one helicity amplitude

$$\sigma_{\parallel}^{\gamma\gamma \rightarrow \pi\pi} - \sigma_{\perp}^{\gamma\gamma \rightarrow \pi\pi} \sim |T_{++}^{\gamma\gamma \rightarrow \pi\pi}|^2. \quad (6.34)$$

Hence such data can provide an additional information which allows one to perform a better separation of the helicity amplitudes and to perform extraction of the soft-overlap form factors $B^{(0)\pm}(s)$.

In our consideration the values of the amplitudes $B_{+\pm}^{(0)}(s)$ depends on the model of pion DA. For model defined by set-II we obtain that $|T_{++}^{\gamma\gamma \rightarrow \pi\pi}| \gg |T_{+-}^{\gamma\gamma \rightarrow \pi\pi}|$ and contrariwise for

the CZ-model. The consideration within the handbag model in Ref.[17] predicts $T_{++}^{\gamma\gamma\rightarrow\pi\pi} \simeq 0$.

Our estimations of the cross section $\sigma_{\parallel} - \sigma_{\perp}$ at $W = 3.05\text{GeV}$ are shown in Fig.24. We consider two different scenarios associated with the two different models of pion DA as discussed above. In order to draw these plots we use and the values $B_{++}^{(0)}(s)$ obtained in Tables 2 and 3. The shaded area shows the 1σ error bands which corresponds to the uncertainties in the determination of $B_{++}^{(0)}(s)$. From this figure we see that the difference between the two calculations is not very large. Hence one needs precise data in order to distinguish between the different scenarios. Nevertheless we expect that new data for the cross sections $\sigma_{\parallel}^{\gamma\gamma\rightarrow\pi\pi} - \sigma_{\perp}^{\gamma\gamma\rightarrow\pi\pi}$ can be very helpful in order to understand the reaction mechanism of the large angle pion production at intermediate values of the energy and momentum transfer.

7 Discussion

We have discussed a contribution of the subleading power corrections in the process $\gamma\gamma \rightarrow \pi\pi$ in the region where all Mandelstam variables are large $s \sim -t \sim -u \gg \Lambda^2$ (large angle scattering). The leading power behavior of the corresponding amplitude is described by the hard scattering mechanism suggested in Ref.[1]. The factorization of power suppressed corrections can be described as a sum of the hard and soft-overlap contributions. We develop a systematic approach for description of such configurations within the SCET framework.

Factorizing the hard modes in SCET we obtain that the soft-overlap contribution can be described by matrix elements of suitable SCET-I operators. We present an analysis of the appropriate SCET-I operators which are required for description $1/Q^2$ corrections to the leading power approximation. We demonstrate that the T -products of the SCET-I operators mix in SCET-II with the pure collinear operators describing hard subleading contributions. Such mixing is possible due to an overlap of collinear and soft domains and leads to the endpoint singularities in soft and collinear convolution integrals. In order to factorize consistently the hard and soft-overlap contributions one has to define a specific regularization which allows one to define the integrals in the endpoint region. In present case such scheme can be avoided if one uses the so-called physical subtraction scheme.

The subleading hard contributions are described by the matrix elements of the different higher twist collinear operators. All such contributions provide the power correction of order $1/s^2$. In present work we took into account only the specific twist-3 collinear operators which can provide the largest numerical corrections. Such terms are described by the two-particle operators and known as chiral enhanced corrections. Such approximation also allows us to simplify the theoretical consideration.

We compute the corresponding leading-order hard kernels and obtain that the hard amplitudes have the endpoint singularities. Therefore in order to be consistent we must add the SCET-I operators which can overlap with this subleading hard contribution. We obtain that such contribution can be only described by one suitable hard-collinear operator. Corresponding SCET-I matrix element defines the one soft-overlap amplitude which

depends only from the total energy s . The angular dependence in this case is given by the hard subprocess. Combining the hard and soft-overlap contributions we show that the endpoint singularities are cancel in the physical subtraction scheme. This allows us to compute the angular dependence of the amplitudes in a model independent way.

The final expression for the power suppressed amplitude depends on the two unknown amplitudes $B_{+\pm}^{(0)}(s)$ which are some functions of the total energy s . These amplitudes are defined by subprocess associated with the hard-collinear scale $\mu_{hc} \sim \Lambda\sqrt{s}$ where the soft scale Λ is of order of the typical momenta of soft particles. The hard-collinear scale is still small in the kinematical region $\sqrt{s} = 3 - 4\text{GeV}$ where we have data and we consider the amplitudes $B_{+\pm}^{(0)}(s)$ as the nonperturbative quantities.

The obtained results have been used in order to perform a phenomenological analysis of existing data. We obtain that to a very good accuracy the angular behavior of the cross section for the production of charged pions is proportional to the $\sin^{-4}\theta$ that is in the reasonable agreement with the data. This allows us to fix the nonperturbative functions $B_{+\pm}^{(0)}(s)$ by fitting the differential cross sections in the region $\sqrt{s} = 3 - 4\text{GeV}$ and $|\cos\theta| < 0.6$. Combining the leading and subleading amplitudes we obtain a reasonable description of the cross sections and their ratio $R = d\sigma^{\pi^0\pi^0}/d\sigma^{\pi^+\pi^-}$.

We find that the results for the functions $B_{+\pm}^{(0)}(s)$ are sensitive to the models of pion distribution amplitude used in the numerical calculations. For the CZ-model the best fit is obtained if $|B_{+-}^{(0)}(s, 0)| \gg |B_{++}^{(0)}(s, 0)|$. For the other models the angular separation of the amplitudes $B_{+\pm}^{(0)}(s)$ can not be performed with a good precision indicating the qualitative estimate $|B_{++}^{(0)}(s)| \gg |B_{+-}^{(0)}(s)|$. Following this observation we consider the model with $B_{+-}^{(0)}(s) \approx 0$. We find that in this case the data can be described quite well.

We expect that additional experimental information can help us to reduce the model dependence in the phenomenological analysis. More accurate data, especially for larger values of energy s will be very helpful but one has to remember that our description so far is also restricted only by the leading-order accuracy in α_s . The other possibility to improve the phenomenological analysis is to consider an additional observable which is sensitive to a different combination of the helicity amplitudes. A required cross section can also be measured in the process $e^+e^- \rightarrow e^+e^-\pi\pi$ using the modulation with respect to a angle between the electron scattering planes in the colliding electron c.m.s., see e.g. Ref.[56]. In this case one can access the combination $\sigma_{\parallel}^{\gamma\gamma \rightarrow \pi\pi} - \sigma_{\perp}^{\gamma\gamma \rightarrow \pi\pi} \sim |T_{++}^{\gamma\gamma \rightarrow \pi\pi}|^2$, where the $\sigma_{\parallel, \perp}^{\gamma\gamma \rightarrow \pi\pi}$ denotes cross sections for the scattering of photons with parallel (σ_{\parallel}) and orthogonal (σ_{\perp}) linear polarizations. This observable is only sensitive to the amplitude $B_{++}^{(0)}(s)$ that allows one to perform an accurate extraction of the amplitudes $B_{+\pm}^{(0)}(s)$. We expect that this will be very helpful for understanding of the dominant mechanism in the large angle meson production.

A Higher twist distribution amplitudes

For convenience in this Appendix we briefly discuss higher twist pion distribution amplitudes. More detailed discussion can be found in Ref.[50]. Below we present a standard QCD formulation. In order to obtain the equivalent SCET description one has to split the quark

fields into large ξ_n and small η_n components and use the equation of motion in order to eliminate the field η_n . A discussion of the some higher twist collinear matrix elements in the SCET framework can be found in Ref.[44].

In the QCD formulation there are three twist-3 collinear operators. Two of them are 2-particle operators and their light-cone matrix elements are defined as

$$\langle p' | \bar{q}(\lambda_1 \bar{n}) W_n(\lambda_1 \bar{n}) i \gamma_5 W_n^\dagger(\lambda_1 \bar{n}) q(\lambda_2 \bar{n}) | 0 \rangle = f_\pi \mu_\pi \int_0^1 du e^{iu\lambda_1 p'_- + i\bar{u}\lambda_2 p'_-} \phi_p(u), \quad (\text{A.1})$$

$$\langle p' | \bar{q}(\lambda_1 \bar{n}) W_n(\lambda_1 \bar{n}) \sigma^{\alpha\beta} \gamma_5 W_n^\dagger(\lambda_2 \bar{n}) q(\lambda_2 \bar{n}) | 0 \rangle = i f_\pi \mu_\pi \left(p^\alpha z^\beta - p^\beta z^\alpha \right) \quad (\text{A.2})$$

$$\int_0^1 du e^{iu\lambda_1 p'_- + i\bar{u}\lambda_2 p'_-} \frac{\phi_\sigma(u)}{6}, \quad (\text{A.3})$$

with $z^\alpha = (\lambda_1 - \lambda_2) \bar{n}^\alpha$, $p'_- \equiv (p' \cdot \bar{n})$ and

$$\mu_\pi = \frac{m_\pi^2}{m_u + m_d}, \quad p' \simeq p'_- \frac{\bar{n}}{2}. \quad (\text{A.4})$$

For the sum of the quark masses we use following estimate

$$(m_u + m_d)(2\text{GeV}) = 8.5\text{MeV}. \quad (\text{A.5})$$

There is only one twist-3 three-particle operator and its matrix element defines the three-particle DA $\phi_{3\pi}(\alpha_i)$

$$\langle \pi^+(p') | \bar{u}(\lambda \bar{n}) \sigma^{\bar{n}\alpha\perp} \gamma_5 g G_{\bar{n}\alpha\perp}(v\lambda \bar{n}) d(-\lambda \bar{n}) | 0 \rangle = i f_{3\pi} p'^2 \int \mathcal{D}\alpha_i e^{i\lambda p'_-(\alpha_u - \alpha_d + v\alpha_g)} \phi_{3\pi}(\alpha_i), \quad (\text{A.6})$$

Here $\mathcal{D}\alpha_i = d\alpha_u d\alpha_d d\alpha_g \delta(\alpha_u + \alpha_d + \alpha_g - 1)$, $G_{\bar{n}\alpha\perp} = G_{\mu\alpha\perp} \bar{n}^\mu$. Using QCD equations of motion one can show (see details in Refs.[50, 55]) that 2-particles DAs $\phi_{p,\sigma}$ can be presented as

$$\phi_p(u) = 1 + R V_p(u, \alpha_i) * \phi_{3\pi}(\alpha_i), \quad (\text{A.7})$$

$$\phi_\sigma(u) = 6u\bar{u} + R V_\sigma(u, \alpha_i) * \phi_{3\pi}(\alpha_i), \quad (\text{A.8})$$

where $V_{p,\sigma}$ denotes a certain dimensionless kernel, the asterisks denote the convolution integrals with respect to the fractions α_i and $R = f_{3\pi}/f_\pi \mu_\pi \simeq 0.014$ [50, 55]. One can assume that corrections associated with the admixture $\phi_{3\pi}$ in Eqs.(A.7) and (A.8) are relatively small because the factor R is numerically small comparing to the constant μ_π defined in Eq.(A.4). Therefore neglecting the 3-particle contributions with $\phi_{3\pi}$ in Eqs.(A.7) and (A.8) one finds

$$\phi_p(u) \simeq 1, \quad \phi_\sigma(u) \simeq 6u\bar{u}. \quad (\text{A.9})$$

The discussion of the twist-3 matrix elements within the SCET framework can also be found in Ref.[44].

The twist-4 operators can be divided on the following groups: two-, three- and four-particle operators. The two-particles operator are not independent and can be expressed

through the other DAs, see Ref.[50]. In phenomenological applications the four-particle twist-4 contributions are assumed to be small and as a rule neglected. Following to Ref.[50] one can define four three-particle DAs of twist four (for simplicity we do not write the collinear Wilson lines W_n)

$$\langle \pi^+(p') | \bar{u}(\lambda \bar{n}) \gamma_{\perp}^{\alpha} \gamma_5 g G_{\alpha_{\perp} \bar{n}}(v \lambda \bar{n}) d(-\lambda \bar{n}) | 0 \rangle = 2 f_{\pi} m_{\pi}^2 p'_{\perp} A_{\perp}(v, \lambda p'_{\perp}), \quad (\text{A.10})$$

$$\langle \pi^+(p') | \bar{u}(\lambda \bar{n}) \gamma_{\perp}^{\alpha} g \tilde{G}_{\alpha_{\perp} \bar{n}}(v \lambda \bar{n}) d(-\lambda \bar{n}) | 0 \rangle = 2 f_{\pi} m_{\pi}^2 p'_{\perp} V_{\perp}(v, \lambda p'_{\perp}), \quad (\text{A.11})$$

$$\langle \pi^+(p') | \bar{u}(\lambda \bar{n}) \not{n} \gamma_5 g G_{\bar{n} n}(v \lambda \bar{n}) d(-\lambda \bar{n}) | 0 \rangle = f_{\pi} m_{\pi}^2 p'_{\perp} A_{\parallel}(v, \lambda p'_{\perp}), \quad (\text{A.12})$$

$$\langle \pi^+(p') | \bar{u}(\lambda \bar{n}) \not{n} g \tilde{G}_{\bar{n} n}(v \lambda \bar{n}) d(-\lambda \bar{n}) | 0 \rangle = f_{\pi} m_{\pi}^2 p'_{\perp} V_{\parallel}(v, \lambda p'_{\perp}), \quad (\text{A.13})$$

with the

$$\{V_i, A_i\}(v, \lambda p'_{\perp}) = \int \mathcal{D}\alpha_i e^{i\lambda p'_{\perp}(\alpha_u - \alpha_d + v\alpha_g)} \{V_i, A_i\}(\alpha_i). \quad (\text{A.14})$$

and we used

$$\tilde{G}_{\alpha\beta} = \frac{1}{2} \varepsilon_{\alpha\beta\mu\nu} G^{\mu\nu}. \quad (\text{A.15})$$

We will not describe in detail the structure of these DAs because we neglect corresponding contributions in the our calculations.

B The list of SCET interactions

$$\mathcal{L}^{(1,n)} [\bar{\xi}_n^c A_{\perp} A_{\perp} \xi_n] \simeq \int d^4x \bar{\xi}_n^c A_{\perp} (\bar{n}\partial)^{-1} A_{\perp} \frac{\not{n}}{2} \xi_n, \quad (\text{B.1})$$

$$\mathcal{L}^{(2,n)} [\bar{\xi}_n^c A_{\perp} A_{\perp}^{(s)} \xi_n] \simeq \int d^4x \bar{\xi}_n^c \{A_{\perp}^s (\bar{n}\partial)^{-1} A_{\perp} + A_{\perp} (\bar{n}\partial)^{-1} A_{\perp}^s\} \frac{\not{n}}{2} \xi_n, \quad (\text{B.2})$$

$$\mathcal{L}^{(2,n)} [\bar{q} A_{\perp} \xi_n^c] \simeq \int d^4x \bar{q} A_{\perp} \xi_n^c. \quad (\text{B.3})$$

$$\mathcal{L}^{(2,n)} [\bar{\xi}_n^c A_{\perp}^c A_{\perp} \xi_n] \simeq \int d^4x \bar{\xi}_n^c A_{\perp}^c (\bar{n}\partial)^{-1} A_{\perp} \frac{\not{n}}{2} \xi_n, \quad (\text{B.4})$$

$$\mathcal{L}^{(3,n)} [\bar{q} A_{\perp} A_{\perp} \xi_n^c] \simeq \int d^4x \bar{q} A_{\perp} (\bar{n}\partial)^{-1} A_{\perp} \frac{\not{n}}{2} \xi_n^c. \quad (\text{B.5})$$

$$\mathcal{L}^{(4,n)} [\bar{q} A_{\perp}^s A_{\perp} \xi_n^c] = \int d^4x \bar{q} \{A_{\perp}^s (\bar{n}\partial)^{-1} A_{\perp} + A_{\perp} (\bar{n}\partial)^{-1} A_{\perp}^s\} \frac{\not{n}}{2} \xi_n^c \quad (\text{B.6})$$

Acknowledgments

This work was supported by the Helmholtz Institute Mainz. The author is grateful to M. Vanderhaeghen, M. Distler and L.Tiator for many useful discussions and to S. Eydelman and H. Nakazava for the helpful correspondence.

References

- [1] S. J. Brodsky and G. P. Lepage, Phys. Rev. D **24** (1981) 1808.
- [2] M. Benayoun and V. L. Chernyak, Nucl. Phys. B **329** (1990) 285.
- [3] J. Dominick *et al.* [CLEO Collaboration], Phys. Rev. D **50** (1994) 3027 [hep-ph/9403379].
- [4] A. Heister *et al.* [ALEPH Collaboration], Phys. Lett. B **569** (2003) 140.
- [5] H. Nakazawa *et al.* [BELLE Collaboration], Phys. Lett. B **615** (2005) 39 [hep-ex/0412058].
- [6] S. Uehara *et al.* [BELLE Collaboration], Phys. Rev. D **79** (2009) 052009 [arXiv:0903.3697 [hep-ex]].
- [7] J. Brodzicka *et al.* [Belle Collaboration], PTEP **2012** (2012) 04D001 [arXiv:1212.5342 [hep-ex]].
- [8] C. Vogt, hep-ph/0010040.
- [9] V. L. Chernyak, Phys. Lett. B **640** (2006) 246 [hep-ph/0605072].
- [10] V. L. Chernyak, arXiv:1212.1304 [hep-ph]; V. L. Chernyak, Chin. Phys. C **34** (2010) 822 [arXiv:0912.0623 [hep-ph]];
- [11] A. Khodjamirian, Eur. Phys. J. C **6** (1999) 477 [hep-ph/9712451].
- [12] S. V. Mikhailov and A. V. Radyushkin, Phys. Rev. D **45** (1992) 1754.
- [13] S. S. Agaev, V. M. Braun, N. Offen and F. A. Porkert, Phys. Rev. D **86** (2012) 077504 [arXiv:1206.3968 [hep-ph]].
- [14] A. P. Bakulev, S. V. Mikhailov, A. V. Pimikov and N. G. Stefanis, Nucl. Phys. Proc. Suppl. **219-220** (2011) 133 [arXiv:1108.4344 [hep-ph]].
- [15] A. P. Bakulev, S. V. Mikhailov, A. V. Pimikov and N. G. Stefanis, Phys. Rev. D **86** (2012) 031501 [arXiv:1205.3770 [hep-ph]].
- [16] V. M. Braun, A. Khodjamirian and M. Maul, Phys. Rev. D **61** (2000) 073004 [hep-ph/9907495].
- [17] M. Diehl, P. Kroll and C. Vogt, Phys. Lett. B **532** (2002) 99 [hep-ph/0112274].
- [18] M. Diehl and P. Kroll, Phys. Lett. B **683** (2010) 165 [arXiv:0911.3317 [hep-ph]].
- [19] C. W. Bauer, S. Fleming and M. E. Luke, Phys. Rev. D **63**, 014006 (2000).
- [20] C. W. Bauer, S. Fleming, D. Pirjol and I. W. Stewart, Phys. Rev. D **63**, 114020 (2001).
- [21] C. W. Bauer and I. W. Stewart, Phys. Lett. B **516**, 134 (2001).
- [22] C. W. Bauer, D. Pirjol and I. W. Stewart, Phys. Rev. D **65**, 054022 (2002).
- [23] M. Beneke, A. P. Chapovsky, M. Diehl and T. Feldmann, Nucl. Phys. B **643**, 431 (2002).
- [24] M. Beneke and T. Feldmann, Phys. Lett. B **553**, 267 (2003).
- [25] J. Gasser, M. A. Ivanov and M. E. Sainio, Nucl. Phys. B **745** (2006) 84 [hep-ph/0602234].
- [26] G. P. Lepage and S. J. Brodsky, Phys. Lett. B **87**, 359 (1979).
- [27] V. L. Chernyak and A. R. Zhitnitsky, Phys. Rept. **112**, 173 (1984).
- [28] N. Isgur and C. H. Llewellyn Smith, Phys. Rev. Lett. **52**, 1080 (1984).
- [29] N. Isgur and C. H. Llewellyn Smith, Nucl. Phys. B **317**, 526 (1989).

- [30] N. Isgur and C. H. Llewellyn Smith, Phys. Lett. B **217**, 535 (1989).
- [31] V. A. Nesterenko and A. V. Radyushkin, Phys. Lett. B **115** (1982) 410.
- [32] A. P. Bakulev, A. V. Radyushkin and N. G. Stefanis, Phys. Rev. D **62** (2000) 113001 [hep-ph/0005085].
- [33] V. L. Chernyak and A. R. Zhitnitsky, Nucl. Phys. B **201** (1982) 492 [Erratum-ibid. B **214** (1983) 547].
- [34] G. Duplancic and B. Nizic, Phys. Rev. Lett. **97** (2006) 142003 [hep-ph/0607069].
- [35] M. Beneke and V. A. Smirnov, Nucl. Phys. B **522** (1998) 321 [hep-ph/9711391].
- [36] V. A. Smirnov and E. R. Rakhmetov, Theor. Math. Phys. **120** (1999) 870 [Teor. Mat. Fiz. **120** (1999) 64] [hep-ph/9812529].
- [37] V. A. Smirnov, Springer Tracts Mod. Phys. **177** (2002) 1.
- [38] J. C. Collins and F. Hautmann, Phys. Lett. B **472**, 129 (2000) [arXiv:hep-ph/9908467].
- [39] A. V. Manohar and I. W. Stewart, Phys. Rev. D **76**, 074002 (2007) [arXiv:hep-ph/0605001].
- [40] J. -Y. Chiu, A. Jain, D. Neill and I. Z. Rothstein, JHEP **1205** (2012) 084 [arXiv:1202.0814 [hep-ph]].
- [41] C. W. Bauer, S. Fleming, D. Pirjol, I. Z. Rothstein and I. W. Stewart, Phys. Rev. D **66** (2002) 014017 [hep-ph/0202088].
- [42] C. W. Bauer, D. Pirjol and I. W. Stewart, Phys. Rev. D **68** (2003) 034021 [hep-ph/0303156].
- [43] M. Beneke and T. Feldmann, Nucl. Phys. B **685** (2004) 249 [hep-ph/0311335].
- [44] A. Hardmeier, E. Lunghi, D. Pirjol and D. Wyler, Nucl. Phys. B **682** (2004) 150 [hep-ph/0307171].
- [45] Y. Y. Balitsky, V. M. Braun and A. V. Kolesnichenko, Sov. J. Nucl. Phys. **48** (1988) 348 [Yad. Fiz. **48** (1988) 547]; Nucl. Phys. B **312** (1989) 509.
- [46] G. 't Hooft, Nucl. Phys. B **72** (1974) 461.
- [47] E. Witten, Nucl. Phys. B **160** (1979) 57.
- [48] M. Beneke, G. Buchalla, M. Neubert and C. T. Sachrajda, Nucl. Phys. B **591** (2000) 313 [arXiv:hep-ph/0006124].
- [49] M. Beneke and T. Feldmann, Nucl. Phys. B **592** (2001) 3 [arXiv:hep-ph/0008255].
- [50] V. M. Braun and I. E. Filyanov, Z. Phys. C **48** (1990) 239 [Sov. J. Nucl. Phys. **52** (1990) 126] [Yad. Fiz. **52** (1990) 199].
- [51] N. Kivel and M. Vanderhaeghen, Phys. Rev. D **83** (2011) 093005 [arXiv:1010.5314 [hep-ph]].
- [52] J. Chay and C. Kim, Phys. Rev. D **82** (2010) 094021 [arXiv:1007.4395 [hep-ph]].
- [53] M. Beneke, Nucl. Phys. Proc. Suppl. **111** (2002) 62 [hep-ph/0202056].
- [54] R. Mertig, M. Bohm and A. Denner, Comput. Phys. Commun. **64** (1991) 345; R. Mertig and R. Scharf, Comput. Phys. Commun. **111** (1998) 265 [hep-ph/9801383]; see also web-page <http://www.feyncalc.org>
- [55] P. Ball, V. M. Braun and A. Lenz, JHEP **0605** (2006) 004 [hep-ph/0603063].
- [56] V. M. Budnev, I. F. Ginzburg, G. V. Meledin and V. G. Serbo, Phys. Rept. **15** (1975) 181.

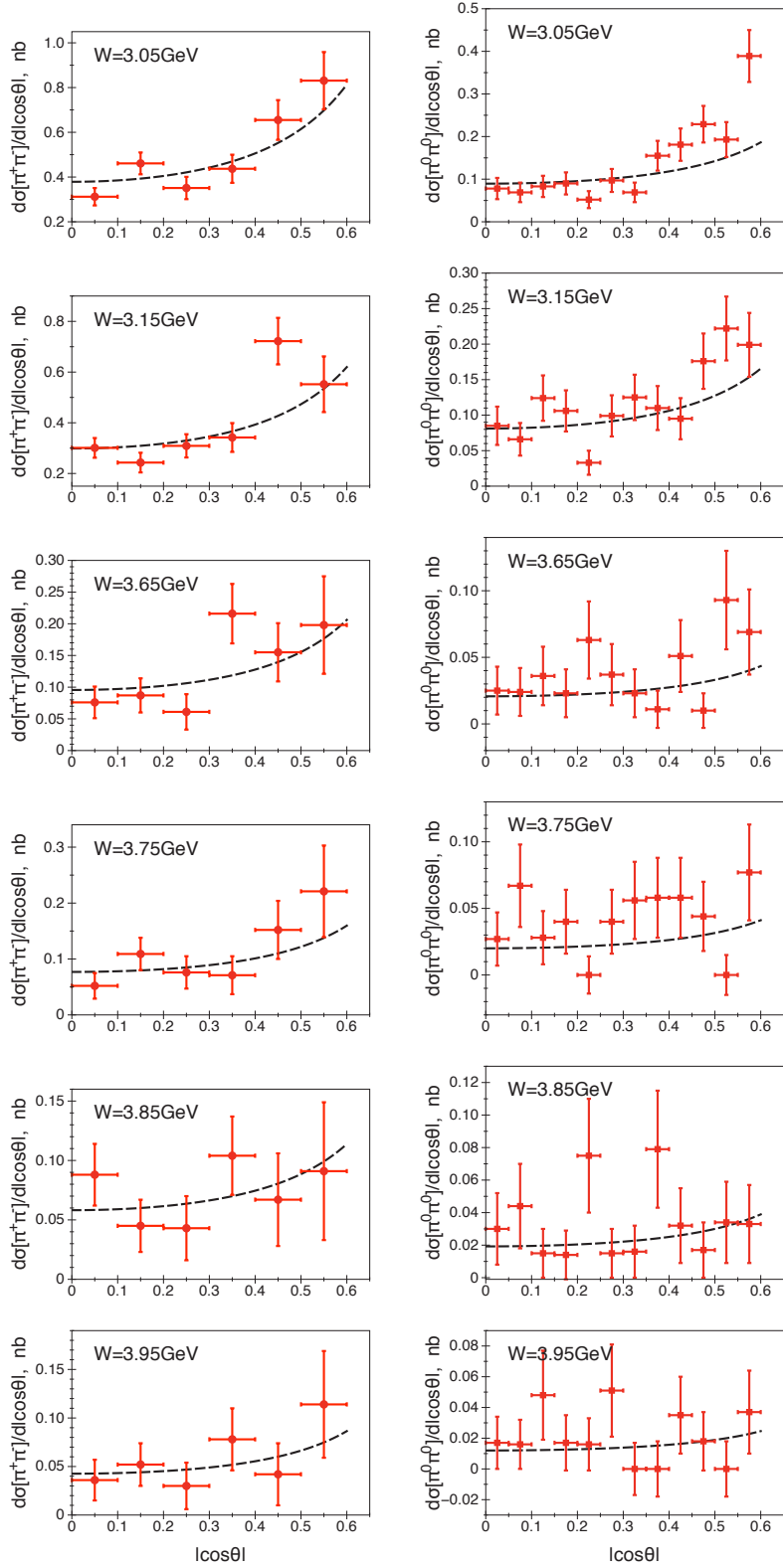


Figure 20. Results of the fit of BELLE data [5, 6] for the differential cross sections at different energies.

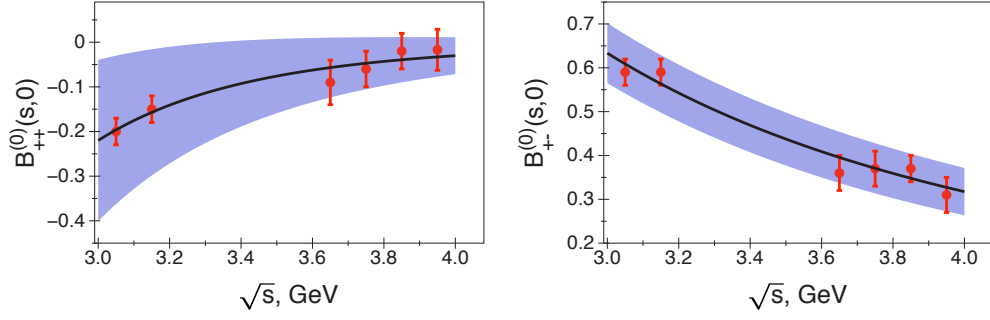


Figure 21. The amplitudes $B_{++}^0(s,0)$ and $B_{+-}^0(s,0)$ as a functions of energy obtained from the fit of the differential cross sections.

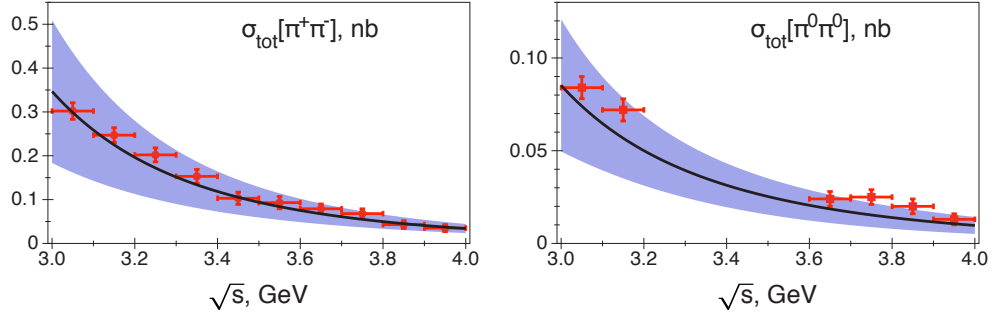


Figure 22. The total cross sections as functions of energy.

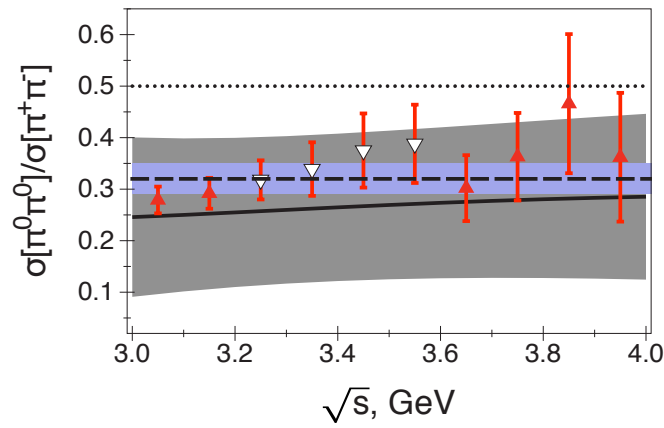


Figure 23. The ratio $\sigma^{\pi^0\pi^0}/\sigma^{\pi^+\pi^-}$ as functions of energy. The notations are the same as in Fig.19.

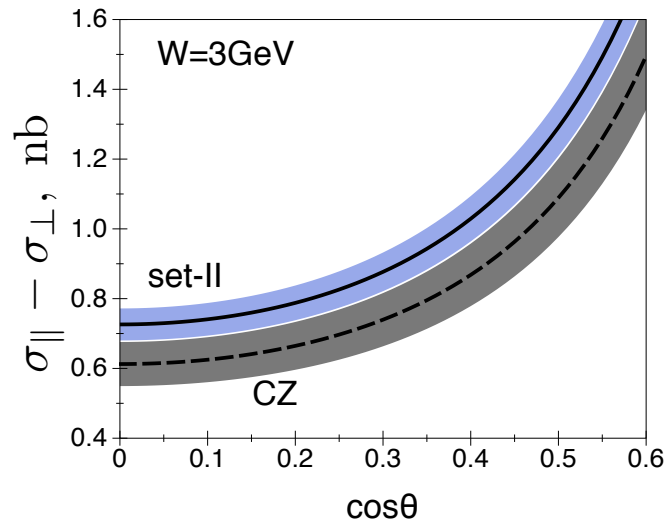


Figure 24. Predictions of the cross sections $\sigma_{\parallel}^{\gamma\gamma\rightarrow\pi\pi} - \sigma_{\perp}^{\gamma\gamma\rightarrow\pi\pi}$ for the two different model of pion DA. See discussion in the text.